Unravelling spatio-temporal water balance patterns in topographically complex landscapes

by

Daniel Metzen

ORCID ID: 0000-0002-0330-8698

Submitted in total fulfillment of the requirements

of the degree of Doctor of Philosophy

September 2017

The University of Melbourne

Faculty of Science

School of Ecosystem and Forest Sciences

Abstract

The Budyko framework for understanding how precipitation (P) is partitioned into evapotranspiration (ET) and streamflow has been shown to be remarkably robust at large spatial scales. The Budyko model simply uses P and potential ET as variables. However, at smaller spatial scales additional predictor variables are required to partition precipitation. In steep uplands, topography appears to exert strong control on the water balance at the hillslope scale. Organization of vegetation suggest heterogeneity in the water balance at these scales. This topographic control though is poorly characterized in most environments and therefore not well represented in models.

The aim of this thesis is to quantify the effect of local topography (aspect and drainage position) on forest water balance as a first step towards a down-scaling of the Budyko model in steep upland terrain.

Six intensively instrumented sited were established on three drainage positions and two aspects in mixed species eucalypt forests (MSEF), with all other variables remaining constant. Continuously monitored water balances were extrapolated across a $\sim$70 ha catchment using a Random Forest model and LiDAR characterization of stand density and structure.

The study demonstrated that spatial vegetation patterns emerged in response to topographic control on water-availability via soil depth, water redistribution and sub-canopy radiation loads. Moreover, short-term variations of overstory transpiration (T_O) were

driven by atmospheric forcing, whereas seasonal and annual T_O patterns were explained by sapwood area index (A_S, R^2:0.89). Understory and forest floor evapotranspiration (ET_U) was controlled by sub-canopy short-wave radiation. Further, the combined effect of aspect and drainage position on water balance partitioning markedly diverged along the south and north-facing transect. All plots on northern aspects had a positive water balance (P>ET), whereas only the ridge plot on the south-facing slope had a positive water balance, while the lower hillslope had higher ET rates than rainfall inputs. ET measurements from the distributed plots could be up-scaled using terrain and vegetation information derived from LiDAR and unveiled strong spatial variability of T_O (4.5-fold), ET_U (3.5-fold) and total ET rates (2-fold) over as little as 200 m distance. The observed ET range corresponds to eucalypt forests typically located >100s of kilometers apart, with the lower end similar to arid open woodlands in Western Australia and the upper end to tall mountain ash forests in the Victorian highlands. Predicting ET using the Budyko framework revealed strongly biased ET estimates in relation to landscape position, where ∼18% of the catchment area plotted above the theoretical water limit, confirming the importance of topographic water redistribution. Further, model residuals were explained well by A_S and terrain patterns.

My thesis presented strong links between vegetation patterns, topography, soil depth and energy and water fluxes in upland MSEF. Ultimately, the study demonstrated the potential of remotely sensed vegetation and terrain patterns to infer and scale water-balance patterns in heterogeneous upland forests.

Declaration

This is to certify that:

(i) the thesis comprises only my original work.

(ii) due acknowledgment has been made in the text to all other material used; and

(iii) the thesis is fewer than 100,000 words in length exclusive of tables, maps, references and appendices.

Daniel Metzen

8 September 2017

Acknowledgments

The study was funded by the Victorian Department of Environment, Land, Water and Planning Integrated Forest Ecosystem Research program. I was supported by a Melbourne International Research Scholarship, a Melbourne International Fee Remission Scholarship and SF Ponds Traveling Scholarship. I'd like to thank my supervisors Patrick Lane, Gary Sheridan and Paul Bolstad, for guidance and support in every possible way throughout my Candidature. I am very grateful to Richard Benyon for providing intellectual and technical support as well as providing sap flow gear used in this study. Further, I would like to thank Phillip Noske, Anne Griebel, Petter Nyman, Craig Baillie, Assaf Inbar, Christoph Langhans and Tom Fairman for assistance in the field or fruitful discussion in the office as well as my partner, friends and family that made my PhD experience a fun one.

Contents

List of Tables

List of Figures

Chapter 1

Introduction

Forests provide a range of crucial ecosystems services, e.g. water storage and filtration, carbon sequestration, thermal regulation etc. (Field et al. 2015; Watanabe and Ortega 2011). Most of those services are tightly coupled to the forest water balance, of which evapotranspiration (ET) is usually the largest component (Schlesinger and Jasechko 2014). Further, small scale spatial vegetation patterns might be important to predict ecosystem response to disturbance, e.g. wildfires, management practices, e.g. fuel reduction burns (Nyman et al. 2015) and silviculture, e.g. thinning (Hawthorne et al. 2013). Thus, accurate predictions of ET will aid managing forest and water resources.

Budyko (1974) developed a framework that enables to predict the partitioning of precipitation into evapotranspiration and stream flow. Known as the "Budyko curve", the evaporative index (ϵ, ET/P) is expressed as a function of the aridity index (AI, PET/P). Over large scales the model has been shown to be remarkably robust given it only uses precipitation (P) and potential evapotranspiration (PET) as inputs (Budyko 1974).

However, the Budyko framework does not account for catchment properties such as variations in vegetation, soils and topography. Hence, forests are treated as being homogeneous just because they are in the same rainfall and temperature category. This oversimplification might cause biased predictions at the scale of interest in heterogeneous

ecosystems with strong non-linear interactions between vegetation, energy and moisture patterns (Ivanov et al. 2008), particularly under changing climate.

Several attempts have been made to account for variations of vegetation, topography and climate by calibrating an additional empirical shape parameter to improve predictions at catchment scale (Choudhury 1999; Zhang et al. 2004; Donohue et al. 2007; Donohue et al. 2012). More recently, the importance of lateral water redistribution (Rouholahnejad Freund and Kirchner 2017) and groundwater storage changes (Condon and Maxwell 2017) on sub-catchment ET estimates using the Budyko framework were illustrated. Hence, at smaller spatial scales (i.e. sub-catchment) additional predictor variables are required to partition precipitation.

One possible way to increase the accuracy of predictions at smaller scales are spatial distributed models, which emerged from the late 1970s onwards. The general idea of those models is to represent the spatial distribution of catchment properties and forcings. However, while the underlying fine-scale model physics might match point scale observations, processes at the spatial domain at which the model is operating are potentially not captured. For example, models predicting water-movement using the Richards equation might match with a few point scale soil moisture observations, yet produce poor streamflow estimates in ecosystems where preferential flow-paths shape the hydrologic response (Weiler and McDonnell 2007).

Further, spatial heterogeneities and process interactions on scales larger than the models internal structures are potentially not captured as well. As a result, distributed models are often over-parameterized and require calibration of an extensive number of parameters to account for the discrepancy between model physics and dominant "real-life" processes, which impedes transferability outside domains they were calibrated in (McDonnell et al. 2007).

Further, understanding why landscape heterogeneities occur (e.g. vegetation and soil depth patterns) and their influence on hydrologic processes potentially allows to improve hydrologic predictions using easily mappable catchment features (e.g. DEMs, optical remote sensing).

Recent introduction of the "Critical Zone" (CZ) concept, the zone spanning from the top of the vegetation to the bottom of aquifers, and the establishment of an associated network of long-term observatories acknowledged the need for a more holistic, inter-disciplinary research approach of understanding ecosystem processes, particularly under changing climate. Functioning of the CZ, and the hydrological cycle in particular, is determined by dynamic processes and interactions as well as its structure (Lin 2010; Grant and Dietrich 2017). Thus, combined investigation of interdependent processes, structures and spatial patterns will extend our understanding not only of hydrologic processes, but also what processes shape the CZ and how changing climate might affect the system, ultimately leading to transferable knowledge of CZ functioning. Further, insights on spatial patterns and heterogeneities in the CZ might enable to down-scale predictions from lumped models.

Within the CZ, the hydrologic cycle plays a central role in shaping the terrain via erosion, transport and accumulation of material, but also in mobilizing nutrients, providing water and in combination with climate (temperature) determines biological activity (Lin 2010). Over large spatial and temporal scales ("geological time scale") the CZ structure is determined by a combination of geologic, geomorphologic and hydro-climatic processes (Fig. 1.1). Tectonic and volcanic processes create elevation gradients and define the parent material, which is then shaped by geomorphologic processes in response to given climate and precipitation patterns to the topography we observe today. Soil erosion, accumulation and production rates interact on shorter-time scales ("ecological time scale") with biogeochemical and biological processes determining soil development and thus growing

conditions for plants. Biomass accumulation in turn reduces soil erosion and enhances biological activity leading to deeper, more developed soils and thus increased water storage capacity, potentially creating a feedback loop which increases ecosystem productivity and CZ development.

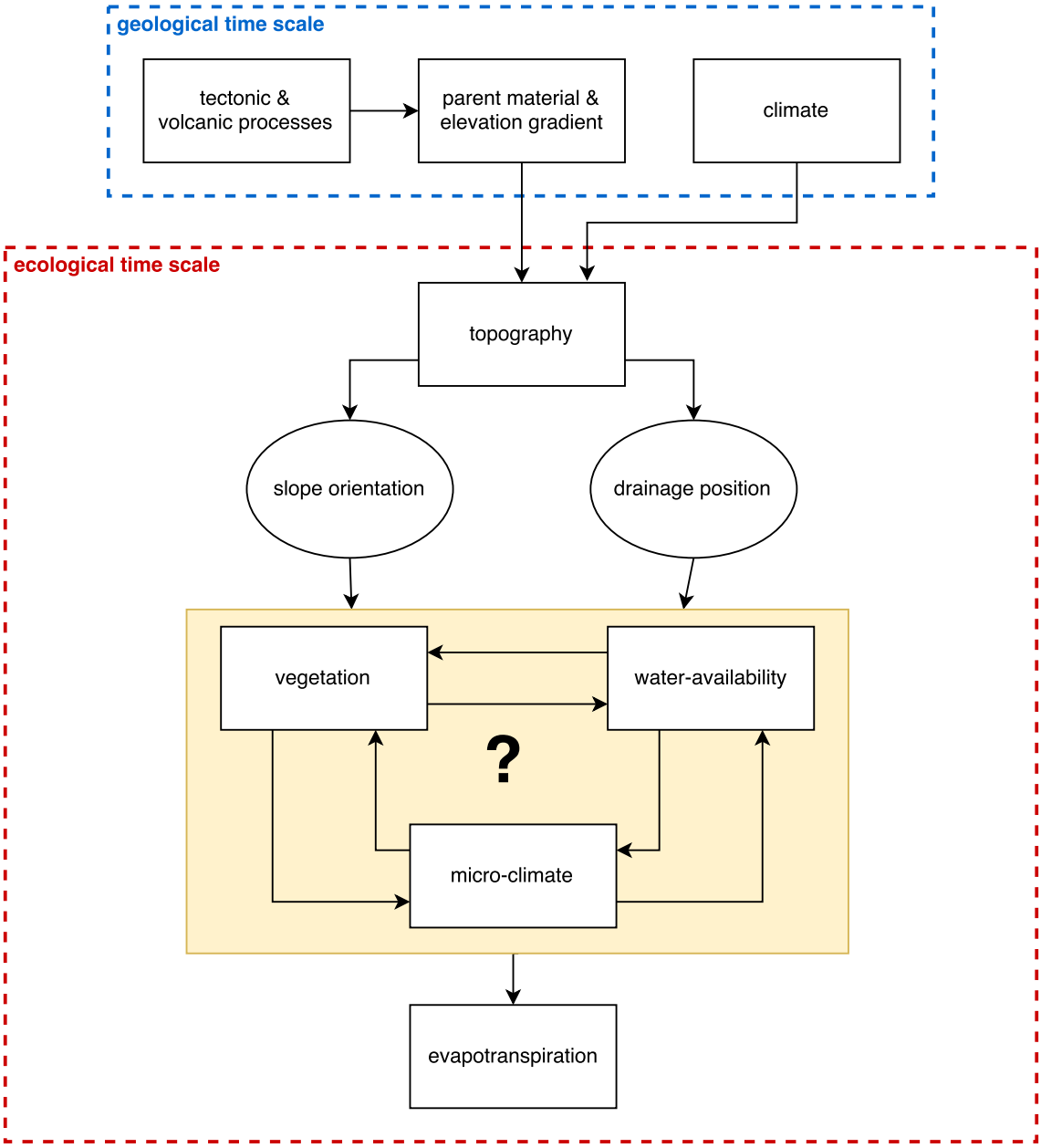

Figure 1.1: Conceptual model describing Critical Zone evolution and addressing knowledge gaps on topographic control of evapotranspiration.

Over smaller spatial extents, where geology, climate and precipitation patterns are

similar, topography can still exert strong control on the CZ structure via slope orientation and drainage position. Slope angle and aspect modify the surface energy balance at a given location by altering the incident angle of solar radiation and thus the radiation load per unit surface area (Nyman et al. 2017; Zou et al. 2007). Further, higher radiation loads on equatorial-facing slopes (Tian et al. 2001; Zou et al. 2007; Nyman et al. 2017) lead to higher potential evapotranspiration rates (PET), which in turn cause lower soil water content (SWC) (Nyman et al. 2015; Martinez et al. 2008). Lower SWC and thus available water for biological activity hinders soil development (Geroy et al. 2011; Pachepsky et al. 2001) and biomass accumulation (Jenkins and Coops 2011; D'Odorico et al. 2007). In contrast, lower radiation and PET on polar-facing slopes results in higher SWC that can be utilized by plants and micro-organisms. Increasing vegetation cover shades the soil surface, limiting water-loss to soil evaporation and thus conserving soil water lost via "unproductive" pathways. Hence, in water-limited ecosystems, the CZ is expected to be generally more developed on polar-facing slopes due to higher water-availability for biological, ecological and biogeochemical processes (Zapata-Rios et al. 2016; Gutirrez-Jurado et al. 2013; Rasmussen et al. 2015).

Moreover, drainage position influences the redistribution of water (Thompson et al. 2011) and soils (Pelletier and Rasmussen 2009; Tesfa et al. 2009) along elevation and drainage gradients imposing additional complexity on top of "local" patterns due to slope orientation. "Local" energy and moisture patterns as well as the CZ structure of upslope areas are expected to have large impacts on "non-local" redistribution of water and soil material. Larger soil water storage and infiltration capacity upslope would cause less net downflow of water, whereas more vegetation cover, root reinforcement and higher infiltration rates would result in less soil movement from upslope areas. Hence, similar drainage position (e.g. quantified by the topographic wetness index (Beven and Kirkby 1979)) is expected to have

different impact on the CZ structure between aspects. Contrasting vegetation patterns between polar and equatorial-facing slopes have been observed in a range of ecosystems in the northern hemisphere, from semiarid shrub ecosystems (Gutirrez-Jurado et al. 2013) to montane forests (Brooks et al. 2015). However, in most ecosystems, little is known about the relative and combined influence of slope orientation and drainage position on CZ structure and processes (Fig. 1.1).

In south-east Australia, forest hydrology research has so far mainly focused on catchment-scale response to disturbance (e.g. bushfires, logging) in tall mountain ash (*E. regnans*) forests (Kuczera 1987; Vertessy et al. 1993; Haydon et al. 1997; Watson et al. 1999; Bren et al. 2010; Benyon et al. 2015) and drier mixed species eucalypt forests (Webb et al. 2012; Webb and Jarrett 2013; Bren et al. 2013; Bren and Hopmans 2007; Lane and Mackay 2001; Lane et al. 2010; Nolan et al. 2015). Hence, streamflow response at catchment-scale is well documented for a range of native eucalypt forests, but relatively little is known about sub-catchment internal ET patterns and drivers.

The TOPOG model developed by the Commonwealth Scientific and Industrial Research Organisation (CSIRO) in the late 1980s aimed to provide sub-catchment water balance information (O'Loughlin 1986; Vertessy et al. 1993). It is a fully distributed model simulating spatio-temporal water movement in complex, heterogeneous terrain and has been shown to be able to accurately predict streamflow in a small headwater catchment in Victoria (Vertessy et al. 1993). However, a large amount of spatially explicit information on climate, topography, vegetation and soil is required to run TOPOG. While some of the vegetation parameters can be inferred from remote sensing (e.g. LAI), deriving spatial estimates of others is challenging (e.g. maximum leaf water potential, aerodynamic resistance, maximum canopy conductance). Obtaining spatial information on the required soil parameters (e.g. soil depth, saturated hydraulic conductivity) is equally difficult.

Thus, performance and transferability of TOPOG to sites it has not been calibrated for is impeded by the vast amount of input data, similar to other 'data hungry' complex models.

As mentioned above vegetation patterns in complex terrain emerge as a consequence of topographically driven energy and moisture patterns. Therefore, vegetation patterns might offer a simpler way of gaining insights on sub-catchment scale ET dynamics. Recent work in non-water limited mountain ash stands, where forest structure and sap velocity rates (v_{sap}) are relatively homogeneous, illustrated that sapwood area index (A_S, sapwood area per unit ground area) explained annual ET (Benyon et al. 2017). However, large parts of the forests in south-east Australia are mixed-species eucalypt forests (MSEF) typically located in an aridity index (AI, ratio of PET to precipitation) range of 1-2, around the energy-limited to water-limited boundary. Forest structure and species composition are very responsive to changes in the energy and water balance in the moderately dry aridity range (1-2) (Nyman et al. 2014; Givnish et al. 2014; Kirkpatrick and Nunez 1980).

So far, a range of plot studies have established that transpiration rates of eucalypt species abundant in MSEF are mainly controlled by vapor pressure deficit (VPD) (Gharun et al. 2014; Mitchell et al. 2009; Nolan et al. 2014; Yunusa et al. 2010) and PET (Mitchell et al. 2012b). Further, stand transpiration rates (Benyon et al. 2006), ecosystem ET (O'Grady et al. 2011) and plant hydraulics (Zolfaghar et al. 2015) have been shown to adapt when trees have access to groundwater access. Consequently, changes of energy and moisture patterns due to non-local contributions (topographic redistribution, groundwater) of plant-available water in combination with slope orientation might be of considerable importance in MSEF in complex terrain. Strong vegetation patterns of MSEF in relation to topography are expected to relate to strong ET patterns as well, yet the nature and magnitude of this topographic control on vegetation and evapotranspiration has received little quantitative research attention.

Early work by Barrett et al. (1996) illustrated different transpiration rates along the eucalypt and temperate rainforest transition in a small head water catchment. On northern aspects, transpiration rates in the rainforest plot were higher than in the eucalypt plot, whereas on the southern aspects transpiration rates between eucalypts and rainforest species were similar. Different patterns between aspects were related to variations in leaf area index in response to the rainforest-eucalypt boundary, which occurred further upslope on the northern aspects. Topographic controls on rainfall, soil type, temperature (Bowman and Connors 1996) and fire patterns (Wood Sam W. et al. 2011) has also been shown to cause shifts between eucalypt and non-eucalypt dominated ecosystems elsewhere in Australia.

More recently, the need to account for the spatial heterogeneity of MSEF when addressing the catchment water balance was acknowledged (Mitchell et al. 2012b; Mitchell et al. 2012a; Gharun et al. 2013; Gharun et al. 2014) but contrasting findings were reported. While Mitchell et al. (2012a) found no significant v_{sap} differences between tree sizes, species and landscape position, Gharun et al. (2015) reported v_{sap} patterns in relation to slope aspect and angle. The lack of spatial v_{sap} heterogeneity allowed Mitchell et al. (2012a) to scale ET using mapped A_S, whereas Gharun et al. (2015) did not report stand structural parameters. Therefore, large uncertainties remain on ET patterns in spatially heterogeneous forest ecosystems as well as the potential use of vegetation patterns to infer ET patterns.

Further, overstory and understory structure as well as ET patterns might vary substantially at the same landscape position, because of different access to light and water. Larger rooting depth of overstory vegetation will increase water-availability compared to understory vegetation. More canopy cover in turn will have ambiguous impacts on understory vegetation. While, light access of understory vegetation will be impeded, atmospheric demand will also be reduced and thus soil water conserved. So far, only a few studies have

investigated understory ET (ET_U) eucalypt ecosystems. In a dry, open eucalypt woodland ET_U has been identified as the largest ET component, accounting for 38 - 64% of total ET (Mitchell et al. 2009). ET_U also contributed substantially to the total ET flux in MSEF. Mitchell et al. (2012b) reported annual ET_U of 144 mm (18% of total ET), whereas Nolan et al. (2014) attributed 24-33% (285-323 mm) of total ET to ET_U. Even in tall mountain ash forests annual ET_U totals ranged from 8 to 26% (116-297 mm) (Benyon et al. 2017). These findings illustrate a large range of ET_U in contrasting eucalypt forest stands, where ET_U was either strongly correlated to sub-canopy energy (Nolan et al. 2014; Mitchell et al. 2012b; Benyon et al. 2017) or moisture patterns (Mitchell et al. 2009). Hence, large uncertainties on spatial ET_U patterns and controls remain in complex upland forests.

While catchment scale models, which integrate over sub-catchment variability, might produce acceptable streamflow estimates for management purposes, certain areas of catchments might have different resilience towards drought or changing climate. Thus, vegetation in different catchment areas (e.g. gully vs. ridge) could take different trajectories going forward, which not necessary cancel out on catchment scale. Therefore, lumped models calibrated under current condition might not work under changing climate with differential sub-catchment ecosystem response. In order to predict ecosystem response to climate change a quantitative assessment of the interactions between aspect and drainage position and their effect on ecosystem structure and functioning is crucial.

Links between the hydrologic cycle and the Critical Zone illustrated above might enable to infer hydrologic functioning from spatial CZ patterns across a range of ecosystems. Spatial vegetation and terrain patterns are particularly appealing for three reasons. Firstly, they are remotely observable at high resolutions with increasing spatial coverage around the globe. Secondly, vegetation patterns potentially capture information on several Critical Zone processes because vegetation growth is influenced or limited by a range of factors

that determine growing conditions (e.g. temperature, light, water-availability, nutrients etc.). Thirdly, water, carbon and nutrients used by plants can be stored within the CZ and thus spatial vegetation patterns integrate over short-term variability of rainfall and climate patterns.

Hence, remotely sensed vegetation and terrain properties might offer the potential to down-scale broad-scale ET predictions in heterogeneous upland forests using the Budyko framework, and thus bridging the gap between lumped and distributed process-based models.

The aim of this thesis is to quantify the topographic controls (aspect and drainage position) on the forest water balance in a domain where detailed data is rare, because common methods to estimate ecosystem ET (e.g. eddy co-variance) fail in complex terrain and heterogeneous ecosystems.

Further, the potential of using remotely sensed vegetation and topographic information to scale sub-catchment ET patterns is evaluated in a first step towards down-scaling of the Budyko model in steep upland terrain.

Field sites were set-up along transects with contrasting aspects (energy input) while simultaneously altering drainage position from ridge to mid-slope and gully at both aspects. In chapter 2, overstory vegetation, soil depth and overstory transpiration patterns are quantified along the transects and dominant controls on stand structure, overstory sap velocity and transpiration identified. Chapter 3 addresses sub-canopy micro-climate, soil moisture and understory ET dynamics and controls. Plot-scale water balance patterns and partitioning in relation to landscape position are investigated in the chapter 4. Chapter 5 evaluates using high-resolution remotely sensed vegetation and terrain data to scale ET in heterogeneous forests and infer spatio-temporal ET patterns in response to landscape position.

Bibliography

Barrett, D. J. et al. (1996). "Transpiration by trees from contrasting forest types". In: *Australian Journal of Botany* 44.3, pp. 249–263.

Benyon, R. G. et al. (2006). "Impacts of tree plantations on groundwater in south-eastern Australia". In: *Australian Journal of Botany* 54.2, p. 181.

Benyon, R. G. et al. (2015). "Use of a forest sapwood area index to explain long-term variability in mean annual evapotranspiration and streamflow in moist eucalypt forests: streamflow predicted from sapwood area". In: *Water Resources Research* 51.7, pp. 5318–5331.

Benyon, R. G. et al. (2017). "Stand-level variation in evapotranspiration in non-water-limited eucalypt forests". In: *Journal of Hydrology* 551, pp. 233–244.

Beven, K. J. and M. J. Kirkby (1979). "A physically based, variable contributing area model of basin hydrology". In: *Hydrological Sciences Bulletin* 24.1, pp. 43–69.

Bowman, D. M.J. S. and G. T. Connors (1996). "Does Low Temperature Cause the Dominance of Acacia on the Central Australian Mountains? Evidence from a Latitudinal Gradient from 11 to 26 South in the Northern Territory Australia". In: *Journal of Biogeography* 23.2, pp. 245–256.

Bren, L. and P. Hopmans (2007). "Paired catchments observations on the water yield of mature eucalypt and immature radiata pine plantations in Victoria, Australia". In: *Journal of Hydrology* 336.3, pp. 416–429.

Bren, L. et al. (2010). “Longer-term water use of native eucalyptus forest after logging and regeneration: The Coranderrk experiment”. In: *Journal of Hydrology* 384.1, pp. 52–64.

Bren, L. et al. (2013). “Impacts of native forest harvesting on flows into the MurrayDarling Basin system”. In: *Australian Forestry* 76.2, pp. 91–100.

Brooks, P. D. et al. (2015). “Hydrological partitioning in the critical zone: Recent advances and opportunities for developing transferable understanding of water cycle dynamics”. In: *Water Resources Research* 51.9, pp. 6973–6987.

Budyko, M. I. (1974). *Climate and Life*. Orlando, Fl: Academic.

Choudhury, B. (1999). “Evaluation of an empirical equation for annual evaporation using field observations and results from a biophysical model”. In: *Journal of Hydrology* 216.1, pp. 99–110.

Condon, L. E. and R. M. Maxwell (2017). “Systematic shifts in Budyko relationships caused by groundwater storage changes”. In: *Hydrology and Earth System Sciences* 21.2, pp. 1117–1135.

D’Odorico, P. et al. (2007). “On soil moisture-vegetation feedbacks and their possible effects on the dynamics of dryland ecosystems”. In: *Journal of Geophysical Research: Biogeosciences* 112 (G4).

Donohue, R. J. et al. (2007). “On the importance of including vegetation dynamics in Budykos hydrological model”. In: *Hydrology and Earth System Sciences* 11, pp. 983–995.

Donohue, R. J. et al. (2012). “Roots, storms and soil pores: Incorporating key ecohydrological processes into Budykos hydrological model”. In: *Journal of Hydrology* 436-437, pp. 35–50.

Field, J. P. et al. (2015). “Critical Zone Services: Expanding Context, Constraints, and Currency beyond Ecosystem Services”. In: *Vadose Zone Journal* 14.1.

Geroy, I. et al. (2011). "Aspect influences on soil water retention and storage". In: *Hydrological Processes* 25.25, pp. 3836–3842.

Gharun, M. et al. (2013). "Validation of canopy transpiration in a mixed-species foothill eucalypt forest using a soilplantatmosphere model". In: *Journal of Hydrology* 492, pp. 219–227.

Gharun, M. et al. (2014). "A test of how coupling of vegetation to the atmosphere and climate spatial variation affects water yield modelling in mountainous catchments". In: *Journal of Hydrology* 514, pp. 202–213.

Gharun, M. et al. (2015). "Mapping spatial and temporal variation in tree water use with an elevation model and gridded temperature data". In: *Agricultural and Forest Meteorology* 200, pp. 249–257.

Givnish, T. J. et al. (2014). "Determinants of maximum tree height in Eucalyptus species along a rainfall gradient in Victoria, Australia". In: *Ecology* 95.11, pp. 2991–3007.

Grant, G. E. and W. E. Dietrich (2017). "The frontier beneath our feet". In: *Water Resour. Res.* 53.4, pp. 2605–2609.

Gutirrez-Jurado, H. A. et al. (2013). "On the observed ecohydrologic dynamics of a semiarid basin with aspect-delimited ecosystems: ecohydrologic dynamics of a semiarid basin". In: *Water Resources Research* 49.12, pp. 8263–8284.

Hawthorne, S. N. et al. (2013). "The long term effects of thinning treatments on vegetation structure and water yield". In: *Forest Ecology and Management* 310, pp. 983–993.

Haydon, S. R. et al. (1997). "Variation in sapwood area and throughfall with forest age in mountain ash (Eucalyptus regnans F. Muell.)" In: *Journal of Hydrology* 187.3, pp. 351–366.

Ivanov, V. Y. et al. (2008). "Vegetation-hydrology dynamics in complex terrain of semiarid areas: 2. Energy-water controls of vegetation spatiotemporal dynamics and topographic niches of favorability". In: *Water Resources Research* 44.3.

Jenkins, R. B. and N. C. Coops (2011). "Landscape Controls on Structural Variation in Eucalypt Vegetation Communities: Woronora Plateau, Australia". In: *Australian Geographer* 42.1, pp. 1–17.

Kirkpatrick, J. B. and M. Nunez (1980). "Vegetation-Radiation Relationships in Mountainous Terrain: Eucalypt-Dominated Vegetation in the Risdon Hills, Tasmania". In: *Journal of Biogeography* 7.2, p. 197.

Kuczera, G. (1987). "Prediction of water yield reductions following a bushfire in ash-mixed species eucalypt forest". In: *Journal of Hydrology* 94.3, pp. 215–236.

Lane, P. N. and S. M. Mackay (2001). "Streamflow response of mixed-species eucalypt forests to patch cutting and thinning treatments". In: *Forest Ecology and Management* 143.1, pp. 131–142.

Lane, P. et al. (2010). "Modelling the long term water yield impact of wildfire and other forest disturbance in Eucalypt forests". In: *Environmental Modelling & Software* 25.4, pp. 467–478.

Lin, H. (2010). "Earth's Critical Zone and hydropedology: concepts, characteristics, and advances". In: *Hydrology and Earth System Sciences* 14.1, p. 25.

Martinez, C. et al. (2008). "Spatiotemporal distribution of nearsurface and root zone soil moisture at the catchment scale". In: *Hydrological Processes* 22.14, pp. 2699–2714.

McDonnell, J. J. et al. (2007). "Moving beyond heterogeneity and process complexity: A new vision for watershed hydrology". In: *Water Resources Research* 43.7, n/a–n/a.

Mitchell, P. J. et al. (2009). "Partitioning of evapotranspiration in a semi-arid eucalypt woodland in south-western Australia". In: *Agricultural and Forest Meteorology* 149.1, pp. 25–37.

Mitchell, P. J. et al. (2012a). "Capturing within catchment variation in evapotranspiration from montane forests using LiDAR canopy profiles with measured and modelled fluxes of water: capturing variation in evapotranspiration using lidar". In: *Ecohydrology* 5.6, pp. 708–720.

Mitchell, P. J. et al. (2012b). "Responses of evapotranspiration at different topographic positions and catchment water balance following a pronounced drought in a mixed species eucalypt forest, Australia". In: *Journal of Hydrology* 440-441, pp. 62–74.

Nolan, R. H. et al. (2014). "Changes in evapotranspiration following wildfire in resprouting eucalypt forests". In: *Ecohydrology*, pp. 1363–1377.

Nolan, R. H. et al. (2015). "Trends in evapotranspiration and streamflow following wildfire in resprouting eucalypt forests". In: *Journal of Hydrology* 524, pp. 614–624.

Nyman, P. et al. (2014). "Downscaling regional climate data to calculate the radiative index of dryness in complex terrain". In: *Australian Metrological and Oceanographic Journal* 64.2, pp. 109–122.

Nyman, P. et al. (2015). "Quantifying the effects of topographic aspect on water content and temperature in fine surface fuel". In: *International Journal of Wildland Fire* 24.8, pp. 1129–1142.

Nyman, P. et al. (2017). "Evaluating models of shortwave radiation below Eucalyptus canopies in SE Australia". In: *Agricultural and Forest Meteorology* 246, pp. 51–63.

O'Grady, A. P. et al. (2011). "Can we predict groundwater discharge from terrestrial ecosystems using existing eco-hydrological concepts?" In: *Hydrology and Earth System Sciences* 15.12, pp. 3731–3739.

O'Loughlin, E. M. (1986). "Prediction of Surface Saturation Zones in Natural Catchments by Topographic Analysis". In: *Water Resour. Res.* 22.5, pp. 794–804.

Pachepsky, Y. A. et al. (2001). "Soil water retention as related to topographic variables". In: *Soil Science Society of America Journal* 65.6, pp. 1787–1795.

Pelletier, J. D. and C. Rasmussen (2009). "Geomorphically based predictive mapping of soil thickness in upland watersheds". In: *Water Resources Research* 45.9.

Rasmussen, C. et al. (2015). "Quantifying Topographic and Vegetation Effects on the Transfer of Energy and Mass to the Critical Zone". In: *Vadose Zone Journal* 14.11.

Rouholahnejad Freund, E. and J. W. Kirchner (2017). "A Budyko framework for estimating how spatial heterogeneity and lateral moisture redistribution affect average evapotranspiration rates as seen from the atmosphere". In: *Hydrology and Earth System Sciences* 21.1, pp. 217–233.

Schlesinger, W. H. and S. Jasechko (2014). "Transpiration in the global water cycle". In: *Agricultural and Forest Meteorology* 189, pp. 115–117.

Tesfa, T. K. et al. (2009). "Modeling soil depth from topographic and land cover attributes". In: *Water Resources Research* 45.10.

Thompson, S. E. et al. (2011). "Spatial scale dependence of ecohydrologically mediated water balance partitioning: A synthesis framework for catchment ecohydrology". In: *Water Resources Research* 47.10.

Tian, Y. Q. et al. (2001). "Estimating solar radiation on slopes of arbitrary aspect". In: *Agricultural and Forest Meteorology* 109.1, pp. 67–74.

Vertessy, R. A. et al. (1993). "Predicting water yield from a mountain ash forest catchment using a terrain analysis based catchment model". In: *Journal of Hydrology* 150.2, pp. 665–700.

Watanabe, M. D. B. and E. Ortega (2011). "Ecosystem services and biogeochemical cycles on a global scale: valuation of water, carbon and nitrogen processes". In: *Environmental Science & Policy* 14.6, pp. 594–604.

Watson, F. G. R. et al. (1999). "Large-scale modelling of forest hydrological processes and their long-term effect on water yield". In: *Hydrol. Process.* 13.5, pp. 689–700.

Webb, A. A. and B. W. Jarrett (2013). "Hydrological response to wildfire, integrated logging and dry mixed species eucalypt forest regeneration: The Yambulla experiment". In: *Forest Ecology and Management* 306, pp. 107–117.

Webb, A. A. et al. (2012). "Longer-term changes in streamflow following logging and mixed species eucalypt forest regeneration: The Karuah experiment". In: *Journal of Hydrology* 464, pp. 412–422.

Weiler, M. and J. J. McDonnell (2007). "Conceptualizing lateral preferential flow and flow networks and simulating the effects on gauged and ungauged hillslopes". In: *Water Resources Research* 43.3.

Wood Sam W. et al. (2011). "Firescape ecology: how topography determines the contrasting distribution of fire and rain forest in the southwest of the Tasmanian Wilderness World Heritage Area". In: *Journal of Biogeography* 38.9, pp. 1807–1820.

Yunusa, I. A. et al. (2010). "Topographical and seasonal trends in transpiration by two co-occurring Eucalyptus species during two contrasting years in a low rainfall environment". In: *Agricultural and Forest Meteorology* 150.9, pp. 1234–1244.

Zapata-Rios, X. et al. (2016). "Influence of terrain aspect on water partitioning, vegetation structure and vegetation greening in high-elevation catchments in northern New Mexico: Terrain Aspect, Water Partitioning, Vegetation Greening in High-elevation Catchments". In: *Ecohydrology* 9.5, pp. 782–795.

Zhang, L. et al. (2004). “A rational function approach for estimating mean annual evapotranspiration”. In: *Water Resources Research* 40.2.

Zolfaghar, S. et al. (2015). “The hydraulic architecture of Eucalyptus trees growing across a gradient of depth-to-groundwater”. In: *Functional Plant Biol.* 42.9, pp. 888–898.

Zou, C. B. et al. (2007). “Effects of topography and woody plant canopy cover on near-ground solar radiation: Relevant energy inputs for ecohydrology and hydropedology”. In: *Geophysical Research Letters* 34.24.

Chapter 2

Stand sapwood area explains stand transpiration patterns along energy and moisture gradient

2.1 Introduction

Slope aspect and inclination is known to increase in-coming short-wave radiation loads on equatorial-facing slopes, while decreasing radiation load on polar aspects (Tian et al. 2001). In water-limited ecosystems, lower radiation loads and less evaporative losses result in higher water-availability on polar-facing slopes (Gutirrez-Jurado et al. 2013; Zhou et al. 2013), as quantified by the aridity index (AI=P/PET) (Budyko 1974). Higher soil water content translates to more biological activity, which ultimately leading to more developed, deeper soils and more biomass on polar aspects (Amundson et al. 2015). Vegetation patterns and associated canopy shading amplify the topographic aridity patterns via a negative feedback (Zou et al. 2007; Nyman et al. 2017) and alters the allocation of soil water from evaporation to transpiration. This feedback is larger in magnitude than the topographic forcing due to aspect, and can cause the large vegetation change with comparatively small changes in energy input due to slope orientation (Gutirrez-Jurado et al. 2013; Rasmussen et al. 2015; Nyman et al. 2014). Non-local water inputs from upslope areas (Thompson et al. 2011) or groundwater (O'Grady et al. 2011) potentially contribute to (plant) available

water at downslope positions, further enhancing spatial heterogeneity. Hence, the combined effect of slope orientation and drainage position can create complex spatial patterns in biological productivity and pedogenesis, which in turn have the potential to alter the local hydrology.

Recent introduction of the Critical Zone concept, spanning from free flowing groundwater to the top of the canopy, highlight the need for holistic, interdisciplinary investigation of the water cycle. However, most observations and recent studies reporting interactions between vegetation, topography and hydrology were carried out in semi-arid or deciduous and coniferous forest ecosystems in the northern hemisphere (Troch et al. 2015; Gutirrez-Jurado et al. 2013; Zapata-Rios et al. 2016; Brooks et al. 2015), which can differ considerably in ecosystem properties and functioning from evergreen temperate forests. Thus, established concepts derived from northern forests may not be directly transferable to evergreen eucalypt forests growing in Australia's climate with a less distinct seasonality.

In south-east Australia, forest hydrology research has so far mainly focused on catchment-scale response to disturbance (e.g. bushfires, logging) in tall mountain ash (*E. regnans*) forests (Kuczera 1987; Vertessy et al. 1993; Haydon et al. 1997; Watson et al. 1999; Bren et al. 2010; Benyon et al. 2015) and drier mixed species eucalypt forests (Webb et al. 2012; Webb and Jarrett 2013; Bren et al. 2013; Bren and Hopmans 2007; Lane and Mackay 2001; Lane et al. 2010; Nolan et al. 2015). Hence, streamflow response at catchment-scale is well documented for a range of native eucalypt forests, but relatively little is known about sub-catchment internal ET patterns and drivers.

However, large parts of forests in south-east Australia are mixed-species eucalypt forests (MSEF) typically located in lower rainfall ranges than mountain ash forests. Here, topographic controls presumably shift ecosystems further past the energy to water-limit boundary (aridity index of 1), and therefore spatial vegetation patterns are assumed to

be greater in MSEF compared to mountain ash forests. Forest structure and species composition of MSEF have been shown very responsive to changes in slope aspect and inclination (Bale et al. 1998; Nyman et al. 2014; Givnish et al. 2014; Pook and Moore 1966). However, the combined effect of slope orientation and drainage position on forest structure in MSEF has received little research attention (Kirkpatrick and Nunez 1980).

Furthermore, strong vegetation patterns of MSEF in relation to topography are expected to relate to strong ET patterns, yet the nature and magnitude of this topographic control on vegetation structure and evapotranspiration has received little quantitative research attention. While recent studies recognized the need to account for the spatial heterogeneity of MSEF when addressing the catchment water balance (Mitchell et al. 2012b; Gharun et al. 2013; Gharun et al. 2014), comparatively little is known about the eco-hydrologic processes at hillslope scale that shape such spatially heterogeneous systems, where species composition and forest structure vary over small spatial extents. Gaining detailed, transferable process understanding of how water and energy fluxes propagate in complex terrain is essential to infer organization and hydrological functioning across the landscape. To achieve this, high resolution measurements across gradients of energy and water-availability are needed to untangle the effects of local topography and drainage position on ET.

This study aims to untangle effects of slope orientation and drainage position on transpiration rates along an energy and moisture gradient in complex terrain. Understanding the key drivers of this small scale variability will enable better prediction of transpiration patterns at larger spatial scales. The specific questions being investigated are:

1. To what degree does forest structure adjust to topography?

2. Are annual or seasonal transpiration patterns affected by landscape position?

3. What are the key drivers of transpiration rates in complex terrain?

2.2 Methods

2.2.1 Study site

The study sites are located in a ∼70 ha sized forested head-water catchment roughly 80 km north-east of Melbourne, VIC, Australia. Mean annual precipitation in the area is 1200 to 1300 mm, peaking in winter and spring. Average daily air temperature in summer (January) is 19°C and average winter (July) temperatures reach 7°C (Nyman et al. 2015). The catchment spans from 290 to 616 m a.s.l in an east-west direction, and thus most of the slope area is either facing towards north or south (Fig. 3.1). Six monitoring plots with a 15 m slope-corrected radius were set-up on a polar and equatorial-facing hillslope at varying drainage position (ridge, mid-slope, gully), while minimizing variations in other factors, e.g. geology, rainfall patterns, short-wave radiation patterns, etc. Plots were set-up in transects on slightly converging hillslopes, so that the water balances of bottom-slope plots could be interpreted with information on the water balance of upslope plots. Potential plot locations were identified using long-term mean annual aridity index (Budyko 1974) and drainage area (D∞ contributing area (Tarboton 1997)) rasters at 20 m spatial resolution. Two levels of aridity and 3 levels of drainage position were aimed for. Plots were chosen with the aim of keeping aridity as constant as possible within the north-facing and south-facing transects, while evenly spacing the three plots across the drainage area range ($\sim$ 1000 to 15000 m^2). The coordinates of the plots that best suited the criteria were loaded on a hand-held GPS (Garmin etrex 10) and the plot center marked upon arrival at the GPS location. Hence, there was a random component of plot selection due to the precision of the GPS (5-10 m). A plPlot size of 15 m was chosen in order to line up with the spatial resolution of the digital elevation model used to generate the aridity index rasters.

Our measurement period lasted from 01.03.2015 to 29.02.2016 and was characterized by

a mean temperature of 11.8°C (mean daily max. of 17.6°C and mean daily min of 7.3°C), mean daily maximum vapor pressure deficit (VPD) of 0.92 kPA and total precipitation of 918 mm.

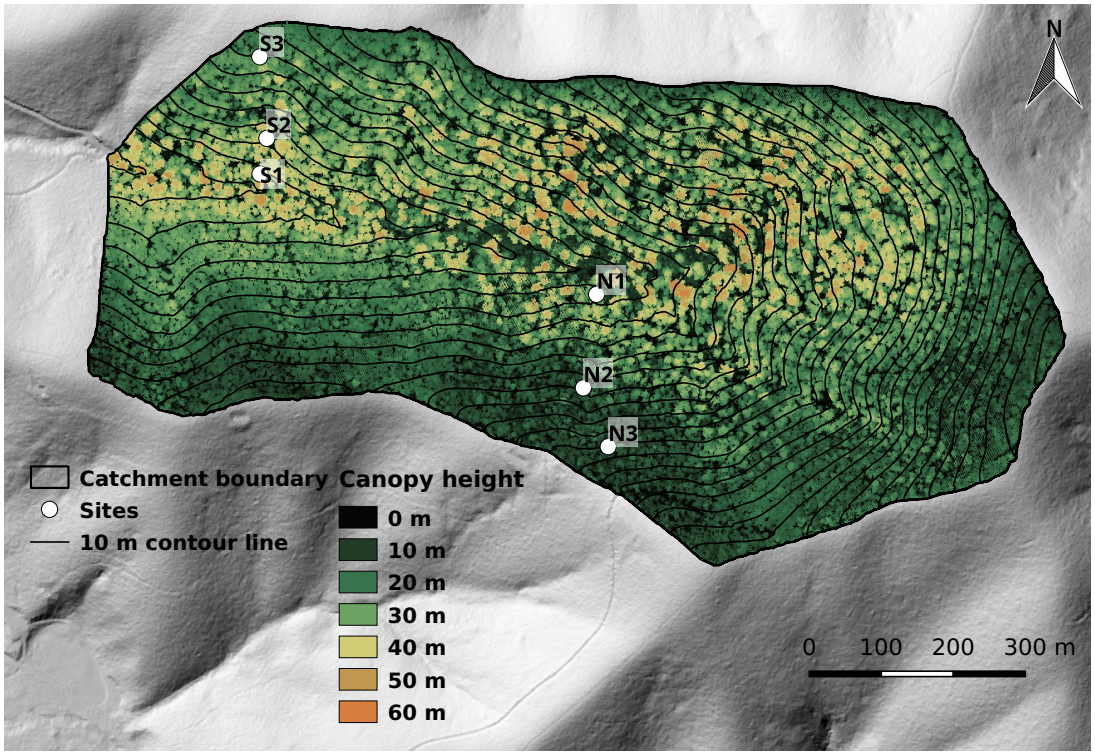

Figure 2.1: Map of the research sites with 1m canopy height model derived from LiDAR imposed on analytical hillshade.

Sap flux and relevant micro-climatic variables were measured on individual plots, complemented by nearby climate stations. Soil moisture was measured at each plot in 10, 30, 50, 75 and 100 cm depth where possible (EC-5, Decagon Devices Inc., Pullman, WA, USA), incoming short-wave radiation at a height of 1.5 m (SP-110, Apogee Instruments Inc., Logan, UT, USA), and sap flux at a height of 1.3 m. Soil moisture sensors were calibrated with the respective site-specific soils. One weather station monitoring sub-canopy micro-climate was set-up at each hillslope and in a clearing close-by (∼4 km from site). All weather stations measured solar radiation (SP-110, Apogee Instruments Inc., Logan, UT,

USA), air temperature and relative humidity (CS215, Campbell Scientific Inc., Logan, UT, USA) as well as wind speed (014A, Met One Instruments Inc., Grants Pass, OR, USA). Two rain gauges (TB3, Hydrological Services Pty. Ltd, Warwick Farm, NSW, Australia), logging at 5 minute intervals, were installed at high and low elevation to account for orographic rainfall gradients (1-4 km away from the site).

Terrain analysis, calculation of TWI and the height above nearest drainage (HAND) (Nobre et al. 2011; Renno et al. 2008) were done on a 20 × 20 m DEM using QGIS and SAGA GIS.

Watershed history

Spatial datasets of fire history and logging activities provided by the Department of Environment, Land, Water and Planning (DWELP) were analyzed and no disturbance was recorded for the watershed. The watershed was in close proximity to water supply infrastructure of Melbourne Water and therefore fenced off to the public requiring keys to pass gates. Personal communication with Melbourne water confirmed that no disturbance to the watershed was known off. Lastly, visual inspections on ground did not reveal any evidence of ecological disturbances or anthropogenic management in the past decades.

2.2.2 Aridity index rasters

Aridity index rasters were generated following Nyman et al. (2014). Large scale, long-term (>20 years) spatial data sets of solar global horizontal irradiance (GHI, 5×5 km), solar direct normal irradiance (DNI, 5×5 km), air temperature (2.5×2.5 km), precipitation (2.5×2.5 km) and cloud fraction (10×10 km) available from the Bureau of Meteorology (BoM) were used to calculate the aridity index (AI) by

$$AI = R_n/\lambda P \tag{2.1}$$

where R_n is the net radiation, P the precipitation and λ the latent heat of vaporisation, which was calculated as a function of air temperature. Net radiation was calculated by

$$R_n = R_s + R_{ld} - R_{lu} \tag{2.2}$$

where R_s is the net shortwave radiation, R_{ld} the incoming long-wave radiation and R_{lu} the outgoing long-wave radiation. The net shortwave radiation was calculated from

$$R_s = (1 - \alpha_s)\ R_g\ S_{TD} \tag{2.3}$$

Where α_s is the surface albedo, $R - g$ is the global incoming shortwave radiation (GHI) and S_{TD} the topographic downscaling factor. Surface albedo was calculated as a function of LAI, which in turn was assigned spatially by using four board vegetation categories based on the ecological vegetation classification (EVC). DHI was calculated as a function of DNI and solar elevation and the diffuse radiation defined as the difference between GHI and DHI. The topographic downscaling factor (S_{TD}) accounts for effects of topographic shading, slope and aspect and was calculated using Solar Analyst (ArcGIS, ESRI) for each 20×20 m grid cell by

$$S_{TD} = (DIR_m + DIFF_m)/R_{tile} \tag{2.4}$$

Where DIR_m and $DIFF_m$ are the Solar Analyst outputs for each 20×20m cell and R_{tile} is the average incoming shortwave radiation for the entire 5×5 km tile. The incoming longwave radiation (R_{ld}) was calculated as a function of topographically adjusted temperature using the SRAD model (Moore et al. 1993). Outgoing longwave radiation was calculated as a function of atmospheric emissivity, using the cloud fraction, temperature (Crawford and Duchon 1999) and sky view factor (ArcGIS).

2.2.3 Plant Area Index

Cover photography was used to determine the plant area index (PAI) that combines leaf and other plant surfaces (trunks, branches, etc.). Five upwards-facing pictures (plot center and 10 m in each cardinal direction) at 1.5 m height were taken at each plot during spring and autumn and the mean PAI calculated. The images were analyzed using the method outlined in Macfarlane et al. (2014) and Macfarlane et al. (2007). Briefly, the blue channel of RAW images was contrast stretched and converted to JPG using DHP RAW2JPG Software (available at https://supersites.tern.org.au/publications-and-resources/resources-for-supersiteusers). Thereafter, PAI was calculated using the Leaf Area Index DCP-313 Image Analysis Software (available at https://supersites.tern.org.au/publications-and-resources/resources-for-supersiteusers). Crown cover (fc) was calculated as

$$f_c = 1 - \frac{g_L}{P_T} \tag{2.5}$$

and foliage cover (ff) as

$$f_f = 1 - \frac{g_T}{P_T} \tag{2.6}$$

where g_L is the number of pixels with large gaps between crowns, g_T the total number of gap pixels and P_T the total number of pixels. Crown porosity (c_p) was then defined as

$$c_p = 1 - \frac{f_c}{f_f} \tag{2.7}$$

Finally, PAI was calculated from

$$PAI = -f_c \frac{ln(c_p)}{k} \tag{2.8}$$

where k is the extinction coefficient set to 0.5.

2.2.4 Plot inventories

Within each plot all trees with a diameter at breast-height (DBH) of >5 cm were tagged, the species identified, DBH and height measured. Diameters were measured using a tape

measure and heights were recorded with a range finder (Forestry Pro, Nikon Vision Co., Ltd, Tokyo, Japan). Contribution of woody plants with DBH <5 cm was assessed in four randomly selected subplots with 2 m radius at each plot. Bark thickness and sapwood cores were taken from a total 144 of the 363 trees in the plots. Sapwood cores were collected using a 5 mm increment corer (Haglöf, Inc., Långsele, Sweden) and the sapwood thickness was measured after staining with Methyl-Orange. Sapwood area (A_S) was calculated using the mean sapwood depth and the diameter under bark (DBH minus bark thickness). An empirical relationship between DBH and A_S (R^2 : 0.75, data not shown) was used to derive A_S of trees that were not cored. All deformed trees and trees >40 cm DBH were cored in order to minimize errors estimating A_S from DBH.

Outlier treatment

Preliminary analysis indicated a strong correlation between A_S and plant area index (PAI), except for plot S2, which had a much lower ratio of A_S to PAI (data not shown). Increasing the radius of plot S2 to 17 m would add three large trees (62.9, 74.1 and 102.4 cm DBH) located within 1 m of the Plot S2 boundary, increasing A_S from 4.0 $m^2\ ha^{-1}$ to 6.70 $m^2\ ha^{-1}$ and making the ratio of A_S to PAI consistent with the other five plots (Tab. 3.3). The crowns of these three large trees would have influenced the PAI estimates for this plot but using the original 15 m radius plot, their large sapwood areas were excluded. To further assess whether the initial measurement of A_S in plot S2 was an outlier, LiDAR derived vegetation height and density indices (80th percentile return height and percentage of returns above 1.5 m) were used to build an empirical sapwood area model with the data of remaining plots ($r = 0.96$, $p = 0.0089$, data not shown). Modeled A_S for plot S2 was 7.25 $m^2\ ha^{-1}$ and 7.10 ± 0.86 $m^2\ ha^{-1}$ for 10 pixels with similar landscape positions throughout the catchment (AI: 1.1-1.3, TWI: 6.5-7.5, HAND: 5-15 m). In relation to

the modeled A_S the initial value was identified as a clear outlier (Studentized residual: 4.34, Bonferroni p-value: 0.14) compared to the adjusted A_S (Studentized residual: 1.01, Bonferroni p-value: 1.0). Hence, I believe the use of A_S derived from the 17 m radius plot S2 for further analysis is justified.

2.2.5 Sap flux measurements

Sap velocity (v_{sap}) was measured on 5 to 6 trees per plot at a 30 min frequency using the compensation heat pulse (CHP) method (The Heatpulser, Edwards Industries, Taupo, New Zealand) and the heat ratio method (SFM1, ICT International, Armidale, Australia). The heat ratio method (HRM) was mainly used to measure smaller, suppressed trees, as it is more reliable measuring lower transpiration rates (Becker 1998; Burgess et al. 2001). Sap velocity of each tree was measured at 2 to 4 locations in the sapwood, depending on the sapwood depth, to account for radial velocity differences. For the CHP sensors, measured v_{sap} was corrected for variations in probe spacing, gas and water fractions of the sapwood (Edwards and Warwick 1984). For the HRM sensors, the measurements and methods described by Burgess et al. (2001) were used. Sapwood around each sensor was sampled at the end of the monitoring period and a probe-specific wound size correction (5.6 mm mean wound size) for each probe was applied (Swanson and Whitfield 1981; Burgess et al. 2001).

The zero-flow baseline was set by assuming v_{sap} to be zero at night during a prolonged wet winter period with relative humidity close to 100% (Benyon 1999). Average v_{sap} of each tree was multiplied by it's sapwood area to derive sap flux volume (E_{sap}). Data gaps were linearly interpolated for small gaps missing only one measurement. Larger gaps were filled using an empirical model build using data from the sensor with the highest correlation coefficient (Pearson's r >0.85, 9% of gap-filling in total). Most data-gaps resulted from drained batteries due to solar panel shading or broken probes, which were usually replaced

within a fortnight.

Sap flux was scaled from individual tree level to plot-level using the Random Forests model (Pedregosa et al. 2011; Breiman 2001). The model was trained using all 36 sap flux sample trees. E_{sap} and v_{sap} were predicted as a function of climate variables measured at the reference weather station (incoming shortwave radiation, vapor pressure deficit, air temperature, wind speed), soil moisture at each site, vegetation structure (tree height, species, sapwood area) and landscape position (TWI, northness, HAND, see Tab. 3.3) ($R^2 : 0.99$). Plot-scale transpiration was calculated by summing the modeled sap fluxes of every tree in the plot. Plot-scale v_{sap} was calculated by dividing the total sap flux estimated using the Random Forest model by the total plot sapwood area. Hence, mean v_{sap} is weighted according to the sapwood area contribution of each tree. The same Random Forests model was used to infer the main drivers of v_{sap} patterns at 30 minute, daily and monthly temporal resolution.

2.3 Results

2.3.1 Forest structure

Stand characteristics

While tree size increased downslope at both transects, trees on the southern aspect were generally larger than on the north-facing slope (Tab. 3.3). Stand densities on the other hand, tended to be higher on the northern aspects, increasing towards the mid-slope (N2) and ridge plot (N3). At the south-facing transect, the gully plot (S1) had the highest stand density, followed by the ridge plot (S3) and the mid-slope plot (S2). The driest sites (N3 and N2) were dominated by small trees with size distributions peaking at around 10 cm DBH. All other plots peaked between 10-20 cm, but in contrast to the dry sites also had

several big trees (Fig. 2.2).

Basal area (A_B) was generally larger on the south-facing slope compared to the northern aspect (Table. 3.3). Contribution of woody understory plants (1-5 cm DBH) was <1 $m^2\ ha^{-1}$ for all plots but S3, where small woody plants accounted for a basal area of 3 $m^2\ ha^{-1}$. On the north-facing slope, the gully plot (N1) had the largest A_B, followed by the ridge (N3) and the mid-slope (N2). The ridge plot (S3) carried the largest A_B on the southern aspect, followed by the gully (S1) and the mid-slope plot (S2) (Tab. 3.3).

Plant area index (PAI) and A_S increased in downslope direction on both aspects and tended to be larger on the southern aspect compared to the northern aspect, although the rate of increase varied between the transects (Tab. 3.3). PAI increased at a much larger rate on the north-facing transect compared to the south-facing slope (ΔPAI 1.9 vs 0.9 $m^2\ m^{-2}$). In contrast, gains in A_S along the transects were much larger on the southern aspect compared to the north-facing transect (ΔA_S 3.68 vs 1.14 $m^2\ ha^{-1}$).

However, A_S differences were not as large as the variations in tree size distribution would suggest and the slope of the cumulative A_S to cumulative A_B ratio equilibrates at a similar gradient for all plots (Fig. 2.2). Even-though, big trees made up large fractions of A_S of the wetter sites (S1, S2, S3 and N1), the curves mainly diverge in the first square meter of plot basal area. Thus, A_S variations between plots mainly originate from trees with smallest diameter at each plot.

In general, drainage position (HAND) could largely explain variations of PAI ($R^2 : 0.76$) and maximum tree height ($R^2 : 0.72$) , whereas ~90% of A_B variations could be explained by slope orientation (northness). No significant relation between A_S, northness, HAND and TWI was found.

Table 2.1: Vegetation and terrain properties at each plot; N and S indicating slope aspect, numbers indicating slope position, increasing from gully to ridge. A_P: plant area, A_B: basal area, A_S: sapwood area, PAI: plant area index, DBH: diameter at breast-height, TWI: topographic wetness index, HAND: height above nearest drainage, AI: aridity index, P: annual precipitation (2015-03-01 to 2016-02-29), E_{sap}: annual sap flux (2015-03-01 to 2016-02-29).

Site	N1	N2	N3	S1	S2[1]	S3
elevation (m)	354	408	451	306	322	368
TWI ($-$)	7.99	6.44	4.91	7.96	6.94	5.00
AI ($-$)	1.75	1.78	1.86	1.47	1.19	1.32
HAND (m)	3.0	36.4	63.5	1.6	9.1	51.5
soil depth (m)	>3.0	0.8	0.5	>3.0	2.0	0.6
P (mm)	840	855	866	826	831	845
E_{sap} (mm)	431	293	313	791	606	391
PAI ($m^2\ m^{-2}$)	3.5	2.1	1.6	3.6	3.0	2.7
A_B ($m^2\ ha^{-1}$)	32.3	23.1	26.4	38.6	35.7	40.5
A_S ($m^2\ ha^{-1}$)	6.5	5.6	5.4	9.6	6.7	5.9
$A_S : A_P$ ratio ($cm^2\ m^{-2}$)	1.9	2.7	3.3	2.7	2.3	2.2
Eucalypt						
density ($stems\ ha^{-1}$)	254.6	1174.2	1216.7	155.6	353.7	509.3
mean DBH (cm)	32.8	13.5	13.5	42.7	31.5	25.5
mean height (m)	21.8	10.0	8.1	27.8	22.0	16.7
A_B ($m^2\ ha^{-1}$)	28.9	23.0	26.4	32.6	34.5	40.2
A_S ($m^2\ ha^{-1}$)	4.7	5.5	5.3	4.7	6.4	5.7
Non-Eucalypt						
density ($stems\ ha^{-1}$)	424.4	42.4	-	792.2	127.3	127.3
mean DBH (cm)	9.4	5.4	-	9.3	8.0	5.8
mean height (m)	6.8	4.5	-	12.0	6.4	5.2
A_B ($m^2\ ha^{-1}$)	3.4	0.1	-	6.0	0.7	0.3
A_S ($m^2\ ha^{-1}$)	1.8	0.06	-	4.9	0.3	0.2

[1] adjusted $17m$ radius plot

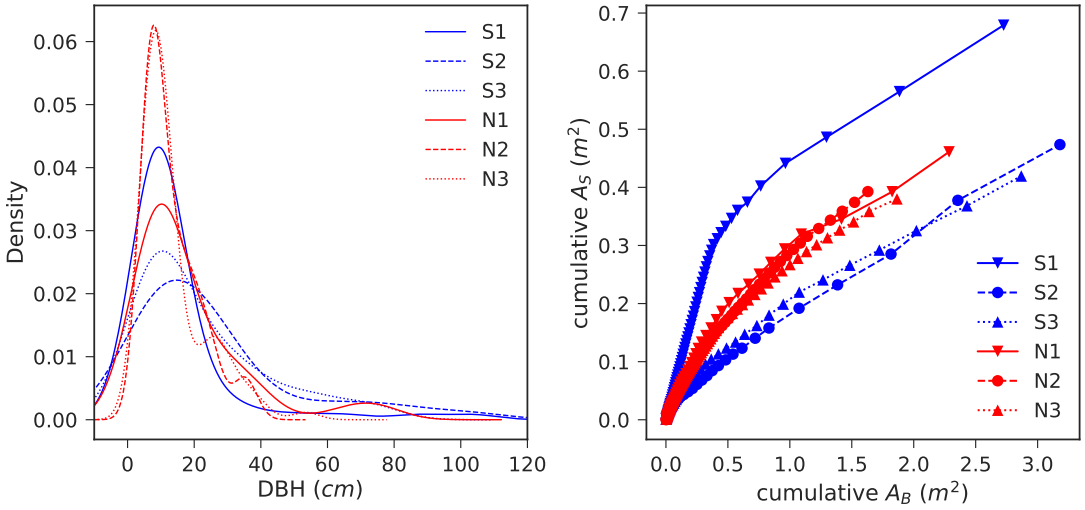

Figure 2.2: Left panel: Kernel density estimate of the DBH distribution for each plot. Right panel: Relationship of cumulative sapwood area to cumulative basal area at each plot. Each point corresponds to a tree and trees are sorted by DBH. Plot S2 with adjusted 17m radius.

Species distribution

The overstory was dominated by three eucalypt species: *Eucalyptus cypellocarpa* (mean DBH 35.0 cm) and the stringybarks *E. baxteri* and *E. obliqua* (mean DBH 21.6 cm), while *E. radiata* and *E. sieberi* tended to be smaller (mean DBH 16.4 cm and 10.7 cm, respectively). *E. radiata* and *E. sieberi* were mainly abundant at the drier sites (N3, N2), where only a few *E. cypellocarpa* were present. The stringybarks were most common at plots S3 and S2, but also accounted for roughly a quarter of encountered species at plot N1 and N3 (Fig. 2.3).

Woody understory species were usually small in size with exception of *Acacia melanoxylon* and *Pomaderris aspera*, which often reached 10 m height. Most of the woody understory species were present on wetter plots (S1, N1, S2, S3). *P. aspera* was almost exclusively abundant in (south-facing) gully positions.

A_B contribution was dominated by the eucalypts at all plots (Tab. 3.3 & Fig. 2.3).

At plots N3 and N2 *E. radiata* made up most of A_B (68% and 58%). The stringybarks dominated plot S3 , while *E. cypellocarpa* was the tallest species and contributed over-proportionally to plot level A_B at the remaining plots.

The species-specific A_S patterns were similar to the A_B patterns. At plot N3 and N2, A_S was mainly attributed to *E. radiata* and to a lesser degree to *E. sieberi* and the stringybarks. *E. cypellocarpa* accounted for >40% of A_S at all other plots. Contribution of tall understory species was generally very low, with exception of the gully plots and especially plot S1, where half of A_S was attributed to *P. aspera* (Fig 2.3).

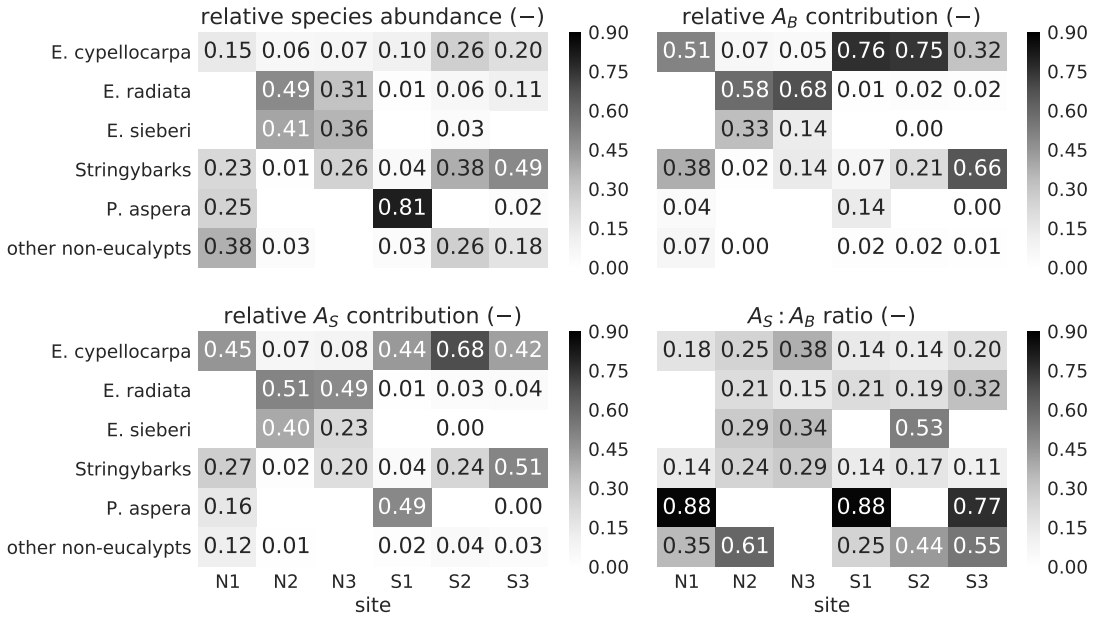

Figure 2.3: Relative proportion of species present at each plot(top-left) and their corresponding basal area contribution (top-right), sapwood area contribution (bottom-left) and sapwood area to basal area ratio (bottom-right).

Typically, the $A_S : A_B$ ratio is expected to be generally larger for small trees as the 'heartwood core' is smaller compared of the 'sapwood ring'. This assumption generally held as the $A_S : A_B$ ratios at plots with larger trees (S1, S2 and N1) were generally lower. However, the cored *P. aspera* were lacking a hardwood core, which resulted in an

over-proportional high ratio of $A_S : A_B$ ratio for this species (Fig 2.3).

2.3.2 Spatio-temporal transpiration patterns

Annual and seasonal dynamics of sap velocity and transpiration rates

Mean E_{sap} gradually increased from ridge to gully on the southern aspect (Fig. 2.4). On the north-facing transect, mean E_{sap} was highest at N1 and similar low at plots N2 and N3. Overall, mean v_{sap} and E_{sap} where higher on the southern aspects compared with the north-facing plots. Annual E_{sap} differed markedly with landscape position (Tab. 3.3). E_{sap} on the north-facing transect was 431 mm at N1, 293 mm at N2 and 313 mm at N3, respectively. Differences between plots were larger on the southern aspect and followed a stronger trend in relation to hillslope position. E_{sap} on the south-facing transect reached 791 mm at S1 and decreased from 606 mm at S2 to 391 mm at S3. Mean annual v_{sap} was relatively constant between plots on the northern aspect, while the ridge plot on the southern transect (S3) had lower v_{sap} than the remaining plots (Fig. 2.4).

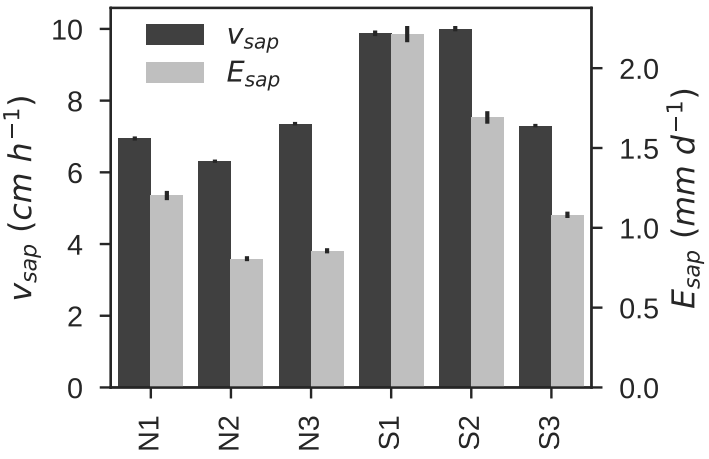

Figure 2.4: Mean annual sap velocity v_{sap} and transpiration rates E_{sap} with standard error of the mean.

On a monthly basis, considerable variations of v_{sap} were observed between plots (Fig. 2.5).

v_{sap} was higher on south than north-facing slopes, with particularly high peaks during mid-day on S1 and S2. In winter, site-specific variations of v_{sap} diminished and almost collapsed into an identical diurnal pattern, with the exception of plot N2, where peaks were still lower compared with all other plots. From October onwards, v_{sap} started to increase over-proportionally at S1 and S2 compared with the remaining plots. Baseline v_{sap} was reached around 8 pm from May to July and v_{sap} picked up again at 7 am. In contrast, from November to February the baseline velocity was only sustained briefly around 5 am, especially at S1 and S2. In general, night-time v_{sap} lows were more stable and sustained longer at all plots during winter compared to the summer months. During the winter months differences in v_{sap} between plots were relatively small, and consequently E_{sap} totals between sites mainly diverged during spring, summer and autumn.

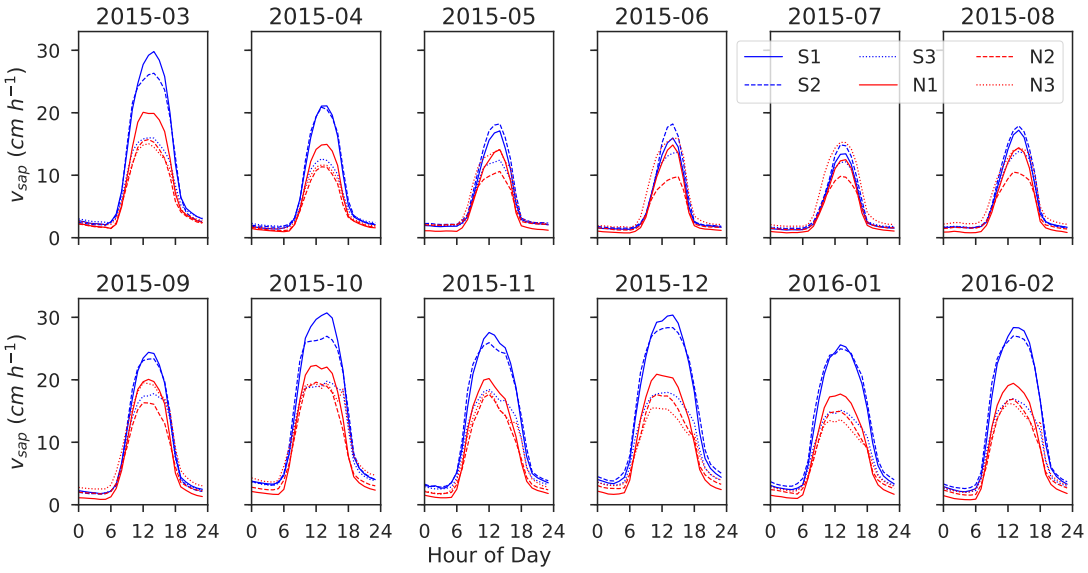

Figure 2.5: Monthly mean diurnal sap velocity (v_{sap}) patterns. Hourly v_{sap} was averaged for each hour across all days within each month at every individual site. Displayed curves are based on the average monthly 24 data points at each site.

Water availability

v_{sap} response to VPD and SWC was strongly influenced by topographic position (Fig. 2.6). At low SWC, v_{sap} was less responsive to VPD on sites with shallow soils (N1, N2, S3), compared with the remaining plots. Plot N3 showed a particularly dynamic response to SWC fluctuations. v_{sap} was very high at high SWC, even at low VPD, but at low SWC v_{sap} barely responded to VPD increases past 0.5 kPA (Fig. 2.6). Differences between high and low SWC were less pronounced for the gully plots and S2, indicating less water limitation on v_{sap}.

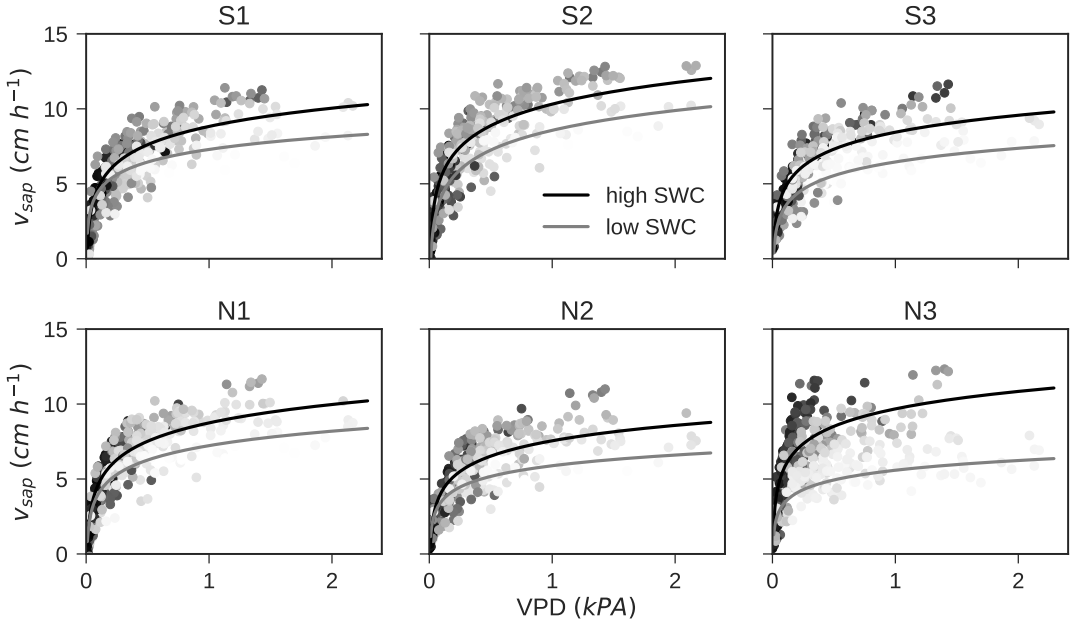

Figure 2.6: Site-specific daily mean sap velocity patterns in relation to VPD and SWC. Dark colors refer to high soil moisture values and light colors to dry soils, with the minimum SWC=0.1 and maximum SWC=0.35 in color coding across all plots. Fitted regression lines are for high (SWC>50th percentile) and low (SWC<10th percentile) soil moisture conditions.

SWC was generally lower (top 1 m of soil profile) and more responsive to rainfall events closer to the ridges, as well as at N2 (Fig. 2.7), where soils were shallower than 1 m (Tab. 3.3). Consequently, water-limitation affected those plots more than the wetter plots

(S1, S2, N1). The temporal patterns of transpiration limitation can be illustrated by plotting the transpiration-atmosphere-coupling (TAC) (Barnard et al. 2017) over time. TAC is defined as the correlation coefficient (R^2) between day-time VPD and v_{sap} for each day. There are generally three scenarios when TAC tends to be low:

1. when VPD is close to zero for the entire day
2. when there is a sharp contrast within one day caused by overcast and clear sky periods
3. when VPD is high and trees can't keep up with v_{sap} rates, especially in combination with low SWC

Scenario 1 and 2 are assumed to occur simultaneously at all plots given the proximity and hence Scenario 3 will cause TAC variations between sites.

TAC tended to be weakest at the 2 ridge plots (N3, S3) and plot N2, as indicated by the number of days with TAC<0.5 (Fig. 2.7). Mean TAC values for the north-facing transect (N1: 0.73, N2: 0.70, N3: 0.64) were lower than the TAC at the southern aspects (S1: 0.77, S2: 0.73, S3: 0.68) and declined towards the ridges at both hillslopes. Plots N3, N2 and S3 were most susceptible to SWC limitations due to shallower soils and presumably less plant-available water. Particularly in late summer, the wetter plots (S1, S2 and N1) could sustain higher v_{sap} and hence a larger TAC (Fig. 2.5 & Fig. 2.7). Simultaneous drops of TAC at all sites points towards above mentioned scenarios 1 and 2, whereas water-limitation tended to cause a more differential TAC response with strong decreases at drier ridge-top sites and less response at the more buffered gully plots.

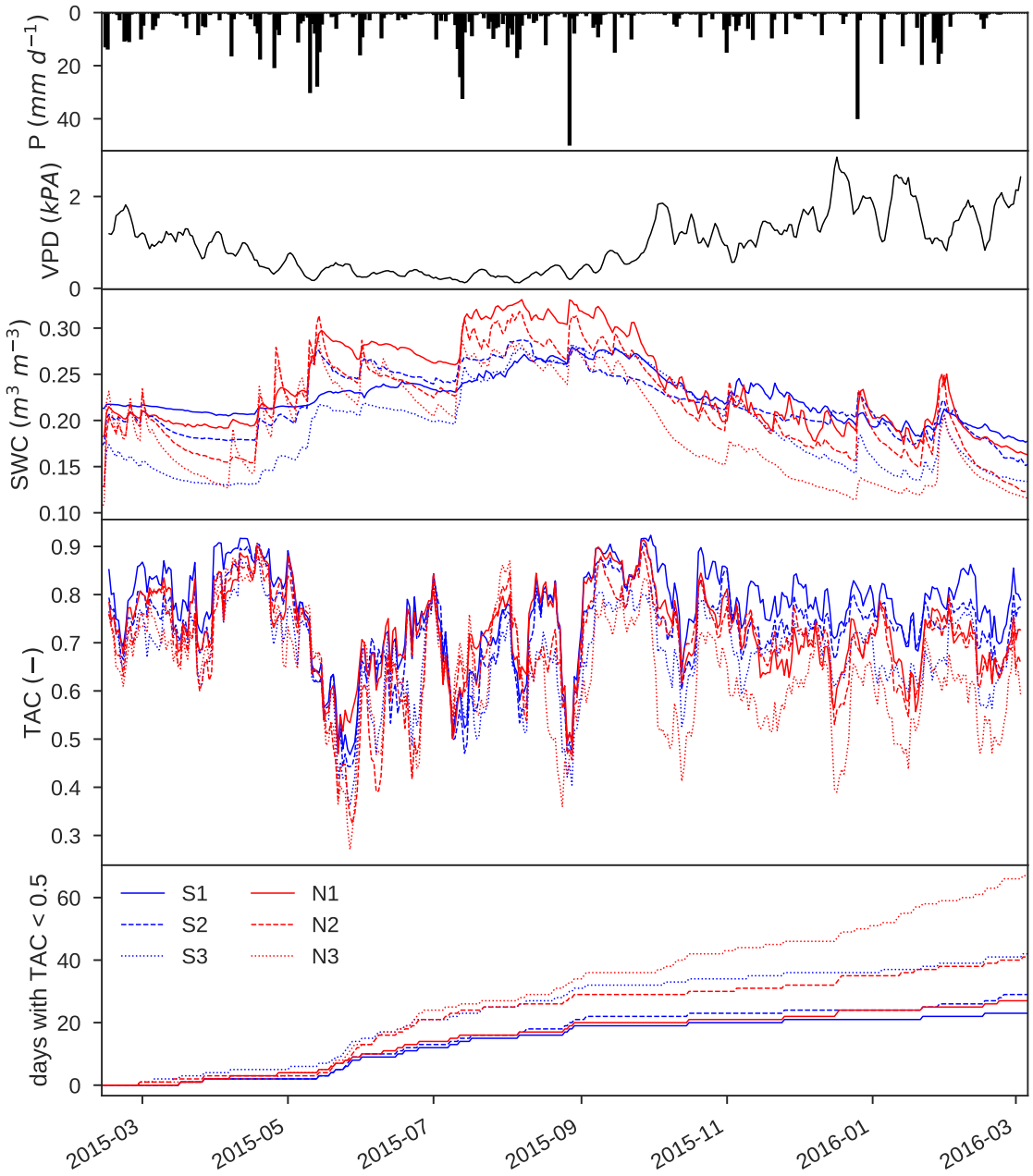

Figure 2.7: Time series of precipitation (top panel), 7-day running mean of maximum daily VPD (2nd panel), mean daily profile SWC (3rd panel), 7-day running mean of the correlation coefficient between day-time (SWR >10 $W\ m^{-2}$) VPD and sap flux for each day (TAC) (4th panel) and cumulative number of days with a TAC <0.5. Only day-time (SWR>10 $W\ m^{-2}$) v_{sap} was included in the analysis.

Dominant versus suppressed trees

In addition to the plot-to-plot variability, within plot v_{sap} variations were characterized by two different regimes in relation to slope orientation and vegetation structure (Fig. 2.9). On the drier (upper) north-facing hillslope, plots N2 and N3 consisted of one relatively open canopy strata with only a few smaller eucalypt trees in the understory (Fig. 2.2). Consequently, sub-canopy radiation was relative high due to sparse canopy cover and equatorial-facing aspects (Fig. 2.8). Plots on the (lower) southern aspect were characterized by few tall eucalypt trees and a second strata of smaller eucalypts and dense cover of *P. aspera* and/or tree ferns. On those polar-facing plots with more vegetation cover, light interception was higher, especially at lower solar altitudes when radiation has a longer path length through upslope canopy during much of the day (Fig. 2.8).

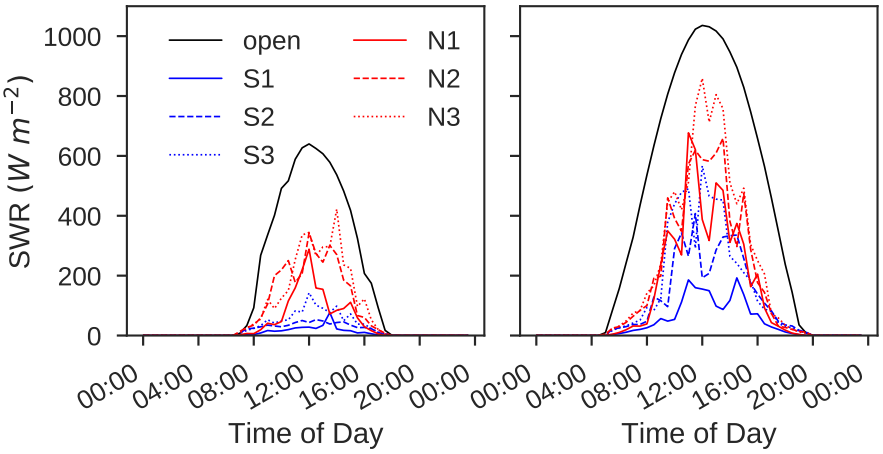

Figure 2.8: Shortwave radiation (SWR) at the open weather station and sub-canopy radiation measured at each plot at 1.5m height in winter (20.08.2015, left panel) and summer (09.01.2016, right panel).

As a result of contrasting sub-canopy radiation patterns, v_{sap} differed between trees at different canopy classes within plots as well as between the same plot locations on contrasting slopes. On the north-facing slope the v_{sap} dynamics between over- and understory trees

were similar and the v_{sap} difference was relative constant throughout the year. However, during the summer months, the v_{sap} of understory trees was less dynamic, indicating stronger water-limitation potentially due to shallower rooting depth. In contrast, v_{sap} of the sub-canopy trees on the southern aspect was close to zero during winter, most likely as a result of low light conditions. v_{sap} increased towards summer but v_{sap} differences between over and understory trees increased as well (Fig. 2.8).

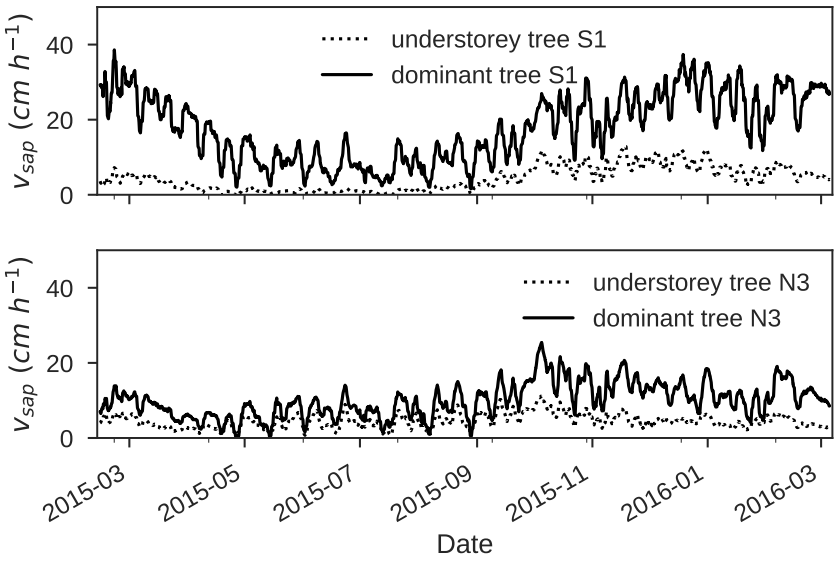

Figure 2.9: 5-day running mean of a understory and dominant tree at the south gully and north ridge plot.

v_{sap} of the dominant trees at plot S1 peaked during the summer months and was largely energy limited indicated by a strong correlation between incoming short-wave radiation (SWR) and v_{sap} for instrumented dominant trees (linear regression with R^2 of 0.74 - 0.82, data not shown). At site N3 the v_{sap} peak occurred in late spring and then v_{sap} declined throughout summer, indicating water limitation during the summer months. Consequently, the correlation between SWR and v_{sap} for dominant trees was lower than at S1 (R^2 between 0.38 - 0.51). The contrast between sites is even larger for the understory trees. At S1 SWR

explained between 69 and 73 % of the understory v_{sap} variability, whereas at N3 only 20 - 36% were explained.

Stem growth patterns also revealed differences between dominant and suppressed trees in relation to landscape position (Fig. 2.10). On the dry sites (N3 and N2), little stem growth and differences between dominant and suppressed trees were observed. However, basal area increments (BAI) increased as well as differences between dominant and suppressed trees with decreasing water-limitation towards the gully plots. Similar to observed transpiration patterns, stem growth patterns from ridge to gully were more gradual on the southern aspect, whereas an abrupt decrease was observed from gully to mid-slope plot on the north-facing transect.

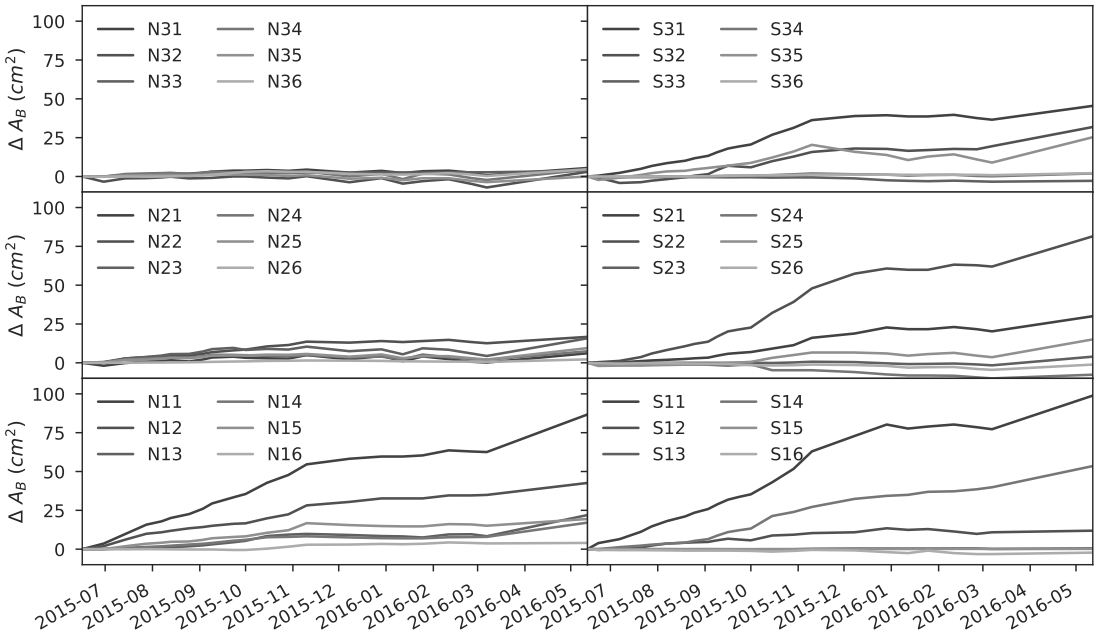

Figure 2.10: Basal area (A_B) change measured at six trees per site using band dendrometers. Left panels: northern aspect, right panels: southern aspects. top row: ridge plots, middle row: mid-slope plots, bottom row: gully plots. The two lowest numbers at each plot represent dominant trees and increasing numbers smaller trees.

Species response

On top of the heterogeneous vegetation structure, different species composition between sites and their transpiration responses add another layer of complexity. Figure 2.11 illustrates the diurnal v_{sap} patterns of each plot grouped by tree species on three days with contrasting conditions (high demand & low SWC, high demand & high SWC, low demand & high SWC).

All species could not sustain high enough v_{sap} rates to keep up with atmospheric demand and closed their stomata during high demand days with relatively dry soils (Fig. 2.11, left column). *E. cypellocarpa*, *E. radiata* and *E. sieberi* posed nearly identical v_{sap} response with a steep increase until 9:00, followed by a mid-day depression around 12:00 and a small peak at 16:00. The Stringybarks generally had lower v_{sap} and lacked the second peak around 16:00. However, most of the instrumented stringybarks at plots N1, S2, S3 were dominated by tall *E. cypellocarpa*, which might explain the generally lower v_{sap} response. Likewise, v_{sap} limitations were evident for *P. aspera*, which is exclusively abundant in the wet gully positions and thus shaded by tall eucalypt trees. At plot-scale, v_{sap} limitation was observed at all sites. The wetter sites generally sustained higher v_{sap} rates, but were characterized by strong mid-day depressions as well.

v_{sap} was less limited during the course of the day, when SWC was higher during days with high VPD and SWR, (Fig. 2.11, middle column). Again, *E. cypellocarpa*, *E. radiata* and *E. sieberi* were able to sustain high v_{sap} almost until mid-day before steadily declining throughout the afternoon. However, night-time v_{sap} was higher for *E. radiata* and *E. sieberi*. The Stringybarks did not show any sign of limitation as v_{sap} closely tracked SWR, but only reached half the peak velocity compared to the other eucalypts. Night-time v_{sap} was highest at plot N3, where most of the instrumented *E. radiata* were abundant, potentially replenishing stem volume capacitance. v_{sap} peaked mid-day at all plots beside

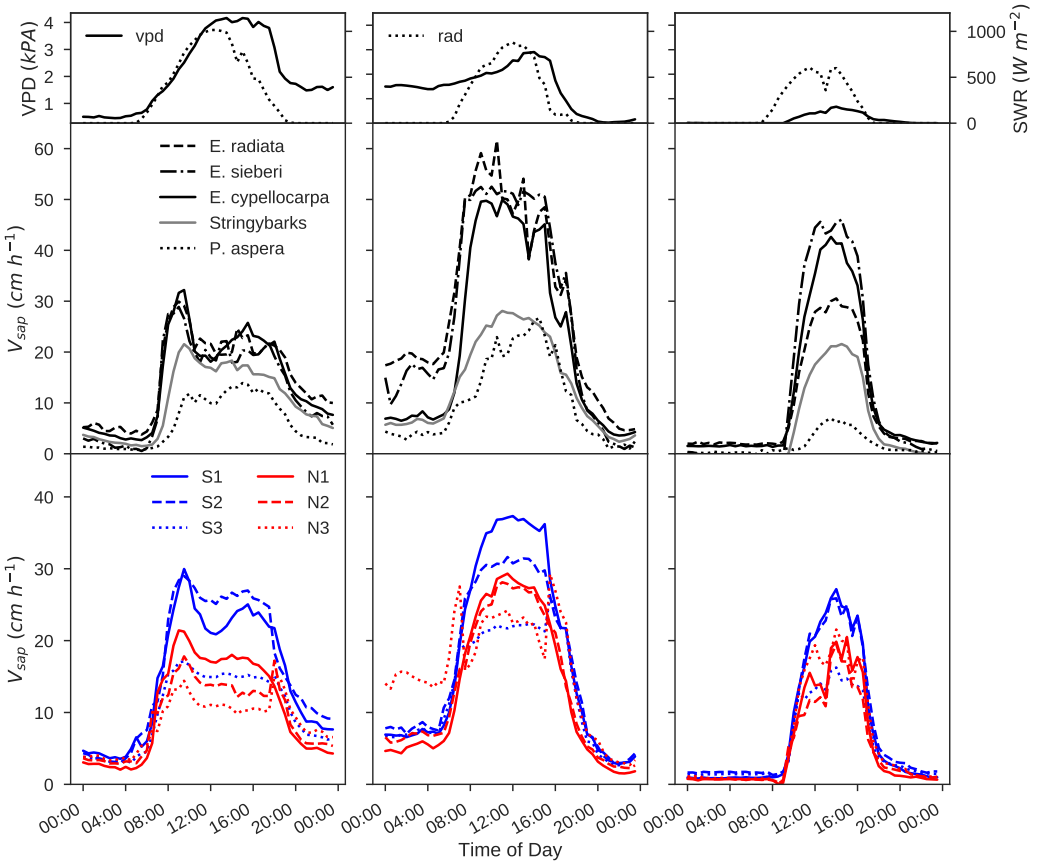

Figure 2.11: Diurnal sap velocity response of only the dominant trees (with exception of *P. aspera*) grouped by species (middle panel) and plots (bottom panel) on days with contrasting conditions (top panels). Left column: high demand day with low SWC (13.1.2016), middle column: high demand day with high SWC (06.10.2015), right: low demand day with high SWC (29.04.2015).

the ridge plots (N3 and S3), where peaks occurred around 16:00. v_{sap} of *P. aspera* was more closely related to VPD than SWR and peaked later compared to the Stringybarks, but almost reached the same peak velocity.

The mid-day depressions subsided in late autumn (Fig. 2.11, right panel), when SWC was high and atmospheric forcing low. Only *E. radiata* and *E. sieberi* responded slightly to

the overcast mid-day. However, during low demand conditions *E. radiata* did not reach the same v_{sap} levels as *E. cypellocarpa* and *E. sieberi*. The Stringybarks again transpired at lower v_{sap} compared to the other eucalypts. *P. aspera* poses very low v_{sap} rates, presumably due to low light conditions in the understory on the southern aspects. At plot-level, S1 and S2 did not respond to the short overcast period, whereas all other plot showed a v_{sap} depression during the overcast period. Besides the depression, v_{sap} rates were less variable between plots. N3 even had the highest peak v_{sap} on the northern aspect under this conditions.

2.3.3 Predicting transpiration patterns at different temporal scales

Drivers of v_{sap} and E_{sap} were identified using the feature importance of the Random Forest model trained at 30 minutes, daily and monthly intervals. On a sub-daily basis, v_{sap} patterns were mainly driven by climatic forcing (Fig. 2.12). Short-wave radiation (SWR) and VPD contributed the most to model performance with a relative feature importance of 0.44 and 0.15, respectively. A_S and tree height were the most important structural parameters at the 30 minute resolution. SWC only played a minor role, with a relative importance of only 0.07 and species, air temperature and all terrain properties were of negligible importance (<0.04). Structural parameters became more important when the temporal resolution was reduced to daily and monthly steps, mainly at the cost of SWR and VPD. Climatic forcing (SWR + VPD) decreased from 0.59 to 0.36 at daily and to 0.22 at monthly scale, while structural parameters (A_S + height) increased from 0.24, to 0.46 and 0.58. All other parameters only played minor roles at the daily and monthly scale (Fig. 2.12).

The E_{sap} model was more responsive towards A_S, as flow volumes are largely dependent on cross-section area of the transport medium. The importance of climatic forcing decreased

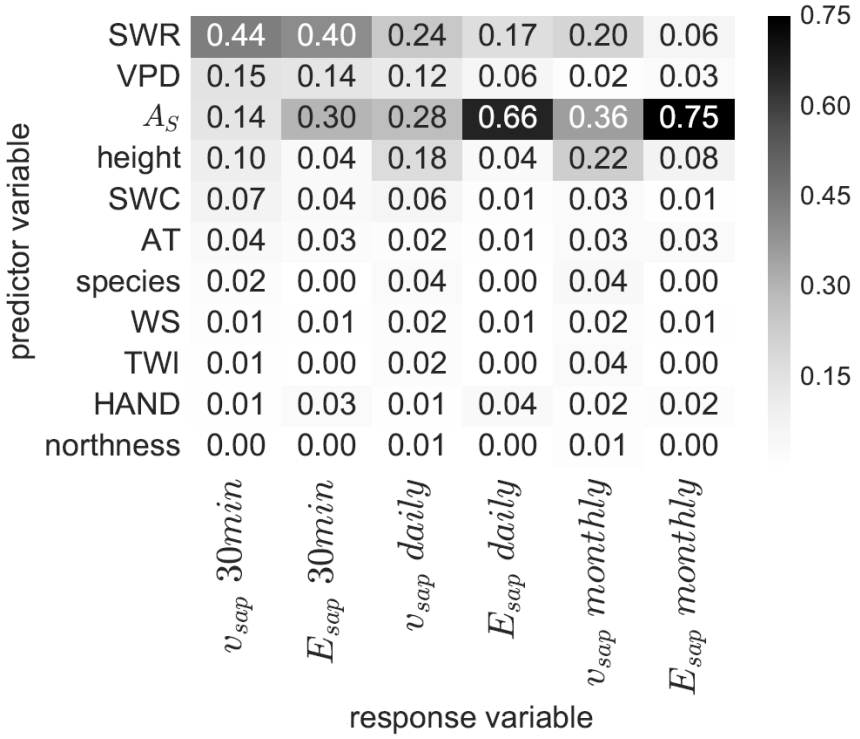

Figure 2.12: Importance of each individual predictor variable in predicting sap velocity (v_{sap}) and sap flux (E_{sap}) using the Random Forest model at 30 minute, daily and monthly temporal resolution.

further in the E_{sap} model compared to the v_{sap} model (from 0.54 to 0.09), while the contribution of A_S to model performance substantially increased from 0.30 at sub-daily to 0.75 at monthly resolution (Fig. 2.12).

The increasing prediction power of structural parameters and particularly A_S with longer temporal scales is further highlighted by the fact that solely A_S could explain 89% of the E_{sap} variation summed over the entire monitoring period (Fig. 2.13). Thus, using solely A_S as predictor for annual E_{sap} only 11% of information is lost, compared to more complex scaling procedures accounting for *vsap* variations due to climate and soil moisture patterns.

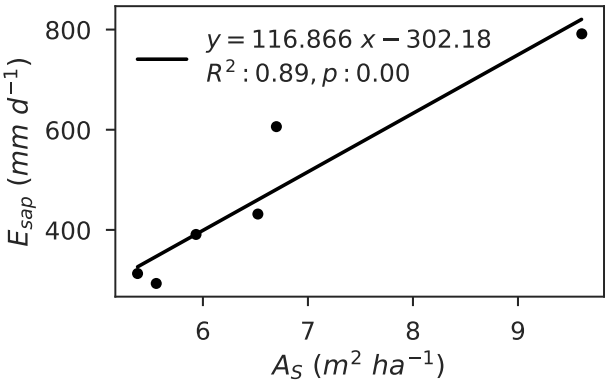

Figure 2.13: Transpiration totals at each plot (E_{sap}) in relation to sapwood area (A_S).

2.4 Discussion

This study demonstrated a clear link between spatial variations of forest structure and landscape position, which resulted in a substantial variation of soil moisture and sapwood area (A_S) patterns that markedly affected transpiration (E_{sap}) patterns. Further, A_S alone did explain ∼90% of modeled annual E_{sap}.

2.4.1 Forest structure

Forest productivity and thus biomass accumulation can be limited either by available energy or water. Energy-limitation has been observed in several eucalypt forests in south-east Australia (Griebel et al. 2017; Drew et al. 2008; Downes et al. 2009). Particularly in winter, low temperatures (Griebel et al. 2017; Drew et al. 2008; Downes et al. 2009) can impede forest growth. Further, low solar elevation during winter month results in less radiation input and might further limit growth, particularly for dominated trees (Griebel et al. 2017; Binkley et al. 2010). On the other hand, water availability can limit growth as well (Berner et al. 2017), particularly in areas with little summer precipitation. In complex terrain, gradients of energy and water availability can be observed over small extents due

to topographic controls on energy and moisture patterns (Nyman et al. 2015; Grimmond et al. 2000; Oliphant et al. 2006). Swetnam et al. (2017) illustrated strong topographic controls on above ground carbon, where highest forest carbon loads were observed at low topographic positions and polar-facing slopes.

In this study, short-wave radiation was higher on north-facing slopes due to slope orientation and hence, soil evaporation is expected to be higher, which in turn resulted in less water available for vegetation growth and pedogenesis. Usually shallower, poorer developed soils provide less nutrients and store less water (Geroy et al. 2011). As a result, contrasting growing environments emerged even over small spatial extent, where vegetation organization can vary strongly with landscape position due to differential resource access and allocation strategies.

On the south-facing transect, tree height, DBH, A_B, A_S and PAI were generally higher than for the corresponding drainage position the north-facing transect. At both transects, tree size and PAI increased in a downslope direction. Limited soil-water storage capacity and higher atmospheric demand would act to reduce the potential for water subsidies from upslope areas at the drier sites on mid and upper hillslope, where soils were shallow. Consequently, changes in tree size and PAI were more gradual on the southern aspect, whereas the reduction of tree size and PAI from the gully plot towards the ridge was more abrupt on the north-facing slope.

Observation of smaller tree sizes and stem growth rates at the driest sites are in agreement with other observations in eucalypt forests (Givnish et al. 2014; Pfautsch et al. 2016) and the safety vs. efficiency trade-off theory (Hacke et al. 2006). In drier, more water-limited environments, evergreen trees adapt by decreasing vessel size and increasing sapwood density (Poorter et al. 2010; Pfautsch et al. 2016). Smaller vessel diameters lead to a deceasing risk of cavitation, and reduced growth rates via lower canopy conductance, and

hence shorter trees (Poorter et al. 2010). Shorter trees and resulting shorter hydraulic path length in combination with tighter vessels provides more drought insurance at dry sites and under warming climates (McDowell and Allen 2015).

In addition, potentially differential fire frequencies due to contrasting fuel moisture regimes (Nyman et al. 2015) might also contribute to long-term structural differences. Smaller canopy extents of smaller trees permitted generally higher stand densities on the equatorial-facing slope and closer to the ridges (Tab. 3.3), with exception of the south gully plot (S1), where *P. aspera* replaced the smaller eucalypt trees in the mid-story (10-20 m height range) and was able to sustain extremely high densities in those low-light conditions.

The potentially lacking upslope water subsidies, might also explain the difference in overstory composition between plot N2, N3 and all other plots. *E. radiata* and *E. sieberi* make up most of the overstory on the drier plots (N3 and N2), whereas stringybarks and *E. cypellocarpa* were more abundant towards the wetter gully plots with deeper soils. These findings are in agreement with Ellis (1971), who attributed a species shift from *E. obliqua* to *E. sieberi* to *E. radiata* as a result of increasingly poorer, undeveloped soils.

P. aspera has an exceptionally high $A_S : A_B$ ratio (Fig. 2.3) and consequently A_S at S1 was considerably higher than at all other plots. Stand densities of *P. aspera* were high, because large A_S could be sustained due to favorable drainage position and low atmospheric demand during winter resulting in higher SWC throughout the year.

Several other studies investigated the effect of aridity on eucalypt forest structure, by relating inventory measurements along a rainfall gradient. Ellis and Hatton (2008) showed that LAI of eucalypt trees varied with aridity, and could be explained at 37 sites using only mean annual precipitation. Givnish et al. (2014) illustrated a strong correlation of eucalypt tree height to the ratio of precipitation to pan evaporation across 19 sites on well-drained convex slopes in Victoria. The effect of aspect, via alteration of the micro-climate, on forest

structure was investigated by Bale et al. (1998). They set-up 6 site pairs close to ridges and found differences in species composition, canopy cover and tree height between southern and northern aspects. However, the main effect of aspect was in separating the eucalypt and rainforest communities. The only other study - to our knowledge - systematically investigating the combined effect of aspect and drainage position in eucalypt forests is Pook and Moore (1966). In contrast to this study, they did not find significant differences between north and south slopes in tree density and A_B in dry sclerophyll forest on Black Mountain, Canberra, ACT, but noted a change in species composition between aspects.

2.4.2 Transpiration patterns

Surprisingly, mean annual plot v_{sap} was relatively uniform across most plots, despite large temporal site-to-site variability (Fig. 2.5). Moreover, clear E_{sap} patterns emerged when accounting for the spatial A_S variation. E_{sap} was generally higher on the south-facing transect than on the northern aspects (Fig. 2.4), while mean E_{sap} gradually decreased from gully towards the ridge on the south-facing hillslope. On the northern aspect highest mean E_{sap} was also observed at the gully plot, but the midslope (N2) and ridge plot (N3) had almost identically low E_{sap} means. In general, v_{sap} and E_{sap} patterns between plots N3 and N2 were fairly similar, as well as between N1 and S3, indicating that slope orientation had larger implications than drainage position in this environment.

v_{sap} had a pronounced seasonal cycle, as water limitation increased from spring through to summer, especially at the sites on shallow soils (N3 >N2 >S3), where SWC decreased fastest due to limited storage capacity (Fig. 2.7 & Tab.3.3). The gully plots N1 and S1 as well as plot S2 were buffered against water-limitation and hence could sustain a higher TAC throughout summer. SWC measured during this study was only indicative of plant-available water (PAW) at the wet sites, as soils were deeper than the SWC profile

measurements at plot S2, S1 and N1 (Tab. 3.3). However, SWC did not deplete in the top 1 m at the wet sites and hence, additional access to potential deeper water pools should not matter, whereas unaccounted PAW, e.g. stored in the weathered sandstone bedrock, might impact TAC on the drier sites.

During the winter months, v_{sap} patterns across all landscape positions were relative similar (Fig. 2.5). The slope effect on solar exposure is largest at low solar altitudes and consequently relative solar exposure differences between aspects are largest during winter (Zou et al. 2007; Nyman et al. 2017). Consequently, plots on the southern aspect had a stronger v_{sap} decline from summer towards winter due to energy limitation, compared to the north-facing plots. In July the highest peak v_{sap} was recorded at the N3 (Fig. 2.5), presumably as a result of high water-availability and relative high radiation input due to favorable slope orientation.

In general, monthly fluctuations of v_{sap} patterns were higher on the wetter plots (S1, S2, N1) due to large v_{sap} decline in winter caused by energy-limitation. Particularly, understory trees on the (lower) southern aspects did not have access to light during winter, resulting in low transpiration rates (Fig. 2.9). v_{sap} patterns were more uniform throughout the year at the drier sites. Variability of v_{sap} peaks was dampened by stronger water-limitation in summer and more energy input due to slope orientation during the winter months (steep VPD-v_{sap} response in Fig. 2.6) causing less seasonality than on the wetter sites.

Distinct E_{sap} patterns observed in this study align with reported ET variations of to 40% in another MSEF catchments in SE Australia (Mitchell et al. 2012b). Patterns of scaled ET revealed an annual elevation-transpiration dependence, where E_{sap} generally decreased with elevation. In contrast to findings from this study v_{sap} between plots was similar.

Gharun et al. (2015) measured v_{sap} of overstory eucalypt trees and modeled species

specific v_{sap} to infer spatial v_{sap} patterns using gridded temperature data in relation to slope orientation and elevation in the Corin Catchment, ACT. They found similar patterns to ours, where v_{sap} was highest on steep southern aspects and flat terrain, which was attributed to lower potential ET and deeper soils in combination with favorable drainage position. However, they also reported lower v_{sap} at high altitudes due to temperature limitation.

Largest spatial E_{sap} variability typically arises towards the end of dry summer periods when soil moisture differences are high due to spatial patterns of soil water storage capacity (Meerveld and McDonnell 2006) and/or aspect and slope angle effects on atmospheric forcing (Renner et al. 2016).

2.4.3 Transpiration drivers

This study demonstrated that (sub-)daily v_{sap} fluctuations were mainly by driven atmospheric forcing (SWR and VPD) across a wide range forest structure, even in a water-limited ecosystem (AI >1). On longer temporal scales, tree structural parameters became more important in explaining v_{sap} and E_{sap} patterns (Fig. 2.12).

VPD has routinely been used to explain v_{sap} response on individual tree basis (Oishi et al. 2010; Adelman et al. 2008; Oren et al. 1999; Oren and Pataki 2001; Gharun et al. 2013; Oishi et al. 2010; Kumagai et al. 2008), especially in energy-limited ecosystems. In MSEF, VPD (Gharun et al. 2013) and potential ET (Mitchell et al. 2012b) have been used to explain v_{sap} patterns, whereas Pfautsch et al. (2010) found highest correlation to maximum air temperature in a wetter *E. regnans* forest during winter and spring.

SWC was a limiting factor on v_{sap} at the drier sites during summer (Fig. 2.5 & Fig. 2.7). Nevertheless, the feature importance of SWC in the Random Forest model was low due to several reasons. Firstly, vegetation is only constrained during periods of low SWC

integrated throughout the plant-available soil column. Deep roots might even have access to substantial water pools in the weathered bedrock, thus reducing the importance of SWC as PAW was not truly captured. Secondly, SWC was correlated with other predictor variables (VPD, TWI, A_S, AT, etc.) over longer time scales, and therefore some of its predictive capacity could have been lost to other factors. Furthermore, atmospheric forcing can be high during periods of low SWC and potentially offset any effects resulting from SWC limitation (Oishi et al. 2010). Thus the feature importance of SWC is masked by aggregation over unimportant periods (when soils are wet), the correlations with other predictors and potentially unaccounted water sources.

In more humid ecosystems, where v_{sap} patterns tend to be more uniform (Kumagai et al. 2008; Kumagai et al. 2007; Benyon et al. 2015; Benyon et al. 2017) A_S patterns have been recognized to explain spatial ET patterns in a broad range of forest types (Adelman et al. 2008; Kumagai et al. 2008; Meerveld and McDonnell 2006; Benyon et al. 2015; Mitchell et al. 2012a). However, Renner et al. (2016) also identified an inverse relationship between v_{sap} and A_S, resulting in similar E_{sap} at contrasting aspects in a European beech forest *(Fagus sylvatica)*.

Despite the heterogeneity of tree sizes, species composition and spatio-temporal variability of E_{sap} between plots in this study and overstory-to-understorey v_{sap} patterns within each plot only 11% of information is lost using solely A_S as predictor for annual E_{sap}, compared to more complex scaling procedures accounting for v_{sap} variations due to climate and soil moisture patterns. Thus, A_S can conceptualized as a 'time-integrated' composite metric of all other predictor variables, which affect the local growing conditions. Furthermore, the predictive power of A_S over a large range of forest structure and landscape positions indicates an optimization of A_S in relation to local hydro-climatic conditions due to slope orientation and drainage position and points towards the co-evolution of topography, soils,

vegetation and climate (Pelletier et al. 2013; Troch et al. 2015; Yetemen et al. 2015; Rasmussen et al. 2015).

From a predictive perspective, the potential to use A_S as an indicator of ET patterns across a broad range of forest types and structures is promising. More readily available high resolution spatial data sets (UAVs, LiDAR) offer huge potential to explore these links of vegetation patterns and water fluxes at landscape scale, as well as spatial ET mapping for management purposes.

2.5 Conclusion

This study revealed a systematic patterns of tree size, stand density, plant area index and sapwood area along two transects in an ecosystem that is characteristic for large parts of the forested area in SE Australia.

Furthermore, large spatio-temporal variations in transpiration due to landscape position were identified. Sap velocity did not vary systematically between sites, but in combination with stand sapwood area, distinct transpiration patterns evolved. Annual transpiration rates were generally higher in the gullies and on the south-facing slopes compared with equal hillslope position on the northern transect. In isolation, slope orientation had larger implications on transpiration patterns than drainage position in this ecosystem. However, their combined effect resulted in strong gradients of vegetation and transpiration patterns. Transpiration differences between sites were small during winter, but increased throughout summer. Seasonal variability was linked to landscape position and generally increased with increasing transpiration totals.

Even-tough being a water-limited ecosystem in the Budyko framework, atmospheric forcing was the main driver of transpiration patterns. Only sites on shallow soils experienced stronger soil water limitation. Stand sapwood area could explain 89% of the annual

transpiration rates across a large forest structure and topographic gradient. Thus, stand sapwood area can be conceptualized as a powerful transpiration predictor integrating the hydro-climatic conditions present at a given landscape position over longer time scales. Such a powerful, but 'simple' predictor should be promising from a practical management perspective.

Linking detailed ground observations with increasingly available resolution spatial data sets (UAVs, LiDAR, etc.) will offer opportunities to further explore links between vegetation patterns and forest-hydrological processes at landscape scale.

Furthermore, a novel approach to scale sap flux measurements from tree to plot scale was presented, that should be more robust in complex terrain with heterogeneous vegetation than the conventional method of calculating plot-scale mean sap velocities from few observation and scaling using stand sapwood area.

Bibliography

Adelman, J. D. et al. (2008). "Use of temporal patterns in vapor pressure deficit to explain spatial autocorrelation dynamics in tree transpiration". In: *Tree physiology* 28.4, pp. 647–658.

Amundson, R. et al. (2015). "Hillslope soils and vegetation". In: *Geomorphology* 234, pp. 122–132.

Bale, C. L et al. (1998). "The impact of aspect on forest structure and floristics in some Eastern Australian sites". In: *Forest Ecology and Management* 110.1, pp. 363–377.

Barnard, D. M. et al. (2017). "Topoclimate effects on growing season length and montane conifer growth in complex terrain". In: *Environ. Res. Lett.* 12.6.

Becker, P. (1998). "Limitations of a compensation heat pulse velocity system at low sap flow: implications for measurements at night and in shaded trees". In: *Tree Physiology* 18.3, pp. 177–184.

Benyon, R. G. (1999). "Nighttime water use in an irrigated Eucalyptus grandis plantation." In: *Tree Physiology* 19.13.

Benyon, R. G. et al. (2015). "Use of a forest sapwood area index to explain long-term variability in mean annual evapotranspiration and streamflow in moist eucalypt forests: streamflow predicted from sapwood area". In: *Water Resources Research* 51.7, pp. 5318–5331.

Benyon, R. G. et al. (2017). “Stand-level variation in evapotranspiration in non-water-limited eucalypt forests”. In: *Journal of Hydrology* 551, pp. 233–244.

Berner, L. T. et al. (2017). “Water availability limits tree productivity, carbon stocks, and carbon residence time in mature forests across the western US”. In: *Biogeosciences* 14.2, pp. 365–378.

Binkley, D. et al. (2010). “Explaining growth of individual trees: Light interception and efficiency of light use by Eucalyptus at four sites in Brazil”. In: *Forest Ecology and Management*. Productivity in Tropical Plantations 259.9, pp. 1704–1713.

Breiman, L. (2001). “Random forests”. In: *Machine Learning* 45.1, pp. 5–32.

Bren, L. and P. Hopmans (2007). “Paired catchments observations on the water yield of mature eucalypt and immature radiata pine plantations in Victoria, Australia”. In: *Journal of Hydrology* 336.3, pp. 416–429.

Bren, L. et al. (2010). “Longer-term water use of native eucalyptus forest after logging and regeneration: The Coranderrk experiment”. In: *Journal of Hydrology* 384.1, pp. 52–64.

Bren, L. et al. (2013). “Impacts of native forest harvesting on flows into the MurrayDarling Basin system”. In: *Australian Forestry* 76.2, pp. 91–100.

Brooks, P. D. et al. (2015). “Hydrological partitioning in the critical zone: Recent advances and opportunities for developing transferable understanding of water cycle dynamics”. In: *Water Resources Research* 51.9, pp. 6973–6987.

Budyko, M. I. (1974). *Climate and Life*. Orlando, Fl: Academic.

Burgess, S. S. et al. (2001). “An improved heat pulse method to measure low and reverse rates of sap flow in woody plants”. In: *Tree Physiology* 21.9, pp. 589–598.

Crawford, T. M. and C. E. Duchon (1999). “An Improved Parameterization for Estimating Effective Atmospheric Emissivity for Use in Calculating Daytime Downwelling Longwave Radiation”. In: *J. Appl. Meteor.* 38.4, pp. 474–480.

Downes, G. M. et al. (2009). "Measuring and modelling stem growth and wood formation: An overview". In: *Dendrochronologia*. EuroDendro 2008: The long history of wood utilization 27.2, pp. 147–157.

Drew, D. M. et al. (2008). "Daily patterns of stem size variation in irrigated and unirrigated Eucalyptus globulus". In: *Tree Physiol* 28.10, pp. 1573–1581.

Edwards, W. R. N. and N. W. M. Warwick (1984). "Transpiration from a kiwifruit vine as estimated by the heat pulse technique and the Penman-Monteith equation". In: *New Zealand Journal of Agricultural Research* 27.4, pp. 537–543.

Ellis, R. C. (1971). "Growth of Eucalyptus Seedlings on Four Different Soils". In: *Australian Forestry* 35.2.

Ellis, T. and T. Hatton (2008). "Relating leaf area index of natural eucalypt vegetation to climate variables in southern Australia". In: *Agricultural Water Management* 95.6, pp. 743–747.

Geroy, I. et al. (2011). "Aspect influences on soil water retention and storage". In: *Hydrological Processes* 25.25, pp. 3836–3842.

Gharun, M. et al. (2013). "Validation of canopy transpiration in a mixed-species foothill eucalypt forest using a soilplantatmosphere model". In: *Journal of Hydrology* 492, pp. 219–227.

Gharun, M. et al. (2014). "A test of how coupling of vegetation to the atmosphere and climate spatial variation affects water yield modelling in mountainous catchments". In: *Journal of Hydrology* 514, pp. 202–213.

Gharun, M. et al. (2015). "Mapping spatial and temporal variation in tree water use with an elevation model and gridded temperature data". In: *Agricultural and Forest Meteorology* 200, pp. 249–257.

Givnish, T. J. et al. (2014). “Determinants of maximum tree height in Eucalyptus species along a rainfall gradient in Victoria, Australia”. In: *Ecology* 95.11, pp. 2991–3007.

Griebel, A. et al. (2017). “Evergreen and ever growing Stem and canopy growth dynamics of a temperate eucalypt forest”. In: *Forest Ecology and Management* 389, pp. 417–426.

Grimmond, C. S. B. et al. (2000). “Spatial variability of micro-climatic conditions within a mid-latitude deciduous forest”. In: *Climate Research* 15.2, pp. 137–149.

Gutirrez-Jurado, H. A. et al. (2013). “On the observed ecohydrologic dynamics of a semiarid basin with aspect-delimited ecosystems: ecohydrologic dynamics of a semiarid basin”. In: *Water Resources Research* 49.12, pp. 8263–8284.

Hacke, U. G. et al. (2006). “Scaling of angiosperm xylem structure with safety and efficiency”. In: *Tree physiology* 26.6, pp. 689–701.

Haydon, S. R. et al. (1997). “Variation in sapwood area and throughfall with forest age in mountain ash (Eucalyptus regnans F. Muell.)” In: *Journal of Hydrology* 187.3, pp. 351–366.

Kirkpatrick, J. B. and M. Nunez (1980). “Vegetation-Radiation Relationships in Mountainous Terrain: Eucalypt-Dominated Vegetation in the Risdon Hills, Tasmania”. In: *Journal of Biogeography* 7.2, p. 197.

Kuczera, G. (1987). “Prediction of water yield reductions following a bushfire in ash-mixed species eucalypt forest”. In: *Journal of Hydrology* 94.3, pp. 215–236.

Kumagai, T. et al. (2007). “Sap flow estimates of stand transpiration at two slope positions in a Japanese cedar forest watershed”. In: *Tree physiology* 27.2, pp. 161–168.

Kumagai, T. et al. (2008). “Transpiration and canopy conductance at two slope positions in a Japanese cedar forest watershed”. In: *Agricultural and Forest Meteorology* 148.10, pp. 1444–1455.

Lane, P. N. and S. M. Mackay (2001). "Streamflow response of mixed-species eucalypt forests to patch cutting and thinning treatments". In: *Forest Ecology and Management* 143.1, pp. 131–142.

Lane, P. et al. (2010). "Modelling the long term water yield impact of wildfire and other forest disturbance in Eucalypt forests". In: *Environmental Modelling & Software* 25.4, pp. 467–478.

Macfarlane, C. et al. (2007). "Estimation of leaf area index in eucalypt forest using digital photography". In: *Agricultural and Forest Meteorology* 143.3, pp. 176–188.

Macfarlane, C. et al. (2014). "Digital canopy photography: Exposed and in the raw". In: *Agricultural and Forest Meteorology* 197, pp. 244–253.

McDowell, N. G. and C. D. Allen (2015). "Darcy's law predicts widespread forest mortality under climate warming". In: *Nature Climate Change* 5.7, pp. 669–672.

Meerveld, H. Tromp-van and J. McDonnell (2006). "On the interrelations between topography, soil depth, soil moisture, transpiration rates and species distribution at the hillslope scale". In: *Advances in Water Resources* 29.2, pp. 293–310.

Mitchell, P. J. et al. (2012a). "Capturing within catchment variation in evapotranspiration from montane forests using LiDAR canopy profiles with measured and modelled fluxes of water: capturing variation in evapotranspiration using lidar". In: *Ecohydrology* 5.6, pp. 708–720.

Mitchell, P. J. et al. (2012b). "Responses of evapotranspiration at different topographic positions and catchment water balance following a pronounced drought in a mixed species eucalypt forest, Australia". In: *Journal of Hydrology* 440-441, pp. 62–74.

Moore, I. D. et al. (1993). "Modelling environmental heterogeneity in forested landscapes". In: *Journal of Hydrology* 150.2, pp. 717–747.

Nobre, A. et al. (2011). "Height Above the Nearest Drainage: a hydrologically relevant new terrain model". In: *Journal of Hydrology* 404.1, pp. 13–29.

Nolan, R. H. et al. (2015). "Trends in evapotranspiration and streamflow following wildfire in resprouting eucalypt forests". In: *Journal of Hydrology* 524, pp. 614–624.

Nyman, P. et al. (2014). "Downscaling regional climate data to calculate the radiative index of dryness in complex terrain". In: *Australian Metrological and Oceanographic Journal* 64.2, pp. 109–122.

Nyman, P. et al. (2015). "Quantifying the effects of topographic aspect on water content and temperature in fine surface fuel". In: *International Journal of Wildland Fire* 24.8, pp. 1129–1142.

Nyman, P. et al. (2017). "Evaluating models of shortwave radiation below Eucalyptus canopies in SE Australia". In: *Agricultural and Forest Meteorology* 246, pp. 51–63.

O'Grady, A. P. et al. (2011). "Can we predict groundwater discharge from terrestrial ecosystems using existing eco-hydrological concepts?" In: *Hydrology and Earth System Sciences* 15.12, pp. 3731–3739.

Oishi, A. C. et al. (2010). "Interannual Invariability of Forest Evapotranspiration and Its Consequence to Water Flow Downstream". In: *Ecosystems* 13.3, pp. 421–436.

Oliphant, A et al. (2006). "Local-scale heterogeneity of photosynthetically active radiation (PAR), absorbed PAR and net radiation as a function of topography, sky conditions and leaf area index". In: *Remote Sensing of Environment* 103.3, pp. 324–337.

Oren, R. et al. (1999). "Survey and synthesis of intra-and interspecific variation in stomatal sensitivity to vapour pressure deficit". In: *Plant, Cell & Environment* 22.12, pp. 1515–1526.

Oren, R. and D. E. Pataki (2001). "Transpiration in response to variation in microclimate and soil moisture in southeastern deciduous forests". In: *Oecologia* 127.4, pp. 549–559.

Pedregosa, F et al. (2011). “Scikit-learn: Machine Learning in Python”. In: *Journal of Machine Learning Research* 12, pp. 2825–2830.

Pelletier, J. D. et al. (2013). “Coevolution of nonlinear trends in vegetation, soils, and topography with elevation and slope aspect: A case study in the sky islands of southern Arizona”. In: *Journal of Geophysical Research: Earth Surface* 118.2, pp. 741–758.

Pfautsch, S. et al. (2010). “Sap flow measurements reveal influence of temperature and stand structure on water use of Eucalyptus regnans forests”. In: *Forest Ecology and Management* 259.6. 00045, pp. 1190–1199.

Pfautsch, S. et al. (2016). “Climate determines vascular traits in the ecologically diverse genus *Eucalyptus*”. In: *Ecology Letters* 19.3, pp. 240–248.

Pook, E. W. and C. W. E. Moore (1966). “The influence of aspect on the composition and structure of dry sclerophyll forest on Black Mountain, Canberra. ACT”. In: *Australian Journal of Botany* 14.2, pp. 223–242.

Poorter, L. et al. (2010). “The importance of wood traits and hydraulic conductance for the performance and life history strategies of 42 rainforest tree species”. In: *New Phytologist* 185.2, pp. 481–492.

Rasmussen, C. et al. (2015). “Quantifying Topographic and Vegetation Effects on the Transfer of Energy and Mass to the Critical Zone”. In: *Vadose Zone Journal* 14.11.

Renner, M. et al. (2016). “Dominant controls of transpiration along a hillslope transect inferred from ecohydrological measurements and thermodynamic limits”. In: *Hydrology and Earth System Sciences* 20.5, pp. 2063–2083.

Renno, C. D. et al. (2008). “HAND, a new terrain descriptor using SRTM-DEM: Mapping terra-firme rainforest environments in Amazonia”. In: *Remote Sensing of Environment* 112.9, pp. 3469–3481.

Swanson, R. H. and D. W. A. Whitfield (1981). "A numerical analysis of heat pulse velocity theory and practice". In: *Journal of experimental botany* 32.1, pp. 221–239.

Swetnam, T. L. et al. (2017). "Topographically driven differences in energy and water constrain climatic control on forest carbon sequestration". In: *Ecosphere* 8.4, e01797.

Tarboton, D. G. (1997). "A new method for the determination of flow directions and upslope areas in grid digital elevation models". In: *Water Resources Research* 33.2, pp. 309–319.

Thompson, S. E. et al. (2011). "Spatial scale dependence of ecohydrologically mediated water balance partitioning: A synthesis framework for catchment ecohydrology". In: *Water Resources Research* 47.10.

Tian, Y. Q. et al. (2001). "Estimating solar radiation on slopes of arbitrary aspect". In: *Agricultural and Forest Meteorology* 109.1, pp. 67–74.

Troch, P. A. et al. (2015). "Catchment coevolution: A useful framework for improving predictions of hydrological change?" In: *Water Resources Research* 51.7, pp. 4903–4922.

Vertessy, R. A. et al. (1993). "Predicting water yield from a mountain ash forest catchment using a terrain analysis based catchment model". In: *Journal of Hydrology* 150.2, pp. 665–700.

Watson, F. G. R. et al. (1999). "Large-scale modelling of forest hydrological processes and their long-term effect on water yield". In: *Hydrol. Process.* 13.5, pp. 689–700.

Webb, A. A. and B. W. Jarrett (2013). "Hydrological response to wildfire, integrated logging and dry mixed species eucalypt forest regeneration: The Yambulla experiment". In: *Forest Ecology and Management* 306, pp. 107–117.

Webb, A. A. et al. (2012). "Longer-term changes in streamflow following logging and mixed species eucalypt forest regeneration: The Karuah experiment". In: *Journal of Hydrology* 464, pp. 412–422.

Yetemen, O. et al. (2015). “Ecohydrologic role of solar radiation on landscape evolution”. In: *Water Resources Research* 51.2, pp. 1127–1157.

Zapata-Rios, X. et al. (2016). “Influence of terrain aspect on water partitioning, vegetation structure and vegetation greening in high-elevation catchments in northern New Mexico: Terrain Aspect, Water Partitioning, Vegetation Greening in High-elevation Catchments”. In: *Ecohydrology* 9.5, pp. 782–795.

Zhou, X. et al. (2013). “Modeling the ecohydrological role of aspect-controlled radiation on tree-grass-shrub coexistence in a semiarid climate”. In: *Water Resources Research* 49.5, pp. 2872–2895.

Zou, C. B. et al. (2007). “Effects of topography and woody plant canopy cover on near-ground solar radiation: Relevant energy inputs for ecohydrology and hydropedology”. In: *Geophysical Research Letters* 34.24.

Chapter 3

Topography diminishes variability of forest floor and understory ET fluxes across large range of forest structure in complex terrain

3.1 Introduction

In water-limited ecosystems, differences in vegetation densities and heights on contrasting aspects indicate towards topographic control of vegetation patterns (Gutirrez-Jurado et al. 2013; Zapata-Rios et al. 2016). Once overstory vegetation cover is established, the interaction of vegetation and terrain amplifies sub-canopy micro-climate patterns (Zou et al. 2007; Grimmond et al. 2000; Oliphant et al. 2006; Nyman et al. 2017). Lower incident angles of direct solar radiation and longer pathways through the vegetation layer result in exponentially lower radiation loads on polar-facing hillslopes (Nyman et al. 2017). Higher sub-canopy radiation load and consequently larger evaporative losses will reduce surface soil water content (SWC) on equatorial-facing aspects. Higher SWC and thus more available water for pedogenesis manifests in deeper, more developed soils on polar-facing slopes compared to equatorial aspects. Plant-available water content (PAWC) of the understory is less dependent on soil depth due to shallower rooting depth compared to

overstory vegetation. However, overstory vegetation mediates sub-canopy radiation loads as illustrated above, and the catena effect on soil depth therefore exerts indirect control on the understory vegetation. Understory energy and moisture patterns as well as understory vegetation are consequently affected by complex interactions of climate, overstory vegetation structure and topography, which in turn are expected to shape understory and forest floor ET patterns.

Eucalypt forest ecosystems of SE Australia span a large climatic gradient (Givnish et al. 2014) and many ecosystems are located in water-limited climates and upland topography (Nyman et al. 2014). Topographic mediated energy and moisture patterns are expected to have largest implications in water-limited ecosystems, potentially causing large forest structure changes over small spatial extents (Nyman et al. 2014). Consequently, potential shifts from xeric to mesic understory environments along drainage gradients are expected to manifest in heterogeneous ET_U patterns as well.

So far, most research on understory and shrub ET has been carried out in energy-limited systems with profound growing seasons or in semi-arid shrub ecosystems where the overstory layer is missing (Huxman et al. 2005; Steinwand et al. 2001). Understory and forest floor evapotranspiration (ET_U) in forest ecosystems is often neglected under the assumption that overstory ET fluxes are several orders of magnitude higher. In Australia, only a few plot studies have investigated ET_U in eucalypt forest stands, although ET_U has been identified as the largest ET component in a dry, open eucalypt woodland, accounting for 38 - 64% of total ET (Mitchell et al. 2009). In wetter MSEF, ET_U contributed substantially to the total ET flux, where Mitchell et al. (2012b) reported annual ET_U of 144 mm (18% of total ET) and Nolan et al. (2014) attributed 24-33% (285-323 mm) of total ET to ET_U. Even, in tall, non-water limited mountain ash (*E. regnans*) forests ET_U contribution was non-negligible, ranging from 8 to 26% (116-297 mm) of total ET (Benyon et al. 2017).

These findings illustrate a large range of ET_U in contrasting eucalypt forest stands, where ET_U was either strongly correlated to sub-canopy energy (Nolan et al. 2014; Mitchell et al. 2012b; Benyon et al. 2017) or moisture patterns (Mitchell et al. 2009).

Albeit, the recently established importance of ET_U on the forest water balance, little is known about spatial ET_U patterns in heterogeneous MSEFs. In particular, large uncertainty remains about how interactions of non-uniform vegetation structures and complex topographic patterns influences spatio-temporal ET_U dynamics.

Thus, this study aims to investigate how the interaction of overstory vegetation with topography will affect sub-canopy micro-climate, understory vegetation and ET_U dynamics. More specifically the following research questions will be addressed:

1. How does sub-canopy micro-climate change along a valley cross-section with varying slope orientation, drainage position and forest structure?

2. Does understory vegetation organize in response to landscape position?

3. What is the dominant ET_U control?

4. Do spatial ET_U patterns vary systematically in response to landscape position?

3.2 Methods

3.2.1 Study site

The study sites were located in a ∼70 ha sized forested head-water catchment ∼80 km north-east of Melbourne, VIC, Australia. Mean annual precipitation in the area is 1200 to 1300 mm, peaking in winter and spring. Average daily air temperature in summer is 19°C and average winter temperatures reach 7°C. The catchment spans from 286 to 617 m a.s.l in an east-west direction, and thus most of the slope area is either facing towards north or

south (Fig. 3.1). Six monitoring plots with a 15 m slope-corrected radius were set-up on a polar and equatorial-facing hillslope at varying drainage position (ridge, mid-slope, gully), while minimizing variations in other factors, e.g. geology, rainfall patterns, short-wave radiation patterns, and upstream contributing area for corresponding slope positions. Two levels of aridity and 3 levels of drainage position were aimed for. Aridity was quantified with long-term mean annual aridity index (Budyko 1974), while the topographic wetness index (TWI) (Beven and Kirkby 1979) was used to quantify drainage position of each plot. Terrain analysis, calculation of TWI and the height above nearest drainage (HAND) (Nobre et al. 2011) were done on a 20 × 20 m DEM using QGIS and SAGA GIS. Aridity index rasters were generated following Nyman et al. (2014).

The monitoring period lasted from 01.03.2015 to 29.02.2016 and was characterized by a mean temperature of 11.8°C (mean daily max. of 17.6°C and mean daily min of 7.3°C), mean daily maximum vapor pressure deficit (VPD) of 0.92 kPA and total precipitation of 918 mm.

3.2.2 LAI measurements

Shrubs, ferns, grasses <1.5 m height

Understory leaf area index (LAI) below 1.5 m height was measured using the line intercept method (Groeneveld 1997) in four randomly selected sub-plots. A 2 mm, one meter long carbon fiber rod was positioned vertically in an 11 by 11 step grid from each sub-plot center and contact points with green leaves were recorded. When vegetation exceeded 1 m height the rod was extended by attaching a second carbon fiber rod (4 mm diameter). LAI was then calculated as follows:

$$LAI = \frac{N}{n} \cdot k^{-1} \tag{3.1}$$

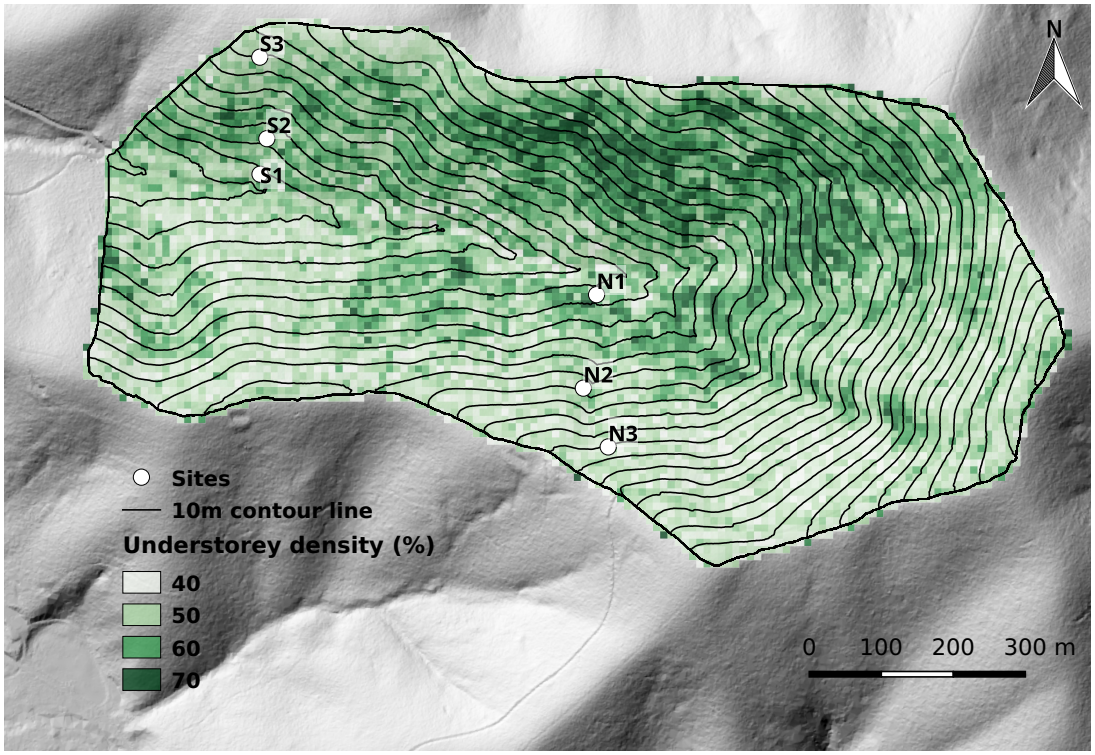

Figure 3.1: Map of the research sites illustrating understory cover derived from LiDAR.

where N is the sum of contact points with green leaves, n is the number of rods places and k is the extinction coefficient. The extinction coefficient is usually set at 0.5, but resulted in unrealistically high values, for sites dominated by small leaved shrubs. Hence, k was derived for a range of plants with different leaf sizes by calibrating the line intercepts against LAI measurements from destructive harvest. Lines were placed in a grid with 10 cm spacing in the projected foliage area of individual plants and the number of line intercepts recorded. Subsequently, all leaves were harvested and the leaf area determined using a leaf area meter (LI-3100C, LI-COR Environmental, Lincoln, NE, USA). Leaf area was the converted to LAI using the projected foliage area (assuming elliptic shape) of the plant and k derived from equation 3.1. Understory plants were binned in 3 classes: large, intermediate and small leaves and the mean k for each class calculated (Tab. 3.1). An ocular estimation of LAI contribution from each class was done at each plot. Line

intercepts were weighted according to class contribution and the corresponding mean k was applied.

Table 3.1: Extinction coefficient (k), leaf area index (LAI) and the corresponding standard errors of the mean (in parenthesis) derived from destructive harvest. Sampled species were binned into three leaf size classes.

leaf size class	large	intermediate	small
k (−)	1.4 (±0.3)	99.4 (±30.8)	21.8 (±3.0)
LAI (m^2 m^{-2})	0.29 (±0.06)	0.07 (±0.03)	0.1 (±0.02)
species	*E. saplings*	*B. spinulosa*	*C. quadrifida*
		C. longifolia	*L. phylicoides*
			L. juniperinum

Tree ferns

Most tree ferns would have been to tall to reliably measure their leaf area using the line-intercept method (mean trunk height 1.6 m ±1.44 m, max. trunk height 5.1 m). Hence, allometrics were developed by sampling a total of 102 fronds from 30 tree ferns and measuring frond width, length and leaf area. Leaves were clipping off the fronds, spread out on a white surface and a picture taken. The leaf area in the picture was converted to polygons and the area calculated. Frond leaf area was well related to frond length times frond width (R^2 : 0.91, data not shown). Tree ferns were censused on each plot, sample frond length and width measured, and frond number counted for each plot, and per fern leaf are index calculated. LAI was then calculated by summing up the leaf area of all ferns per plot and dividing by the plot area.

3.2.3 Micro-climate measurements

One climate station was set-up at each hillslope below the canopy and in a clearing close-by (∼4 km from site). All climate stations measured solar radiation (SP-110, Apogee Instruments Inc., Logan, UT, USA), air temperature, relative humidity (CS215, Campbell Scientific Inc., Logan, UT, USA) and wind speed (014A, Met One Instruments Inc., Grants Pass, OR, USA). Air temperatures were normalized to plot S1 by applying a lapse rate of 7°C per 1000 m elevation difference to isolate impact of vegetation and slope orientation on micro-climate. Two rain gauges (TB3, Hydrological Services Pty. Ltd, Warwick Farm, NSW, Australia), logging at 5 minute intervals, were installed at high and low elevation to account for orographic rainfall gradients (1-4 km from site).

Incoming short-wave radiation (SWR) was measured every minute at each plot at a height of 1.5 m on three randomly chosen locations within each plot (SP-110, Apogee Instruments Inc., Logan, UT, USA). Pyranometers at the mid-slope and ridge plots were installed on August 20th 2015.

3.2.4 Soil moisture measurements

Soil moisture was measured in 15 minute intervals at each plot in 10, 30, 50, 75 and 100 cm depth where possible (EC-5, Decagon Devices Inc., Pullman, WA, USA). Each soil moisture sensors was calibrated using four soil samples sampled at the depth of probe installation using bulk density rings. Soil samples were dried at 105 degree until constant weight was reached and the bulk density calculated. For each sensor location, the amount of sampled soil needed to repack to measured bulk density was wetted, mixed and left for an hour. Thereafter, the wetted soil was weighted, repacked to the measured bulk density and the volumetric water content calculated. Four soil moisture sensors (EC-5) were inserted into the soil and output voltage measured. More water was added to the soil

four more times and the procedure above repeated. Finally, a linear regression between output voltage and volumetric soil water content was fitted for each sensor installation location. The temporal dynamics of the sensor at 10 cm depth were used to scale manual TDR measurements of surface soil moisture (0 -12 cm, R^2: 0.66 - 0.99, data not shown).

3.2.5 Sub-canopy radiation model

The Light Penetration Index model (LPI) or path length model (PL) (Nyman et al. 2017) were used to model sub-canopy short-wave radiation (SWR), depending which posed a higher coefficient of determination at each individual site. Modeled SWR was used for the time before pyranometer installation at the mid-slope and ridge plots as well as to gap-fill. Sub-canopy direct radiation $R_{sc,dir}$ was calculated in the PL model by

$$R_{sc,dir} = R_{ac}(1 - P_{dif})e^{-Lk} \tag{3.2}$$

where R_{ac} the measured above canopy radiation, P_{dif} the estimated diffuse fraction, k the bulk canopy extinction coefficient (0.033) and L the path length. The path length was calculated by

$$L = \frac{H - h}{cos(z)} \tag{3.3}$$

where H is the tree height, h the measurement height of sub-canopy radiation (1.5 m) and z the zenith angle. The above-canopy diffuse fraction (P_{dif}) was calculated from the clearness index, which is the ratio of total radiation on a horizontal surface to the total radiation at the top of the atmosphere (Spencer 1982). Coefficients derived by Spencer (1982) for Melbourne airport were applied to the weather station data setup in the clearing. Finally, the diffuse fraction ($R_{sc,dif}$) was calculated from

$$R_{sc,dif} = R_{ac}P_{dif}v \tag{3.4}$$

where v is the sky view factor derived from hemispherical photography.

In the LPI model the diffuse sub-canopy radiation was calculated using 3.4 as well. However, the direct radiation component was calculated by

$$R_{sc,dir} = R_{ac}(1 - P_{dif})wLPI \tag{3.5}$$

where LPI is the light penetration index defined as the ratio of LiDAR returns above 1.5 m height to all LiDAR returns and w the weighting factor accounting for the incident angle defined as

$$w = \frac{H - h}{L} \tag{3.6}$$

3.2.6 ET_U measurements

An evaporation dome was build from a metal frame which was wrapped with polyvinyl cover (Mitchell et al. 2012b; Nolan et al. 2014; Macfarlane and Ogden 2012). The resulting cylindrical enclosure had a height of 1 m and a diameter of 0.7 m. An air temperature and relative humidity sensor (HMP110, Vaisala Oyj, Vantaa, Finland) was installed inside the enclosure and a pyranometer on top measured SWR parallel to 'domed' surface. A mixing fan ensured that the sensor reading was representative for the entire dome volume. Closed-cell pipe insulation foam was applied at the bottom in order to provide a good seal on uneven ground. The enclosure was then placed over low vegetation or on the forest floor to measure ET_U at six sub-plots per site during five measurement campaigns at each site. Air temperature and relative humidity inside the enclosure were measured for a minute, which were converted to ET following Ward and Micin (2006). Water vapor mass accumulated inside the dome was calculated by

$$w = \frac{217 \times e \times V}{AT + 273.15} \tag{3.7}$$

where w is the water vapor in g, V is the dome volume (0.385 m^3), AT the air temperature and e the vapor pressure, which was calculated by

$$e = \frac{RH}{100} \times 6.1078^{(17.2694 \times AT/AT+237.3)} \tag{3.8}$$

Water vapor mass inside the dome was plotted against time and a linear regression fitted. The slope of the regression line represents the ET rate ($g\ s^{-1}$) and was then converted to $mm\ h^{-1}$. It has to be noted that due to the nature of these campaign measurements interception loss was not accounted for, and therefore ET_U only captured soil evaporation and understory transpiration.

Surface soil moisture (0-12 cm depth) was measured at 4 locations in the sub-plots after the ET measurements using a hand-held TDR probe (HydroSense II, Campbell Sci., Logan, UT, USA). Shrubs were destructively harvested after the last campaign and the LAI measured using a leaf area meter (LI-3100C, LI-COR Environmental, Lincoln, NE, USA). LAI of measurement locations, derived from destructive harvest after last campaign, spanned a range from 0 to 3.28 and was generally representative for the mean plot LAI (Fig. 3.2)

3.2.7 ET_U model

Empirical ET_U models were build using a combination of auxiliary soil water content (SWC) and short-wave radiation (SWR) measurements, as well as leaf are index (LAI) derived from destructive harvest (Tab. 3.2). SWR was the only variable in a single parameter model that achieved a Nash-Sutcliffe model efficiency coefficient (NSE) >0, indicating that ET_U is primarily driven by SWR. Adding SWC or LAI, resulted in similar NSE gains compared to with the one parameter model. However, the Akaike information criterion (AIC) was slightly lower for the model using SWC instead of LAI. Including all three parameters rendered LAI and SWC statistically insignificant, an thus the model using

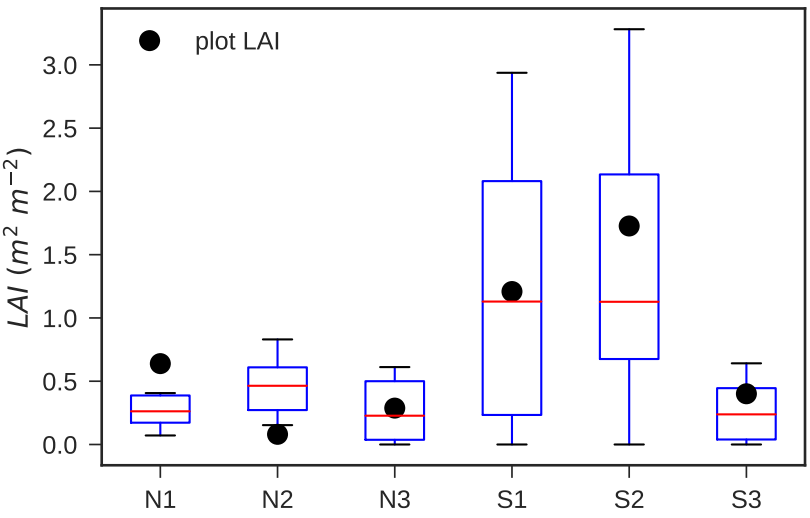

Figure 3.2: LAI derived from destructive harvesting at the six understory ET measurement plots (boxplot) compared to plot scale LAI measured using the line-intercept method (black dot).

Table 3.2: Understory evapotranspiration (ET_U) model selection criteria. ET_U was modeled using incoming short-wave radiation (SWR), soil water content (SWC), leaf area index (LAI) or a combination thereof. The Nash-Sutcliffe model efficiency coefficient (NSE) and the Akaike information criterion (AIC), as well as statistical significance of each regression coefficient is listed for each model. Significant values are shown in bold.

	f(SWR)	f(SWC)	f(LAI)	f(SWR,SWC)	f(SWR,LAI)	f(SWR,SWC,LAI)
NSE	0.49	-0.57	-0.95	0.63	0.63	0.64
AIC	-132.2	-98.6	-92.7	-136.1	-135.6	-134.5
SWR	**<0.001**	-	-	**<0.001**	**<0.001**	**<0.001**
SWC	-	**<0.001**	-	**0.005**	**0.005**	0.378
LAI	-	-	**<0.001**	-	-	0.48

SWR and SWC was used. Each individual dome ET_U measurement could be explained reasonable well (R^2 : 0.42, Fig. 3.3a). Given the spatial variability of sub-canopy radiation,

plot averages of the six sub-plot measurements considerably reduced the noise, model bias and consequently 64% of variation could be explained (Fig. 3.3b). Hence, the model

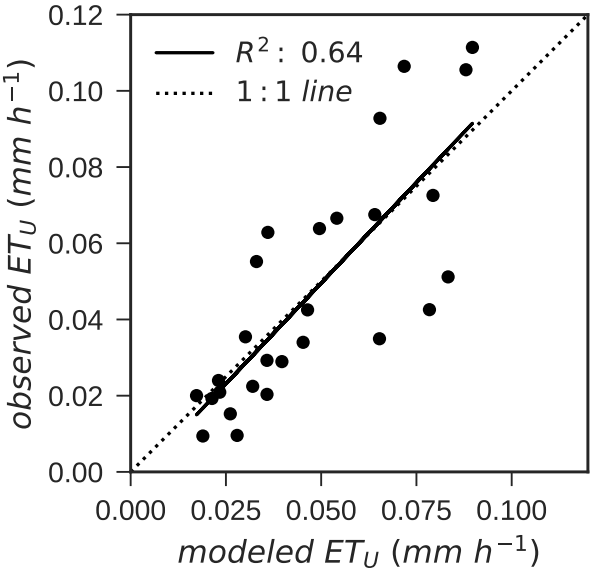

Figure 3.3: Modeled versus observed understory ET for a) all individual measurements and b) binned by plot and date. ET was modeled as function of short-wave radiation, surface soil water content and leaf area index.

obtained using spatial plot averages was applied to daytime hours (SWR >1 $W\ m^{-2}$) and summed up to daily totals. Based on the lack of night-time ET_U measurements and the evidence of nocturnal ET in the range of 5-20% in other ecosystems (Zeppel et al. 2010; Moore et al. 2008; Ogle et al. 2012; Dios et al. 2015; Dawson et al. 2007) nocturnal ET_U was set to 10% of mean day-time ET_U. Hence, ET_U was calculated by

$$ET_U = 0.000142\ SWR + 0.128081\ SWC, \text{ for SWR >1 W} \tag{3.9}$$

, where SWR is the incoming short-wave radiation in $W\ m^{-2}$, SWC the soil water content at 0-12 cm in $m^3\ m^{-3}$ and LAI the leaf area index.

3.2.8 ET_U efficiency

ET_U efficiency (ET_{eff}) was defined as

$$ET_{eff} = \frac{\sum ET_U \times \lambda}{\sum SWR} \tag{3.10}$$

where ET_U is the understory ET, λ is the latent heat of vaporization (2460 $MJ\ m^{-3}$) (Monteith and Unsworth 2013) and SWR the incoming short-wave radiation below the canopy.

3.3 Results

3.3.1 Sub-canopy micro-climate

Mean annual air temperature was fairly similar between the weather stations (Fig. 3.4), with 14.1°C at the open, 12.8°C at the northern aspect and 11.9°C at the south-facing slope. Differences between sub-canopy and open temperature mainly arose in winter when temperatures were low. Air temperature dynamics between slopes were very similar, with temperatures at the northern aspect constantly slightly higher.

In contrast, VPD showed a clear seasonal pattern (Fig. 3.4). During the winter months, sub-canopy VPD ranged between 10 and 40% of the VPD at the open weather station. The differences between the reference station and sub-canopy VPD diminished towards summer. However, in absolute numbers mean VPD differences were relative small. VPD was higher at the open weather station than on both slopes (mean VPD of 0.39 kPA), and slightly higher at the N1 (0.31 kPA) compared to S1 (0.26 kPA).

Two general sub-canopy radiation patterns emerged in relation to landscape position. Firstly, plots on the northern aspect generally had higher SWR than the south-facing slope. Furthermore, SWR decreased moving down the transect at both slopes (Fig. 3.5a). A combination of vegetation, landscape position and slope orientation caused interception

Table 3.3: Understory and terrain properties at each plot; N and S indicate slope aspect, numbers indicate slope position, increasing from gully to ridge, TWI: topographic wetness index, HAND: height above nearest drainage, AI: aridity index, P: elevation adjusted annual precipitation (2015-03-01 to 2016-02-29), LAI_U: total understory leaf area index, PAI_O: total overstory plant area index, TH: tree fern trunk height, CR: tree fern crown radius.

Site	N1	N2	N3	S1	S2	S3
			Site characteristics			
elevation (m)	354	408	451	306	322	368
slope (°)	14.8	24.1	28.9	10.1	18.5	22.1
TWI (-)	7.99	6.44	4.91	7.96	6.94	5.00
AI (-)	1.75	1.78	1.86	1.47	1.19	1.32
HAND (m)	3.0	36.4	63.5	1.6	9.1	51.5
soil depth (m)	>3.0	0.8	0.5	>3.0	2.0	0.6
P (mm)	840	855	866	826	831	845
LAI_U (m^2 m^{-2})	0.6	0.1	0.3	1.2	1.7	0.4
PAI_O (m^2 m^{-2})	3.5	2.1	1.6	3.6	3.0	2.7
Canopy height (m)	37.0	15.7	15.2	44.8	38.4	28.3
			Non-Tree fern understory			
LAI (m^2 m^{-2})	0.62	0.08	0.29	0.02	1.35	0.4
main species	*P. esculentum*	*C. longifolia*	*L. juniperinum*	*B. nudum*	*B. nudum*	*P. esculentum*
	B. nudum	*L. phylicoides*	*H. sericea*	*L. elatius*	*L. elatius*	*G. ovata*
	L. phylicoides	*C. quadrifida*	*C. longifolia*	*A. melanoxylon*	*G. ovata*	*B. arborescens*
	B. arborescens	*P. esculentum*	*E. sapling*	*B. arborescens*	*C. quadrifida*	*L. phylicoides*
	L. elatius	*B. spinulosa*				*C. lawrenceana*
		L. juniperinum				
			Tree fern			
LAI (m^2 m^{-2})	0.02	-	-	1.23	0.38	-
density (stems ha^{-1})	56.6	-	-	1329.8	792.2	-
mean TH (m)	0.98 (±0.78)	-	-	2.04 (±1.42)	1.43 (±1.58)	-
mean CR (m)	0.84 (±0.74)	-	-	1.83 (±0.76)	1.36 (±0.69)	-

of large fractions of SWR (Fig. 3.5b). On the southern aspects, a larger fraction of SWR reached the ground during the summer months compared to winter, a result of high solar elevation and consequently shorter path length through the vegetation. SWR per unit slope area decreased at the north-facing slope in summer, because the solar elevation was larger than the slope angle, effectively decreasing the incident angle of the solar beam.

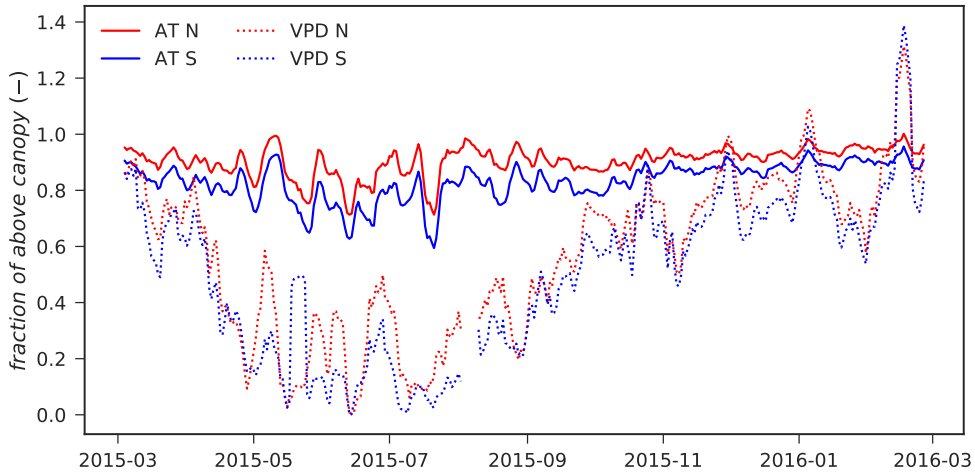

Figure 3.4: Air temperature (AT) and vapor pressure deficit (VPD) measured at the micro-climate stations. Displayed are seven day running means of the fraction observed compared to the open reference station.

In general, the effect of slope orientation was strongest during the winter months on both aspects (Fig. 3.6). On the north-facing slope, slope inclination increased SWR per unit area, especially at low solar elevation during winter. During the summer month, the solar azimuth angles were lower than the slope angle, effectively decreasing the incident angle mid-day and diminishing the slope effect, especially at N3, which had the steepest slope angle (28.9°, Tab. 3.3). The pattern was reversed on the southern aspect, where slope orientation deceased SWR per unit area during winter. Analog to the north-facing transect the slope effect was least pronounced during summer, especially at S1, where slope inclination was only 10.2° (Tab. 3.3)).

3.3.2 Soil moisture dynamics

Surface soil water content (SWC, 0-12 cm depth) showed a clear pattern in relation to hillslope position and aspect (Fig. 3.7). SWC was generally higher on the southern aspect,

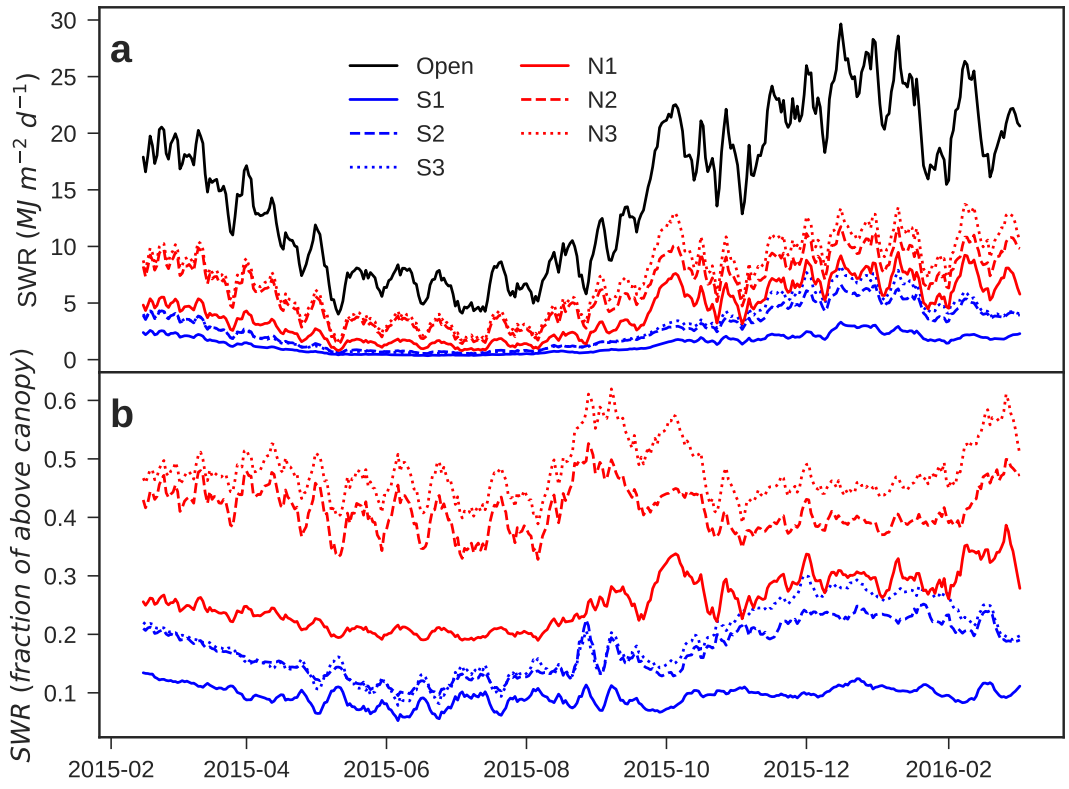

Figure 3.5: a) Incoming short-wave radiation load (SWR) at the weather station (open) and below the canopy at each site. b) Fracation of SWR received at each site compared to the weather station.

compared to the north-facing slope. Mean SWC at the northern transect decreased from 0.13 m^3 m^{-3} at N1 to 0.06 m^3 m^{-3} at N2 and 0.07 m^3 m^{-3} at N3. The SWC decrease from gully to ridge was not as pronounced on the southern aspect, where mean SWC at S1 was 0.16 m^3 m^{-3} and increased to 0.20 m^3 m^{-3} at S2 before decreasing to 0.10 m^3 m^{-3} at S3. Furthermore, SWC was generally more responsive to rainfall events at the ridge and mid-slope plots, where soils were shallower.

Mean SWC patterns were linked to mean sub-canopy SWR and to a lesser degree to topography (Fig. 3.8). Drainage position, represented by HAND, was the most important topography feature and could explain 56 % of the variation between plots (Fig. 3.8b).

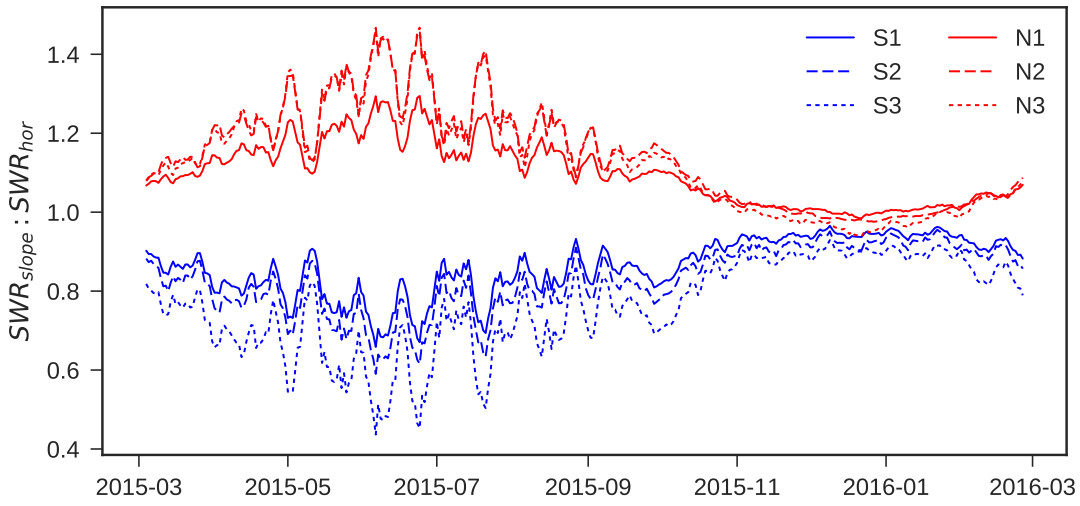

Figure 3.6: Slope effect on short-wave radiation (SWR) patterns. Modeled sub-canopy SWR per area on the actual slope divided by the modeled SWR on a horizontal surface. In both cases path length through vegetation is the same. N and S indicate slope aspect, numbers indicate slope position, increasing from gully to ridge.

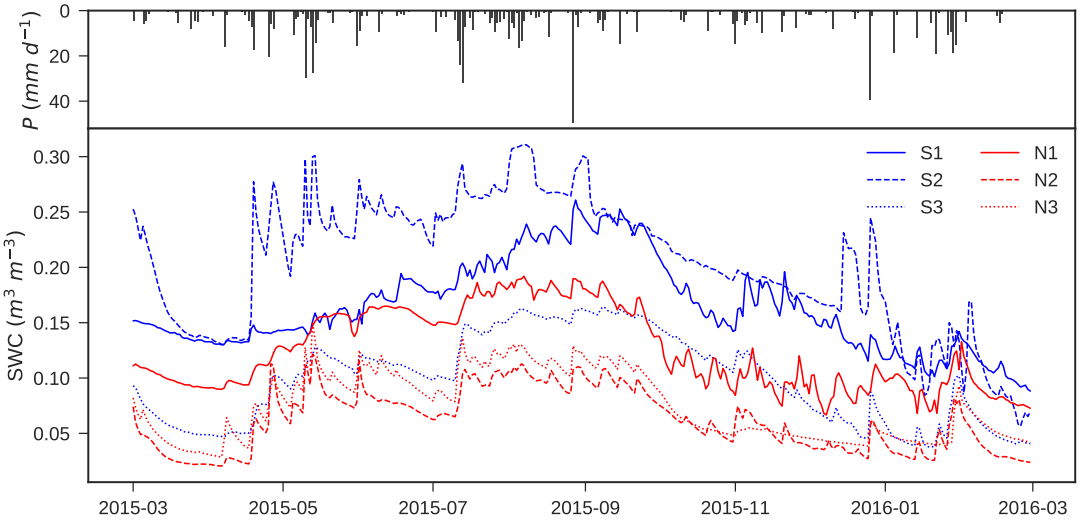

Figure 3.7: Surface soil water content (SWC) dynamics at each plot during the monitoring period.

SWC was not associated with slope aspect (R^2 : 0.04, not shown), however, northness (Rasmussen et al. 2015) - the cosine of aspect times the sine of slope - was able to explained 45 % of the variation (Fig. 3.8c).

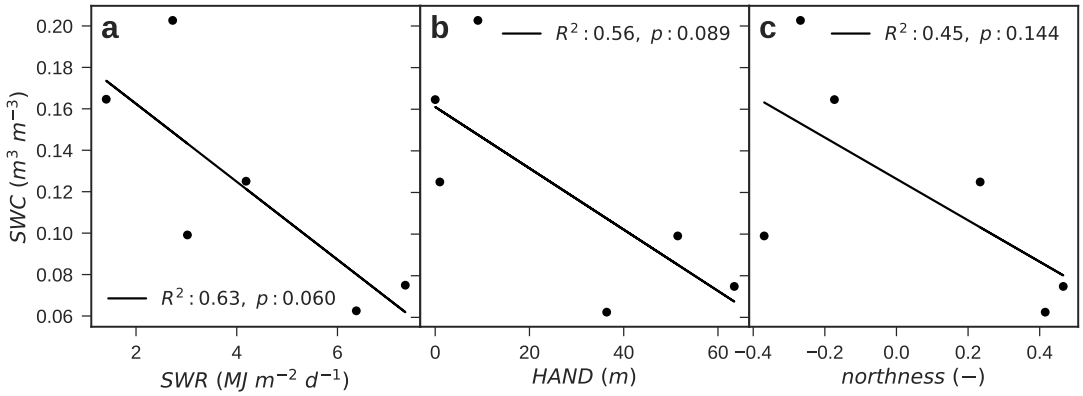

Figure 3.8: Relationship between annual mean surface soil water content (SWC) and a) mean daily short-wave radiation (SWR) b) elevation (z) and c) northness, the product of the sine of the slope and the cosine of aspect (Rasmussen et al. 2015)

3.3.3 Understory vegetation

On the lower south-facing slope (S1) the understory mainly consisted of rough tree ferns (*Cyathea australis*) with very few other broad-leaved species (water ferns (*Blechnum nudum*), sword grass (*Lepidosperma elatius*)) (Tab. 3.3). Tree fern density decreased towards the mid-slope plot (S2) and mainly bracken ferns (*Pteridium esculentum*), water ferns, sword grass and Hop goodenia (*Goodenia ovata*) were present. Apart from those broad-leaved species, occasional prickly currant bushes (*Coprosma quadrifida*) were abundant. In the upper parts of the hillslope the tree ferns disappeared and the understory at S3 mainly consisted of bracken ferns, small-leaved species (e.g. *Leptospermum phylicoides*, *Correa lawrenceana*) and occasional small blanket leaves (*Bedfordia arborescens*). The ridge and mid-slope areas of the northern aspect were dominated by prickly small-leaved species (e.g. *Coprosma quadrifida*, *Leptospermum juniperinum*, *Hakea sericea*) and eucalypt saplings at the ridge plot (N3). Towards the mid-slope plot (N2) bracken ferns (*Pteridium esculentum*), cauliflower bush (*cassinia longifolia*) and hairpin banksia (*Banksia spinulosa*) became more abundant and the eucalypt saplings disappeared. The prickly shrubs were still present

at the gully plot (N1), but bracken ferns, water ferns, tree ferns and other broad-leaved species also were abundant at N1, but at lower densities compared to the southern aspect.

Leaf area index (LAI) was generally higher on the southern aspect compared to the north-facing plots (Fig. 3.9).

On the south-facing slope, the mid-slope plot (S2) carried the highest understory LAI, followed by S1 and with a larger gap S3. Almost all leaf area at plot S1 was attributed to tree ferns, especially tall ones (>1.5 m height). Non-tree fern understory leaf area at S1 was very low due to very sparse cover. At plot S2 tree ferns only contributed ∼25% of the LAI, with majority made up by other broad-leaved understory species. No tree ferns were abundant at S3 and some prickly species replaced water ferns and sword grasses, explaining the relatively steep LAI decrease.

A clear drop-off between the gully (N1) and the remaining plots was observed on the northern aspect. Higher understory cover and a shift to broader leaved species (bracken ferns, water ferns, sword grass) manifested in larger understory LAI at N1, compared with plot N2 and N3. At the ridge plot (N3) most understory leaf area was located in small eucalypt saplings, but their coverage was relatively low. Although more vegetation cover was observed at mid-slope plot, less leaf area was recorded due to the absence of broad-leaved species. Tree ferns only contributed little leaf area at N1 on the northern aspect (Fig. 3.9).

Understory LAI was moderately correlated to mean sub-canopy daily SWR (Fig. 3.10a) and drainage position (Fig. 3.10c), whereas mean surface SWC alone could explain 98% of the LAI variations between plots (Fig. 3.10b).

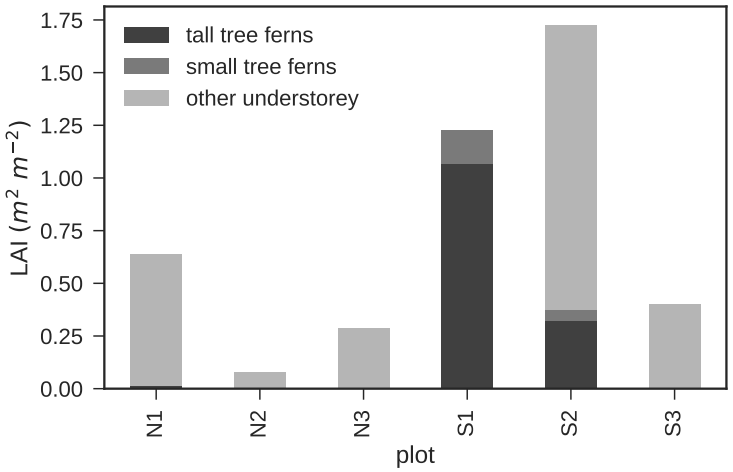

Figure 3.9: Leaf area index (LAI) contribution of tall tree ferns (>1.5 m height), small tree ferns (<1.5 m height) and all other understory species (<1.5 m height) at each plot.

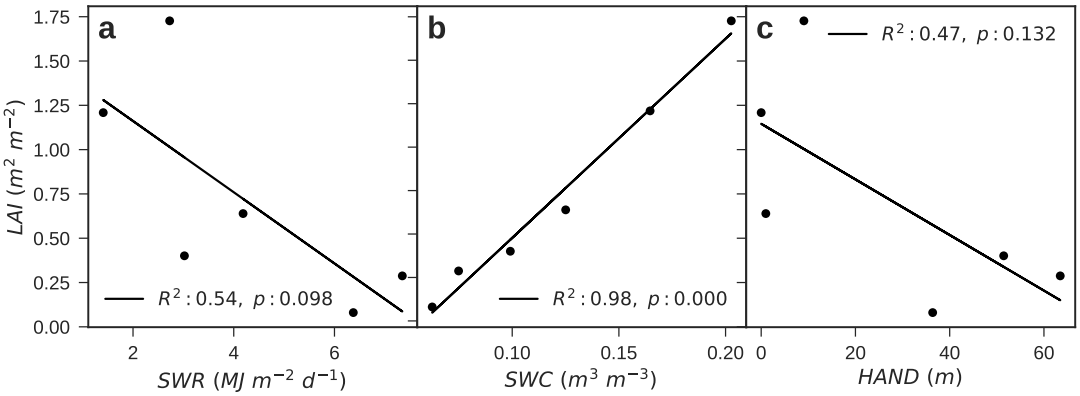

Figure 3.10: Understory leaf area index (LAI) in relation to (a) mean daily short-wave radiation (SWR),(b) mean surface soil water content (SWC) and (c) plot elevation.

3.3.4 Understory and forest floor ET

Annual understory evapotranspiration (ET_U) totals between the transects were relatively similar, with 143 mm at the north-facing slope and 127 mm on the southern aspect (Fig. 3.11b). On the northern aspect, the ridge plot (N3) had the highest ET_U (158 mm), declining to 135 mm at the mid-slope position (N2) and 138 mm in the gully (N1). On the south-facing transect differences between plots were larger, where ET_U increased from 116

mm at the gully plot (S1) to 160 mm at the mid-slope position (S2) before declining to 105 mm at the ridge top (S3). ET_U followed a seasonal pattern at all sites, with highest ET_U rates during (early) summer and generally lower rates throughout the winter month (Fig. 3.11a). ET_U mainly tracked sub-canopy radiation and was generally more dynamic on the northern aspect as a result of higher radiation loads due to slope orientation. Despite low sub-canopy radiation loads, ET_U totals at S1 and S2 were high due to large amounts of leaf area and high SWC (Fig. 3.11 & Tab. 3.3). On the other hand, high radiation loads on the dry upper northern aspects had adverse effect on LAI (Fig. 3.10a) and SWC (Fig. 3.8a) permitting higher ET_U totals.

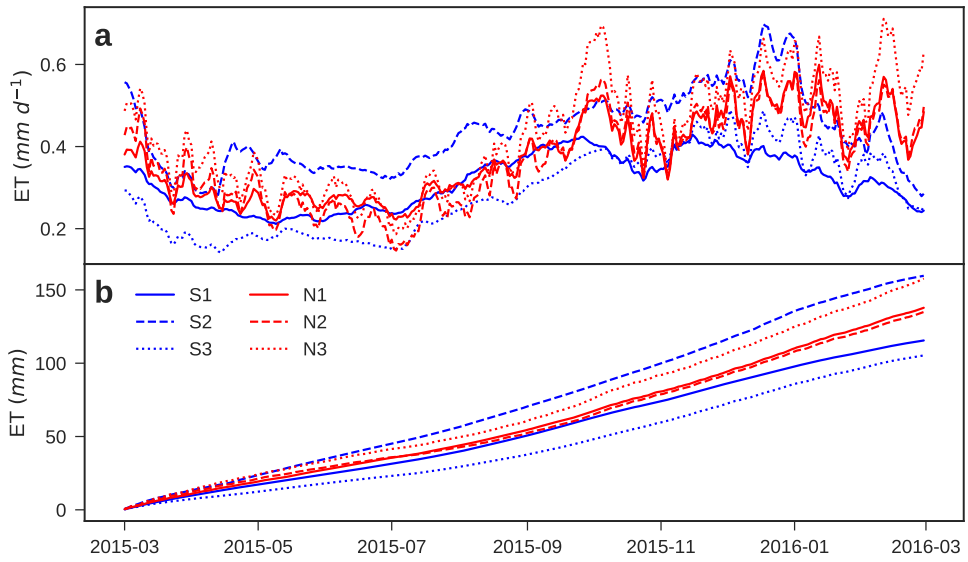

Figure 3.11: Daily (a) and cumulative sums (b) of understory transpiration and soil evaporation (ET) at each monitoring plot.

ET efficiency (ET_{eff}), the ratio of total latent heat of the water vaporized (in $MJ\ m^{-2}$) to the total short-wave radiation (in $MJ\ m^{-2}$), also revealed water-limitation patterns in relation to different landscape positions. ET_{eff} ranged between 0.15 and 0.23 on the northern aspects, whereas ET_{eff} of 0.24 - 0.58 were reached on the south-facing slopes

(Fig. 3.12a). Higher values of ET_{eff} indicate that a larger fraction of short-wave radiation was converted to ET_U fluxes, implying less water-limitation. A more pronounced trend with hillslope position was observed on the southern-aspect, where ET_{eff} constantly increased down-slope. Conversely, no difference between the mid-slope (N2) and ridge (N3) was observed on the northern transect and ET_{eff} only increased at the gully plot (N1). Differences between sites could be related to LAI, which explained 66% of the variability (Fig. 3.12b).

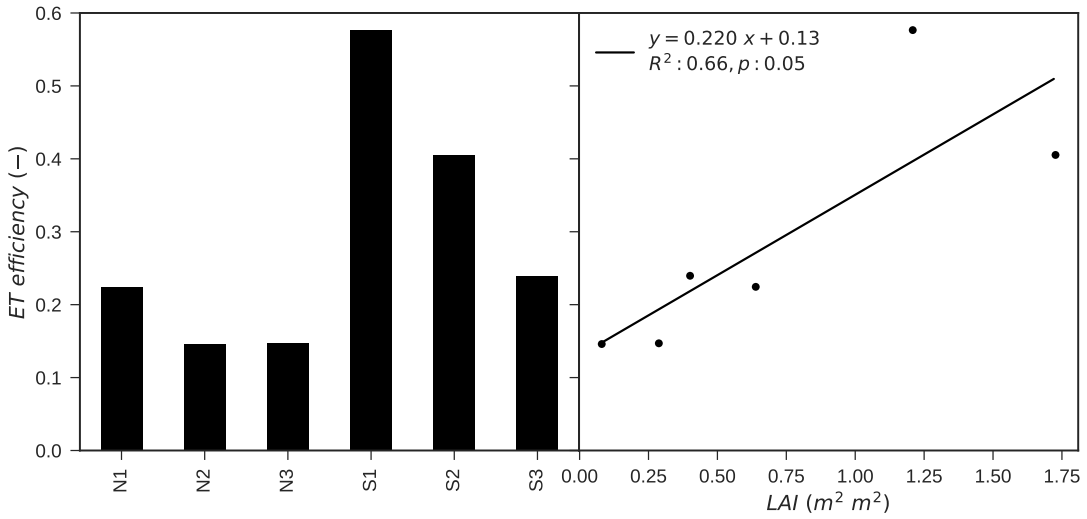

Figure 3.12: Annual ET efficiency per site (a) and in relation to plot leaf area index (LAI)(b). ET efficiency was defined as the ratio of annual latent heat of vaporization sums to the annual short-wave radiation energy.

At annual scale, no significant relation between ET_U totals and landscape position was found (Fig. 3.13). Neither TWI nor HAND, which both characterize the drainage position (Fig. 3.13b,c) were able explain the observed spatial ET_U patterns. Northness, a metric capturing slope effects on local energy and moisture status (Fig. 3.13a), explained 21% of the variation, but the relationship was statistically not significant.

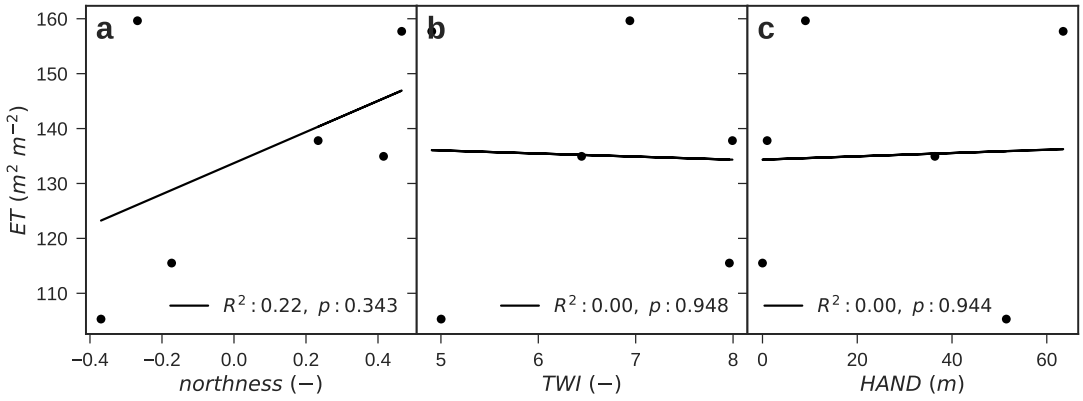

Figure 3.13: Regression analysis of annual understory ET with (a) northness (LAI), (b) the topographic wetness index (TWI) and (c) height above nearest drainage (HAND).

3.4 Discussion

This study showed that annual ET_U did not organize in response to landscape position. Even though understory vegetation characteristics (LAI, species composition) and sub-canopy energy and moisture patterns varied largely along a forested valley cross-section, mean annual ET_U was relatively similar between aspects (127 vs 143 mm). However, intra-transect patterns differed. On the north-facing transect, variations between plots were small and the upper hillslope contributed most, whereas the lower hillslope and mid-slope accounted for most of ET_U on the southern aspect with relatively little contribution from the upper hillslope. Understory LAI was correlated to spatial SWC patterns and species composition shifted from broad-leaved species to smaller leaved, prickly species as SWC decreased. Further, the main micro-climatic difference between sub-canopy and above canopy was the short-wave radiation load.

3.4.1 Micro-climate and SWC patterns in relation to topography

Micro-climatic variation between the two sub-canopy weather stations and the open reference weather station was mainly observed in SWR patterns, which were constantly

between 0.1 and 0.3 times the fraction of the SWR received in the clearing (Fig. 3.4). Canopy effect on air temperature was fairly constant throughout the year, whereas VPD variations were largest during winter (Fig. 3.4). Large spikes in the ratio to the open were usually caused by very low values on a single day at the reference station (e.g. in late February).

The effect of vegetation and topography on SWR patterns has been illustrated in Australia (Nyman et al. 2015; Kirkpatrick and Nunez 1980) as well as elsewhere (Zou et al. 2007; Grimmond et al. 2000; Kirkpatrick and Nunez 1980; Gutirrez-Jurado et al. 2013).

However, the 5-fold difference in mean annual sub-canopy SWR over such small spatial extents is noteworthy. A similar range of sub-canopy SWR was observed at ridge-top plots in the same region along a large rainfall gradient ranging from 759 to 1745 mm (Nyman et al. 2017), illustrating how much control topography exerts on vegetation structure, sub-canopy energy and moisture patterns and ultimately ET_U fluxes.

Slope orientation had the largest effect at both slopes during winter, when solar elevation was lowest (Fig. 3.6). On the southern aspect slope orientation caused decreases down to 40 - 70% compared to SWR received on a horizontal surface under the given vegetation at each plot. In contrast, SWR on the sloping surface increased to 120 - 150% compared to the horizontal surface at the north-facing slope. During summer the slope effect diminished and even caused a slight reduction on the northern aspect, since solar elevation was larger than the slope angle (Fig. 3.6).

SWC was generally higher on the southern aspect compared to the north-facing slope and increased in down-slope direction at both transects. Plot S2 was an exception, posing higher mean SWC than plot S1, which might have been caused increase soil water convergence along the hillslope drainage line at S2. Nevertheless, SWC was clearly linked to landscape position, as indicated by the strong correlation to HAND and northness (Fig. 3.8b,c).

Spatial surface SWC patterns have been attributed to topography in general and to aspect in particular (Western et al. 1999; Famiglietti et al. 1998; McMillan and Srinivasan 2015; Martinez et al. 2008), but aspect alone did not explain the spatial SWC patterns in this study (R^2 : 0.04). However, northness - a proxy for the slope angle in northerly direction - explained 45% of spatial variability (Fig. 3.8c). Furthermore, the fact that HAND was stronger correlated to SWC than observed SWR indicated that topographic redistribution played an important role for surface soil moisture in this ecosystem (Fig. 3.8).

3.4.2 Organization of understory vegetation

Understory vegetation patterns were strongly coupled to sub-canopy moisture and energy patterns (Fig. 3.10), as suggested by the eco-hydrological equilibrium theory (Eagleson 1982). Broad leaved species vanished with decreasing SWC and higher radiation loads, whereas small leaved, prickly species became more abundant at the drier plots (Tab. 3.3). Understory LAI was closely linked to spatial SWC patterns (Fig. 3.10) and corresponded with abundance of broad leaved species (Tab. 3.3).

Tree ferns (*C. australis*) grew almost exclusively on the lower southern hillslope and only few were abundant at the north gully plot (Fig. 3.9). The preference of a shaded habitat is in accordance with observed high light level stress of tree ferns (Volkova et al. 2009). Bracken ferns were the only broad-leaved species that was abundant at all plots, with exception of the north ridge plot. Although bracken fern is relatively drought tolerant (Hollinger 1987; Gordon et al. 1999), it has little control over its leaf temperature during hot sunny days (Miller and Gates 1967), which might explain its absence at the most sun exposed plot (N3). Sedges (*L. elatius*) tend to be hygrophilous (Barrett 2013) and hence were mostly abundant on the wet gully plots. The small-leaved, prickly species contributed little to the plot LAI, thus the dry plots (N3 & N2) had low LAI values. In addition, plot

N3 had higher than expected LAI because a fair amount of small eucalyt saplings (<1 cm DBH) were present which contributed most to LAI.

3.4.3 Dominant controls on ET_U

Few studies have been carried out in Australian eucalypt forests that measured ET_U, and this study is the first to my knowledge that investigated ET_U patterns in eucalypt forests at hillslope scale along water-availability gradients.

However, no general pattern with landscape position could be established (Fig. 3.13). On the contrary, topography seemed to mitigate ET_U differences via contrasting energy and moisture availability. Mean ET_U was relatively similar between slopes despite large differences in understory vegetation characteristics (LAI, species composition), sub-canopy moisture and energy patterns between plots (Tab. 3.3). However, hillslope position had contrasting impacts on ET_U rates at each hillslope. The lower and mid-slope areas had higher ET_U on the southern aspect, whereas ET_U was largest on the upper hillslope of the drier, north-facing transect.

Similar annual ET_U to this study have been reported from eucalypt forests elsewhere in SE Australia. Mitchell et al. (2012b) documented ET_U of 144 mm, which was measured at two bottom-slope plots with a mean canopy height of 31.4 & 33.8 m and LAI 1.3 - 1.8 $m^2\ m^{-2}$. Nolan et al. (2014) reported 166-188 mm in a dry 25 m tall forest (LAI=2.1 $m^2\ m^{-2}$) and 135-154 mm in a damp 40 m tall forest (LAI=2.1 $m^2\ m^{-2}$). Even in tall mountain ash forests annual ET_U totals ranged from 8 to 26% (116-297 mm) (Benyon et al. 2017). Hence, this study confirms that ET_U contribution are significant and should not be neglected in complex terrain either.

In drier, open eucalypt woodlands, forest floor ET has even been identified as the largest ET component (Mitchell et al. 2009), where rates ranged from 0.3 - 1.0 $mm\ d^{-1}$ and

represented 38 - 64% of total ET. Little to no understory presence as well as mean tree height (13 - 18 m) were comparable to the upper north-facing hillslope of this study.

In general, variations in ground vegetation cover has been shown to have little impact on ET_U rates in (semi-) arid ecosystems, because in the absence of vegetation soil water is evaporated regardless (Huxman et al. 2005). However, ET_{eff} across sites in this study revealed clear patterns of water-limitation on ET_U. At the driest sites (N3 & N2), only $\sim$15% of sub-canopy radiation load was converted to ET_U compared to up to 60% on the lower south-facing slope, illustrating the 'excess energy' that could be utilized for ET with more available water.

The strong relationship between annual mean SWC and LAI enables to model understory ET purely as a function of LAI and sub-canopy SWR. Theoretically, higher LAI and SWC should lead to larger ET rates. However, energy is needed to evaporate and to transpire water and SWR was inversely correlated with SWC and LAI (Fig. 3.8). As a result, annual ET_U rates were fairly similar given the large range of LAI, SWR and SWC observations between plots. Sub-canopy LAI and SWR could potentially be derived from LiDAR data, which would offer the potential of scaling ET observations to large areas.

3.5 Conclusion

This study showed that annual understory and forest floor ET (ET_U) did not organize in response to landscape position. Main micro-climatic variation was observed in short-wave radiation patterns, which in turn altered surface soil moisture patterns. Understory LAI as well as species composition organized in response to sub-canopy light and moisture status.

However, the interaction of energy, moisture and vegetation patterns mediated understory ET differences between landscape positions. Sub-canopy radiation was the main driver of ET_U, but also had an ambiguous effect on ET_U. While providing energy to evaporate

water, sub-canopy radiation simultaneously decreased the plant available water through increased evaporation and hence decreased shrub LAI as well, effectively limiting ET_U. This could be illustrated by the ET_U efficiency, which related the incoming energy of short-wave radiation to the outgoing energy from the latent heat of vaporization. ET_U efficiency was high at buffered parts of the landscape, where large LAI resulted in high ET_U rates despite low radiation. In contrast, sun-exposed parts of the landscape had little ET_U efficiency.

Prediction of ET_U as a function of sub-canopy radiation and LAI patterns, offers huge potential for LiDAR application, which can be used to map sub-canopy radiation (LPI model) and understory LAI, and would thus be a useful tool to scale ET_U fluxes across the landscape.

Bibliography

Barrett, R. L. (2013). "Ecological importance of sedges: a survey of the Australasian Cyperaceae genus Lepidosperma". In: *Annals of Botany* 111.4, pp. 499–529.

Benyon, R. G. et al. (2017). "Stand-level variation in evapotranspiration in non-water-limited eucalypt forests". In: *Journal of Hydrology* 551, pp. 233–244.

Beven, K. J. and M. J. Kirkby (1979). "A physically based, variable contributing area model of basin hydrology". In: *Hydrological Sciences Bulletin* 24.1, pp. 43–69.

Budyko, M. I. (1974). *Climate and Life*. Orlando, Fl: Academic.

Dawson, T. E. et al. (2007). "Nighttime transpiration in woody plants from contrasting ecosystems". In: *Tree Physiology* 27.4, pp. 561–575.

Dios, V. R. Resco de et al. (2015). "Processes driving nocturnal transpiration and implications for estimating land evapotranspiration". In: *Scientific Reports* 5, p. 10975.

Eagleson, P. (1982). "Ecological optimality in water-limited natural soil-vegetation systems: 1. Theory and hypothesis". In: *Water Resources Research* 18.2, pp. 325–340.

Famiglietti, J. S. et al. (1998). "Variability in surface moisture content along a hillslope transect: Rattlesnake Hill, Texas". In: *Journal of Hydrology* 210.1, pp. 259–281.

Givnish, T. J. et al. (2014). "Determinants of maximum tree height in Eucalyptus species along a rainfall gradient in Victoria, Australia". In: *Ecology* 95.11, pp. 2991–3007.

Gordon, C. et al. (1999). “Effects of environmental change, including drought, on water use by competing Calluna vulgaris (heather) and Pteridium aquilinum (bracken)”. In: *Functional Ecology* 13 (s1), pp. 96–106.

Grimmond, C. S. B. et al. (2000). “Spatial variability of micro-climatic conditions within a mid-latitude deciduous forest”. In: *Climate Research* 15.2, pp. 137–149.

Groeneveld, D. P. (1997). “Vertical point quadrat sampling and an extinction factor to calculate leaf area index”. In: *Journal of Arid Environments* 36, pp. 475–485.

Gutirrez-Jurado, H. A. et al. (2013). “On the observed ecohydrologic dynamics of a semiarid basin with aspect-delimited ecosystems: ecohydrologic dynamics of a semiarid basin”. In: *Water Resources Research* 49.12, pp. 8263–8284.

Hollinger, D. Y. (1987). “Photosynthesis and Stomatal Conductance Patterns of Two Fern Species From Different Forest Understoreys”. In: *The Journal of Ecology* 75.4, p. 925.

Huxman, T. E. et al. (2005). “Ecohydrological implications of woody plant encroachment”. In: *Ecology* 86.2, pp. 308–319.

Kirkpatrick, J. B. and M. Nunez (1980). “Vegetation-Radiation Relationships in Mountainous Terrain: Eucalypt-Dominated Vegetation in the Risdon Hills, Tasmania”. In: *Journal of Biogeography* 7.2, p. 197.

Macfarlane, C. and G. N. Ogden (2012). “An improved evaporation dome for forest environments”. In: *Computers and Electronics in Agriculture* 89, pp. 126–129.

Martinez, C. et al. (2008). “Spatiotemporal distribution of nearsurface and root zone soil moisture at the catchment scale”. In: *Hydrological Processes* 22.14, pp. 2699–2714.

McMillan, H. K. and M. S. Srinivasan (2015). “Characteristics and controls of variability in soil moisture and groundwater in a headwater catchment”. In: *Hydrology and Earth System Sciences* 19.4, pp. 1767–1786.

Miller, P. C. and D. M. Gates (1967). "Transpiration Resistance of Plants". In: *American Midland Naturalist* 77.1, p. 77.

Mitchell, P. J. et al. (2009). "Partitioning of evapotranspiration in a semi-arid eucalypt woodland in south-western Australia". In: *Agricultural and Forest Meteorology* 149.1, pp. 25–37.

Mitchell, P. J. et al. (2012b). "Responses of evapotranspiration at different topographic positions and catchment water balance following a pronounced drought in a mixed species eucalypt forest, Australia". In: *Journal of Hydrology* 440-441, pp. 62–74.

Monteith, J. L. and M. H. Unsworth (2013). *Principles of environmental physics: plants, animals, and the atmosphere*. 4th ed. Amsterdam ; Boston: Elsevier/Academic Press. 401 pp.

Moore, G. W. et al. (2008). "Nocturnal transpiration in riparian Tamarix thickets authenticated by sap flux, eddy covariance and leaf gas exchange measurements". In: *Tree Physiology* 28.4, p. 521.

Nobre, A. et al. (2011). "Height Above the Nearest Drainage: a hydrologically relevant new terrain model". In: *Journal of Hydrology* 404.1, pp. 13–29.

Nolan, R. H. et al. (2014). "Changes in evapotranspiration following wildfire in resprouting eucalypt forests". In: *Ecohydrology*, pp. 1363–1377.

Nyman, P. et al. (2014). "Downscaling regional climate data to calculate the radiative index of dryness in complex terrain". In: *Australian Metrological and Oceanographic Journal* 64.2, pp. 109–122.

Nyman, P. et al. (2015). "Quantifying the effects of topographic aspect on water content and temperature in fine surface fuel". In: *International Journal of Wildland Fire* 24.8, pp. 1129–1142.

Nyman, P. et al. (2017). “Evaluating models of shortwave radiation below Eucalyptus canopies in SE Australia”. In: *Agricultural and Forest Meteorology* 246, pp. 51–63.

Ogle, K. et al. (2012). “Differential daytime and night-time stomatal behavior in plants from North American deserts”. In: *New Phytologist* 194.2, pp. 464–476.

Oliphant, A et al. (2006). “Local-scale heterogeneity of photosynthetically active radiation (PAR), absorbed PAR and net radiation as a function of topography, sky conditions and leaf area index”. In: *Remote Sensing of Environment* 103.3, pp. 324–337.

Rasmussen, C. et al. (2015). “Quantifying Topographic and Vegetation Effects on the Transfer of Energy and Mass to the Critical Zone”. In: *Vadose Zone Journal* 14.11.

Spencer, J. W. (1982). “A comparison of methods for estimating hourly diffuse solar radiation from global solar radiation”. In: *Solar Energy* 29.1, pp. 19–32.

Steinwand, A. L. et al. (2001). “Transpiration coefficients for three Great Basin shrubs”. In: *Journal of Arid Environments* 49.3, pp. 555–567.

Volkova, L. et al. (2009). “Effects of sudden exposure to high light levels on two tree fern species Dicksonia antarctica (Dicksoniaceae) and Cyathea australis (Cyatheaceae) acclimated to different light intensities”. In: *Australian Journal of Botany* 57.7, p. 562.

Ward, P. R. and S. F. Micin (2006). “The capacity of dryland lucerne for groundwater uptake”. In: *Australian Journal of Agricultural Research* 57.5, p. 483.

Western, A. W. et al. (1999). “Observed spatial organization of soil moisture and its relation to terrain indices”. In: *Water Resources Research* 35.3, pp. 797–810.

Zapata-Rios, X. et al. (2016). “Influence of terrain aspect on water partitioning, vegetation structure and vegetation greening in high-elevation catchments in northern New Mexico: Terrain Aspect, Water Partitioning, Vegetation Greening in High-elevation Catchments”. In: *Ecohydrology* 9.5, pp. 782–795.

Zeppel, M. et al. (2010). “Rates of nocturnal transpiration in two evergreen temperate woodland species with differing water-use strategies”. In: *Tree Physiology* 30.8, pp. 988–1000.

Zou, C. B. et al. (2007). “Effects of topography and woody plant canopy cover on near-ground solar radiation: Relevant energy inputs for ecohydrology and hydropedology”. In: *Geophysical Research Letters* 34.24.

Chapter 4

Forest water balance partitioning in complex terrain

4.1 Introduction

Most ecosystem services provided by forests are influenced by the water balance, some directly (e.g. water supply, ground water recharge) and other indirectly (e.g. forest productivity, carbon sequestration etc.) (Watanabe and Ortega 2011). Within an ecosystem, precipitation is partitioned into evapotranspiration (ET), runoff (R), deep drainage (D) and storage (S). However, rainfall partitioning depends on climatic inputs (Budyko 1974), as well as the ecosystem structure and functional state (Brown et al. 2005; Donohue et al. 2007; Williams et al. 2012; Flerchinger et al. 2010) that is determined amongst others by soil properties, topography, time since disturbance (e.g. fire) and successional phase (Jefferson et al. 2010; Savenije 2010). Precipitation will either be intercepted by vegetation or litter, run-off or infiltrate into the soil. Depending on soil water content (SWC), water will either be stored in the soil column, where it can be utilized by biotic and abiotic processes, or drain deeper into deeper layers eventually contributing to base flow or ground water recharge. Hence, larger fraction of surface run-off manifests in less plant-available water (Troch et al. 2009), higher erosion rates and fashier hydrographs. In addition to

water-availability for biotic and abiotic processes, water quality will be higher when run-off is filtered via longer flowpaths through the soil and stream flow will be buffered against extreme precipitation events (Neary et al. 2009).

Evapotranspiration provides direct (surface cooling) and indirect (carbon sequestration) ecosystem services. However, transpiration (T) is more efficient in cooling the surface as roots can access large subsurface water stores and thus potentially consume higher energy loads than soil evaporation (E) alone, which is limited to surface soil moisture (Silberstein et al. 2001). Furthermore, lower albedo of vegetated surfaces compared to bare and dry soils also alters the energy balance by reflecting a larger fraction of incoming short-wave radiation. Shifting ET allocation more towards T likely increases ecosystem processes (e.g. forest productivity, pedogenesis) as water will percolate through the soil and plants, whereas E will remove water from the topsoil with limited opportunity to be utilized by organisms and plants.

Water balance partitioning and scaling remain a key challenges in eco-hydrology (Asbjornsen et al. 2011) due to complex interactions and feedbacks between climate and ecosystem state, that might vary strongly between climates and ecosystems types. This is particularly challenging in complex terrain, where the transition from water to energy limitation can occur over small scales (Nyman et al. 2014). However, climate and ecosystem state are not independent and vegetation, soils and topography adjust to climatic forcing with increasing time lag.

Further,the eco-hydrological equilibrium theory (Eagleson 1982) states that vegetation optimizes to maximize soil moisture in water-limited ecosystems. For example, in multi-strata forests, the total combined LAI of understory and overstory has been linked to water-availability (Specht 1983; Specht et al. 2006; Specht 1972) and one strata can compensate for loss of LAI in a different strata (e.g. understory LAI increased following

disturbance of the overstory (Macfarlane et al. 2010)). Thus, vegetation patterns organize in response to water-availability, which in turn resulted from co-evolution of climate, vegetation, soils and topography at a given location. However, understory vegetation patterns are expected to be particularly sensitive to soil moisture due to shallower rooting depth. While prolonged dry periods might prohibit understory vegetation cover due prolonged low surface soil moisture, deep rooted plants might still have access to sub-soil moisture storage, an thus water-availability might substantially differ for overstory and understory at a given landscape position. Even overstory trees trade-off productivity for additional safety against hydraulic failure with increasing aridity and water-stress (Hacke et al. 2006; Pfautsch et al. 2016; Poorter et al. 2010). Therefore, vegetation patterns and phenology might be suitable indicators to monitor (via remote sensing) the state of ecosystems (Thompson and Katul 2011). Further, vegetation manipulation is one important management option available to catchment managers, e.g. thinning (Hawthorne et al. 2013), fuel reduction burns. Thus, we need to advance the understanding of interactions between water balance and vegetation across scales and ecosystems.

This study aims to quantify fine-scale sub-catchment water balance partitioning as a function of aspect and drainage position. Further, it aims to test whether vegetation patterns reflect the magnitude of water balance components and could therefore be used to map sub-catchment forest water balance partitioning.

4.2 Methods

4.2.1 Precipitation measurement

Precipitation was measured in two clearings close to the plots (<4 km away). Rain gauges (TB3, Hydrological Services Pty. Ltd, Warwick Farm, NSW, Australia), logging at 5

minute intervals, were installed at high and low elevation to account for orographic rainfall gradients between plot locations.

4.2.2 Throughfall measurement

Throughfall was funneled into 20 L plastic drums using 1.2 m long and 0.14 m wide metal troughs (Fig. 4.1). Three set-ups were randomly placed within each plot and drums were emptied at each site visit (usually every fortnight).

Figure 4.1: Example of throughfall trough installation, illustrating the slope effect on the trough surface area.

4.2.3 Streamflow measurement

Stream flow was measured at a culvert, which was already in place to prevent erosion of the Upper Yarra Aqueduct Track. A small depression before the culvert was concreted to prevent streamflow seeping underneath the culvert. Stage height was recorded in the concreted pool using a capacitance water level sensor (Odyssey Capacitance Water Level Logger, Dataflow Systems Ltd., Christchurch, NZ). The recorded stage height (Fig. 4.2a) was calibrated to streamflow rates (Fig. 4.2b) by measuring outflow volume of the culvert, which was collected in large containers and weighted using a hanging balance. After the

first few flow events, culvert leaks were discovered and the inside of the culvert was line with plastic cover on 29.07.2015.

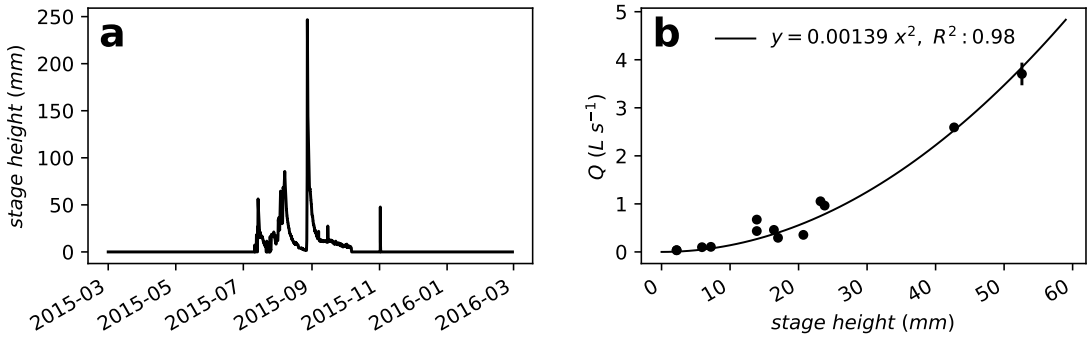

Figure 4.2: Recorded stage height (a) and rating curve (b) relating stage height to stream flow (Q).

4.2.4 Soil water storage calculation

Soil water storage (S) was calculated from continuous soil water content (SWC) sensor data and soil depth measurements. Soil thickness was measured up to 3 m depth by hand augering. SWC sensors were installed at 10, 30, 50, 75 and 100 cm depth when soils thickness permitted. Measured SWC at each depth was assumed to be representative until the half-way point between sensors. S was then calculated by multiplying soil layer thickness by the volumetric SWC. When soil depth exceeded SWC instrumentation the sensor reading at 100 cm was assumed to be representative for the remaining soil profile. Two sensors had to be removed from analysis due to malfunction (erratic noise and extremely low and unresponsive values).

4.2.5 ET measurement

Overstory transpiration was measured using sap flow sensors on five to six trees per plot. Transpiration total of each tree in each plot was predicted using a Random Forest model

trained with sap flow observations of all 36 trees, plot inventory data, climate data, soil moisture data from each plot and topographic data. Plot-scale overstory transpiration totals were derived by summing up transpiration of each tree within a plot. Understory transpiration and soil evaporation measurements with a closed chamber during campaigns were used to build a regression model using below canopy radiation and soil moisture. Bulk interception loss for overstory and understory was calculated from the difference between throughfall measurements and precipitation recorded in a clearing near-by. Detailed procedures were described in the previous chapters.

4.2.6 Water balance

The water balance was calculated as

$$P = Q + ET + \Delta S + D + e \tag{4.1}$$

$$ET = T_O + I + ET_U \tag{4.2}$$

$$I = P - TF - SF \tag{4.3}$$

where P is the precipitation, Q the streamflow, ET the evapotranspiration, ΔS the change in (soil) water storage, D the deep drainage, e an error term accounting for measurement errors, T_O the overstory transpiration, I the canopy interception loss, ET_U the understory and forest floor evapotranspiration, TF throughfall and SF stemflow, where SF was set to 4% of P based on previous studies in similar forests (Crockford and Richardson 2000).

4.3 Results

4.3.1 Precipitation

918 mm of precipitation (P) were recorded during the monitoring period. However, rainfall totals recorded at the nine closest Bureau of Meteorology (BoM) stations during the

monitoring period ranged from 615 to 1040 mm with an average of 797 mm, corresponding to 45 to 96% of the long-term averages with a mean of 72% (Tab. 4.1).

Table 4.1: Rainfall records of all Bureau of Meteorology (BoM) stations within 30 km of the field sites that had a complete record during the observation period an >20 years of records. ID: BoM station number, n: number of years on record, $\overline{P}$: mean annual rainfall, SD: standard deviation of annual rainfall , P: observed rainfall during observation period, % of $\overline{P}$: percentage of observed rainfall to mean rainfall. The summary row contains the total sum of Years on record and the means of $\overline{P}$, SD, P and % of $\overline{P}$.

Location	ID	n	$\overline{P}$ (mm)	SD (mm)	P (mm)	% of $\overline{P}$
NOOJEE	85277	37	1034	305	975	94
NOOJEE	85292	28	1020	234	982	96
VESPER	85305	20	1106	286	1040	94
O'SHANNASSY RESERVOIR	86090	103	1370	300	615	45
POWELLTOWN	86094	76	1182	325	633	54
UPPER YARRA DAM	86271	48	1044	226	811	78
GLADYSDALE	86358	34	951	396	654	69
MARYSVILLE	88044	114	1278	344	878	69
BUXTON	88130	48	972	261	591	61
SUMMARY	-	508	1106	297	797	72

However, P anomalies occurred mostly west and north of the field sites (Fig. 4.3), wheres P values close to long-term means were only recorded at the two gauges in Noojee and in Vesper south-east from the field sites, suggesting prevailing winds were more southerly than usual. Therefore, P was more likely to cease during southerly wind on the southern flanks of Upper Yarra ranges before reaching the field sites and close-by BoM rain gauges. Thus, the rainfall measurements were likely of good quality and below the long-term mean.

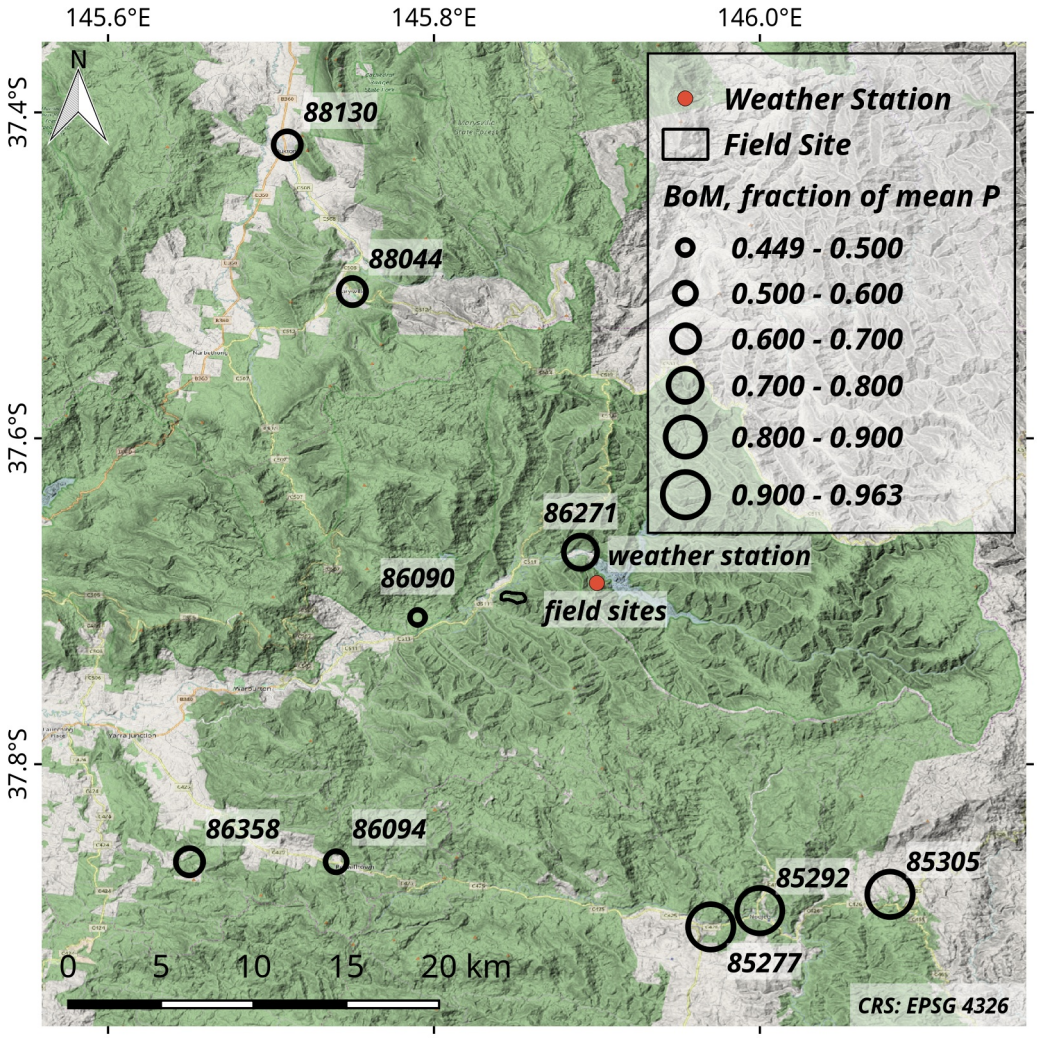

Figure 4.3: Location and fraction of mean precipitation recorded at Bureau of Meteorology (BoM) rain gauges during the monitoring period.

4.3.2 Evapotranspiration

Overstory transpiration (T_O) was the largest water balance component at all plots, followed by interception loss (I), understory and forest floor evapotranspiration (ET_U) and streamflow (Q) (Fig. 4.4). However, contributions varied with respect to landscape position. T_O shares ranged from 44% at the upper northern aspects (N3, N2) to 49-51% at plot N1

and S3 to 62 - 67% at the lower south-facing hillslope (S1, S2). ET_U ranged from 10%

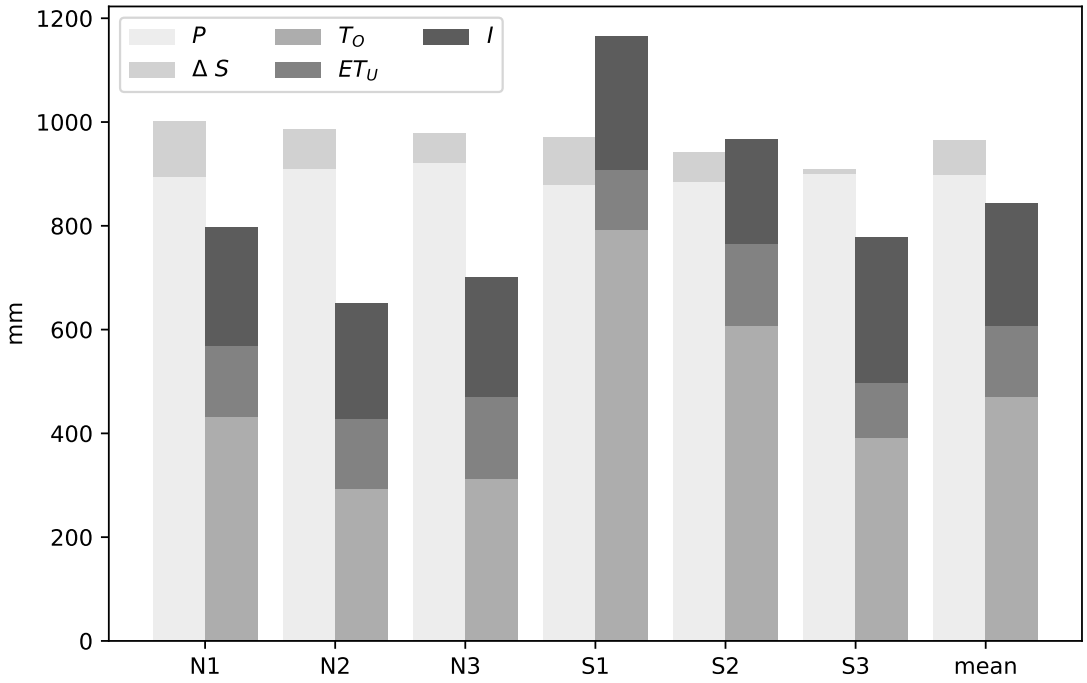

Figure 4.4: Measured water balance components for each monitoring plot and mean across all sites. P: precipitation, Δ S: soil water storage change, T_O: overstory transpiration, ET_U: understory transpiration and forest floor evaporation, I: interception loss.

at S1 to 22% at N3 and its contribution was generally higher on the northern aspects (>17%) than on the south-facing hillslope (<17%). Interception loss (I) accounted for 201 to 281 mm of the water balance and did not vary systematically with landscape position (Fig. 4.4). Interception volumes were on average higher but also more variable on the southern aspect (246 ±41 mm) compared to the north-facing transect (227 ±4 mm). In contrast, the contribution of interception loss to the water balance was on average higher on the north-facing slope (34.5%) compared to the southern aspect (26%). Theoretically, throughfall ratios should decline with increasing LAI due to larger canopy storage capacity (Ashton and Bassett 1997; He et al. 2014). However, we did not find a significant relationship between LAI and the ratio of collected throughfall to precipitation (Fig. 4.5a).

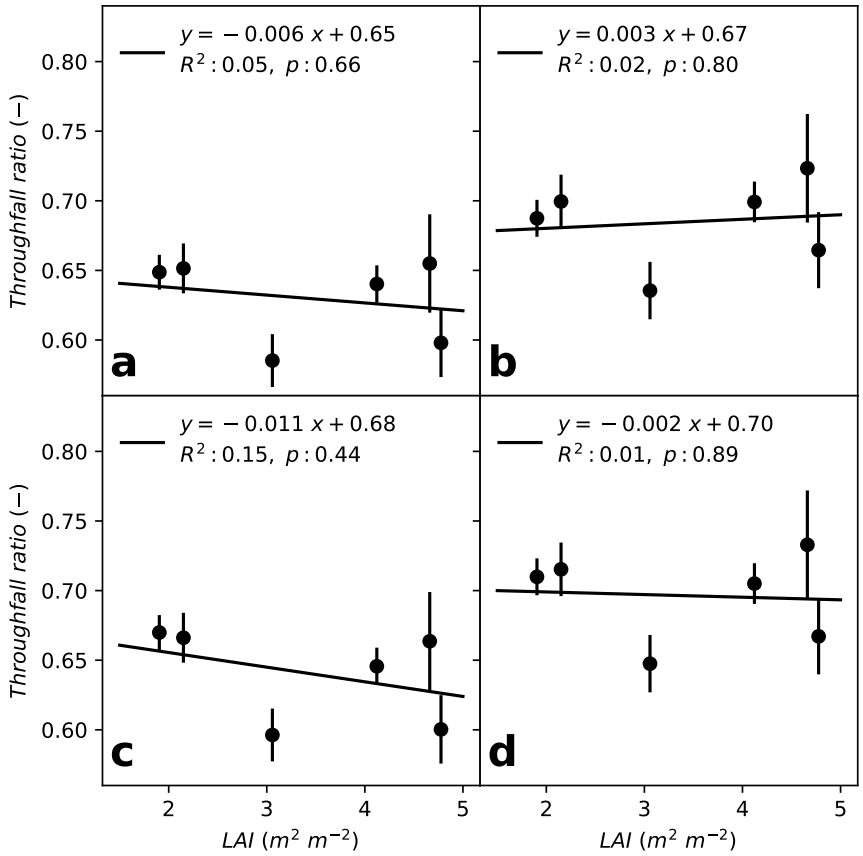

Figure 4.5: Throughfall ratios using a) raw throughfall data and precipitation from the reference weather station, b) corrected for orographic rainfall gradients c) corrected for trough area d) using both corrections.

Thus, corrections to the throughfall dataset were applied which accounted for site-specific rainfall inputs due to orographic gradients (Fig. 4.5b), varying effective trough area due to installation at roughly half the slope angle (Fig. 4.5c & Fig. 4.1) and a combination of both (Fig. 4.5d). However, after all corrections were applied the LAI to throughfall ratio relationship remained insignificant.

Another possible explanation for no LAI-I relationship could be evaporation from the toughs' metal surface or from the collection drums. Evaporation loss would be largest at north-facing sites with little canopy cover, where radiation loads were highest and thus potentially mediating I differences with LAI. However, no patterns between sites were

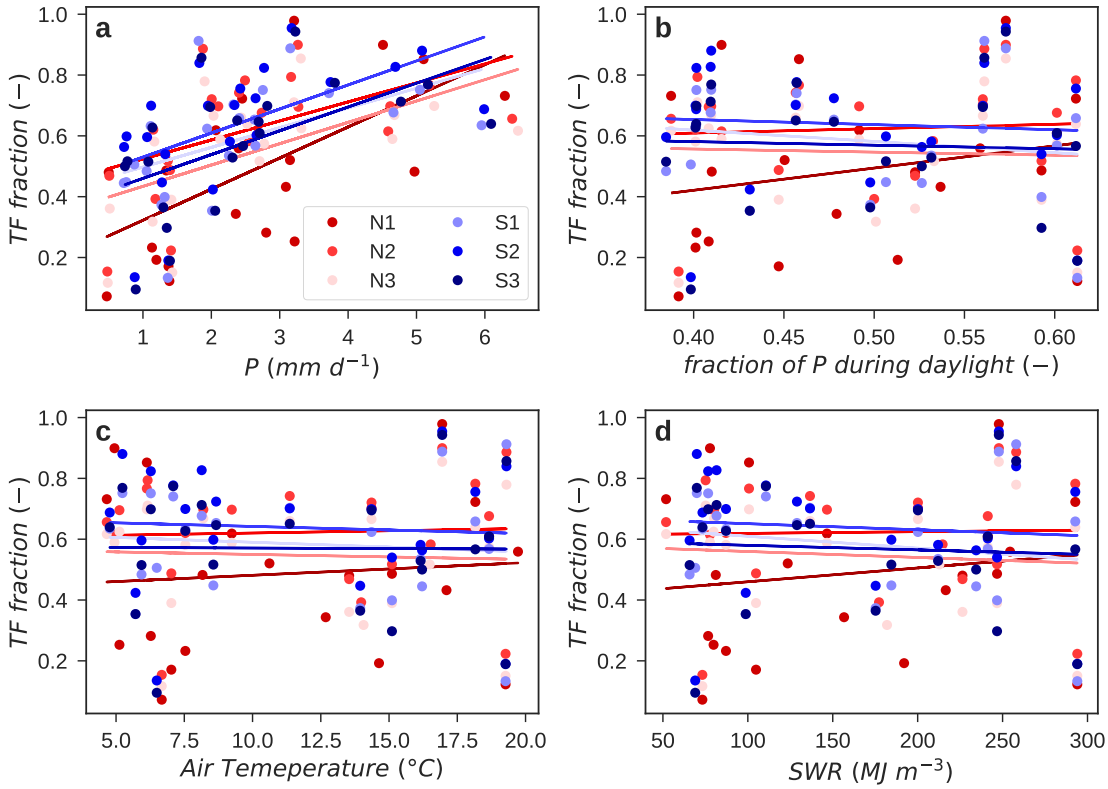

Figure 4.6: Throughfall ratios in relation to (a) daily precipitation (P), (b) the fraction of precipitation recorded during daylight, (c) mean air temperature and (d) mean incoming short-wave radiation (SWR) for each collection interval.

observed relating throughfall ratios to rainfall intensity (Fig. 4.6a), fraction of rainfall during daylight (Fig. 4.6b), mean air temperature (Fig. 4.6c) and mean solar radiation during the collection period (Fig. 4.6d). If evaporation loss from the instruments would have been an issue, differences between north and southern aspects should have emerged, especially during low intensity events and periods with high radiation loads, when contrasting canopy cover would have had the largest impact.

Rainfall distribution could have mitigated the effect of LAI patterns on I as well. High-intensity or long-duration rainfall events, where canopy storage capacity would be exceeded and stay saturated for most part of the rainfall event would lead to more uniform patterns. Similarly, frequent low-magnitude rainfall events that did not saturate the canopy storage

with sufficient time between events to allow depletion of the canopy storage could also explain more uniform throughfall patterns. However, the recorded rainfall distribution agreed well with the long-term distributions of the selected BoM stations (Fig. 4.7). Hence, uniform throughfall patterns across the LAI gradient cannot be attributed to rainfall intensity anomalies during the monitoring period and seem to be a feature of this ecosystem.

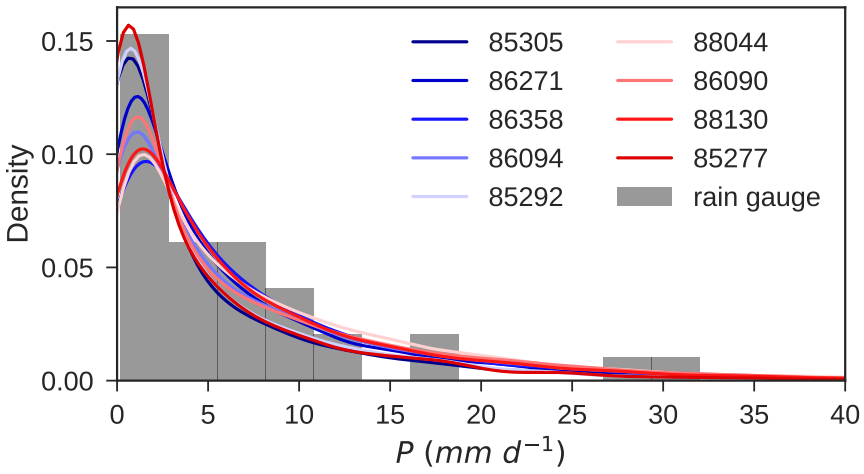

Figure 4.7: Rainfall distribution of the rain gauge at the above-canopy weather station and all Bureau of Meteorology rain gauges within 30km distance (see Tab. 4.1).

4.3.3 Streamflow

Throughout the monitoring period, 15 mm streamflow was recorded with the bulk of the run-off concentrated in two flow events from 5.8.2015 to 10.08.2015 and 27.08.2015 to 06.09.2015 (Fig. 4.8). The streambed was dry most of the year and no streamflow was recorded at all. Thus, annual streamflow values were low compared to the other water balance components (Fig. 4.4).

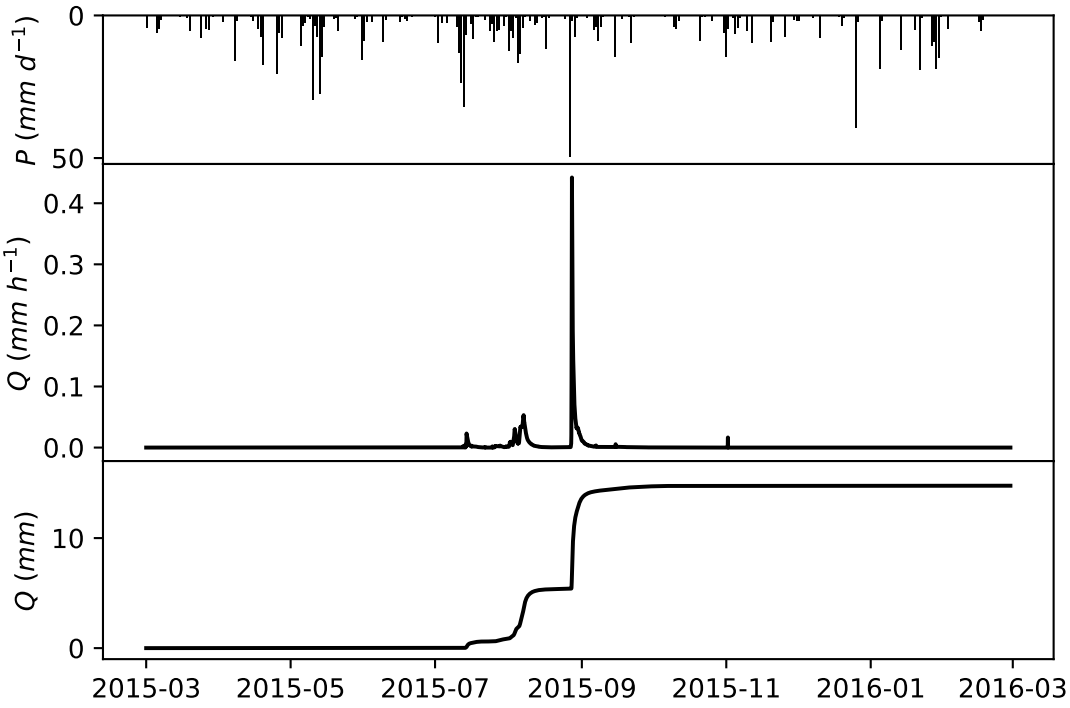

Figure 4.8: (a) Half-hourly recorded streamflow (Q) and (b) cumulative streamflow totals.

4.3.4 Soil water storage

Mean profile SWC at all plots was lower at the end of the monitoring period compared to the start. While SWC deficit varied with drainage position at both transects, it was generally larger on the northern aspect than on the south-facing slope. On the northern aspect, SWC deficit increased from 0.042 m^3 m^{-3} at N1 to 0.101 m^3 m^{-3} at N2 and 0.115 m^3 m^{-3} at N3. In contrast, no clear pattern in relation to drainage position was observed on the south-facing slope, where largest deficit occurred at the mid-slope plot (S2) with 0.052 m^3 m^{-3} followed the gully plot (0.035 m^3 m^{-3}) and 0.020 m^3 m^{-3} and at the ridge plot (S3). Mean soil water storage deficit was 66 mm ±31 mm and ranged from 9 mm at S3 to 107 mm at N1 (Fig. 4.4).

4.3.5 Water balance partitioning

Measured water balance inputs, i.e. P + ΔS, range from 909 mm at S3 to 1001 mm at N1 with a mean of 965±34 mm. Variability of water balance output was larger spanning from 666 mm at N2 to 1179 mm at S1 but mean output was lower (858±191 mm). Plot water balances outputs did underlie the same trend imposed by T_O patterns. On the southern aspect, sums of outflows decreased gradually from gully towards ridge, whereas on the north-facing slope the midslope and ridge plot posed similarly low outflows with increase at the gully plot (Fig. 4.4). Thus, the residuals of the measured water balance components, i.e. deep drainage (D) and measurement errors (e), were extremely variable (-208 to 321 mm) with an average of 107±199 mm. However, D+e was positive on the entire north-facing transect, whereas the lower southern aspects (S1 and S2) did pose negative water balances.

Overstory transpiration (T_O) was the dominant component of total stand evapotranspiration (ET) as illustrated by a very strong positive correlation between the overstory transpiration fraction (f_{T_O}) and ET. In contrast, ET contribution of interception (f_I) and understory and forest floor ET (f_{ET_U}) significantly declined with increasing ET. ET, f_{T_O} and f_I were significantly correlated to LAI_T and LAI_U, whereas LAI_O was only related to f_{T_O}. Relations between f_{ET_U} and any LAI metric were not significant. Landscape position on the other hand, characterized by northness (NN) and height above nearest drainage (HAND), was insignificant for ET and contribution of all ET fractions with exception of f_{ET_U}. Significant positive correlation between f_{ET_U} and NN indicated that slope orientation rather than drainage position drives the overstory vs understory partitioning in this ecosystem. The dominance of f_{T_O} on ET causes a strong negative LAI_T - f_I relationship, as I volumes were relative uniform between sites.

LAI_T and LAI_O did correlate strongly with soil depth (SD) and HAND. However, due

Table 4.2: Correlation matrix showing Pearson's correlation coefficients between: total stand evapotranspiration (ET_{total}), overstory transpiration fraction of ET_{total} (f_{T_O}), understory and forest floor evapotranspiration fraction of ET_{total} (f_{ET_U}), interception loss fraction of ET_{total} (f_I), total stand leaf area index (LAI_T), overstory leaf area index (LAI_O), understory leaf area index (LAI_U), soil depth (SD), northness (NN) and height above nearest drainage (HAND). Significant (α=0.05) correlations are printed in bold.

	ET	f_{T_O}	f_{ET_U}	f_I	LAI_{total}	LAI_O	LAI_U	SD	NN	HAND
ET	1.00									
f_{T_O}	**0.98**	1.00								
f_{ET_U}	**-0.82**	-0.80	1.00							
f_I	**-0.85**	**-0.90**	0.45	1.00						
LAI_{total}	**0.87**	**0.95**	-0.75	**-0.86**	1.00					
LAI_O	0.75	**0.82**	-0.79	-0.64	**0.92**	1.00				
LAI_U	**0.82**	**0.89**	-0.52	**-0.93**	**0.87**	0.61	1.00			
SD	0.72	0.79	-0.56	-0.77	**0.87**	**0.91**	0.62	1.00		
NN	-0.63	-0.66	**0.82**	0.38	-0.66	-0.56	-0.63	-0.24	1.00	
HAND	-0.70	-0.80	0.54	0.80	**-0.89**	**-0.89**	-0.69	**-0.95**	0.30	1.00

to the catena effect, soil depth and HAND were themselves very strongly correlated. Thus, LAI patterns could be driven by patterns of soil water storage (SD), access to non-local water sources (e.g. groundwater, upslope subsidies) or a combination thereof. HAND and the topographic wetness index (TWI) were highly co-linear (r=-0.97) because the transects were set-up on converging hillslopes and therefore TWI tended to be high with low HAND. Further, HAND did show stronger correlation throughout all parameters and thus TWI was not included in the table.

4.3.6 Vegetation - water balance interactions

Leaf area index (LAI) in the overstory (LAI_O) as well as understory (LAI_U) was larger on the southern aspect compared to the north-facing slope (Tab. 4.3).

Table 4.3: Vegetation and terrain characteristics at each monitoring site. LAI_T: total leaf area index, LAI_O: overstory leaf area index, LAI_U: understory leaf area index, A_S: sapwood area, NN: Northness (Rasmussen et al. 2015), TWI: topographic wetness index (Beven and Kirkby 1979), $HAND$: height above nearest drainage (Nobre et al. 2011), SD: soil depth.

	LAI	LAI_O	LAI_U	A_S	NN	TWI	$HAND$	SD
N1	4.12	3.48	0.64	6.52	0.23	8.0	1.0	>3.0
N2	2.15	2.07	0.08	5.56	0.42	6.4	36.4	0.8
N3	1.90	1.62	0.29	5.38	0.47	4.9	63.5	0.5
S1	4.78	3.57	1.21	9.61	-0.17	8.0	0.5	>3.0
S2	4.66	2.93	1.73	6.70	-0.27	7.0	9.1	2.0
S3	3.06	2.66	0.40	5.93	-0.37	5.0	51.5	0.6
mean	3.45	2.72	0.72	6.62	0.05	6.5	27.0	1.7

LAI_O at both gully plots was similar (∼3.5), but decreased rapidly from gully (N1) towards the mid-slope (N2) and ridge plot (N3) on the northern aspect, whereas a more

gradual decline of LAI_O was observed on the south-facing slope. LAI_U contrasts between slopes were stronger than LAI_O, where variations and mean LAI_U on the south-facing transect (1.11) were much higher than on the northern aspect (0.34). While LAI_U decreased from 0.64 at N1 to 0.29 at N3 and 0.08 at N2 on the north-facing transect, LAI_U on the southern aspect increased from S1 (1.21) to S2 (1.73), before dropping to at S3 (0.40).

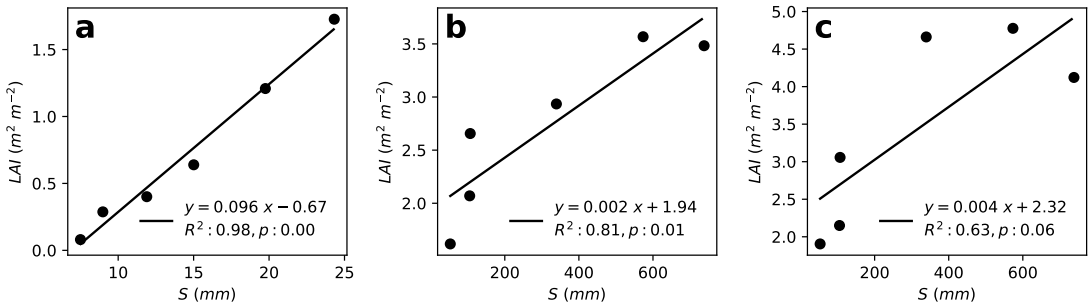

Figure 4.9: Effect of top soil water storage (0 - 120 mm) on (a) understory LAI and total soil water storage on (b) overstory leaf area index (LAI), and (c) total LAI.

Soil water storage could explain >80% of the observed LAI_O , LAI_U and total plot LAI variations (Fig. 4.9).

Spatial LAI patterns were closely linked to soil water storage (Fig. 4.9). Mean topsoil water storage (top 12 cm) was almost perfectly ($R^2 = 0.98$) related to LAI_U patterns (Fig. 4.9a), whereas 81% of plot-scale LAI_O variations could be explained by minimum observed total soil water storage (S) (Fig. 4.9b). Correlation of LAI_T with S was lower and statistically not significant (p=0.06) than for each individual strata ($R^2 = 0.63$).

Furthermore, stand A_S, and total LAI could explain large parts (∼90% and ∼75%, respectively) of total stand ET variations between sites (Fig. 4.10). Thus, vegetation patterns and total stand ET were strongly coupled to water-availability.

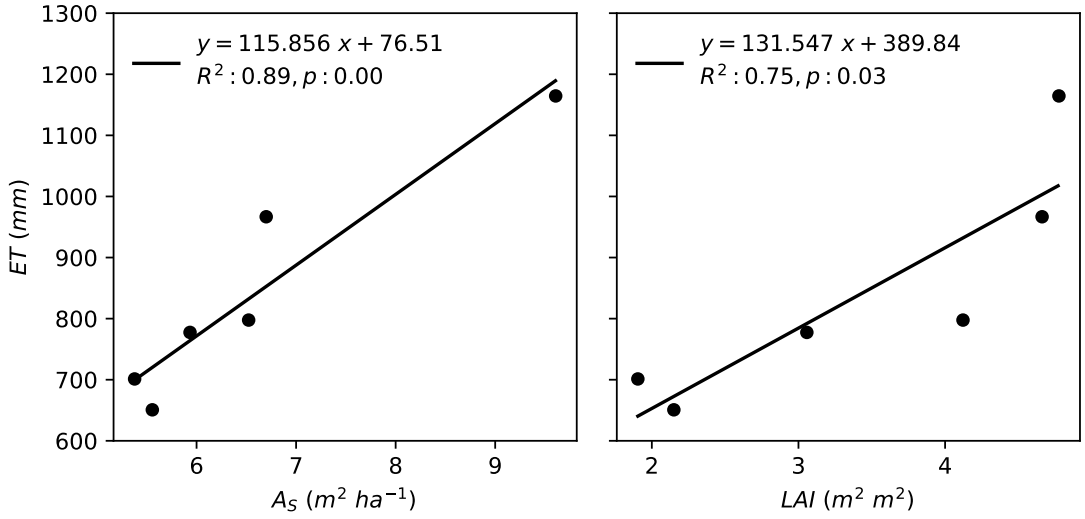

Figure 4.10: Plot-scale total evapotranspiration (ET), in relation to (a) stand sapwood area (A_S) and (b) total stand leaf area index (LAI).

4.4 Discussion

T_O dominated the ET flux at each plot, followed by I, ET_U and Q. Further, landscape position did not systematically affect flux totals of each individual component, with the exception of T_O, which was generally higher on the southern aspects and increased at both transects in down slope direction. ET_U was correlated with northness and thus indicated local topographic control of ET_U. However, no significant relationship could be established between landscape position and other ET components. Further, total LAI and ET patterns organized in response to soil water storage, which in turn was related to landscape position.

4.4.1 Water balance partitioning

Reported values of water balance components for relative similar forest types in SE Australia were within the range of our findings. Nolan et al. (2014) reported T_O ranging from 467 to 529 mm, I of 132-144 and ET_U of 323 to 382 mm. Interestingly, they found higher ET fluxes in drier forests, where they observed 619-646 mm T_O, 246-266 mm I and 285-323 mm

ET_U, which could have been due to above-average precipitation and thus less-than usual water-limitation on the drier sites. In general, ET_U fluxes in the Nolan study were higher than in this study, presumably due to larger contribution form shrubs, which accounted for 24-57% of plot sapwood area. Mitchell et al. (2012b) recorded T_O of 440-448 mm, interception losses ranging from 210-231 mm and ET_U of 144 mm for gully plots in a mixed-species eucalypt forests (MSEF) with comparable mean annual P (1129 $\pm$79 mm). These ranges agree well with the north-facing gully plot (Fig. 4.4), while the ridge plot (southern aspect) in their study (T_O: 241 mm, ET_U: 144 mm) was mostly comparable to the north-facing mid-slope or ridge plot. However, interception values in this study were much larger than the 109 mm they observed, which might be attributed to higher vegetation cover in our study.

In contrast to theoretical expectations that higher LAI and thus larger canopy storage capacity should relate to larger interception loss (Gash 1979; Aston 1979; He et al. 2014), no LAI-I relationship was observed. This might be systematic for eucalypt forests, as other studies also did not observe throughfall trends in relation to LAI (Benyon and Doody 2015; Nolan et al. 2014). Nolan et al. (2014) even found an inverse trend of interception loss and LAI using similar methods than this study, and they attributed higher interception losses in forest types with less LAI to larger evaporative demand at the more xeric sites.

Soil water storage deficits were observed at all six monitoring plots (9 - 107 mm), confirming previous observations that Eucalypts were able to sustain high transpiration rates throughout drought periods (Mitchell et al. 2012b).

4.4.2 Vegetation patterns

The large range of observed differences in plot-scale LAI and water balance components were correlated by variations in soil water storage capacity and subsequent topographic

water redistribution. Soil depth and consequently soil water storage capacity decreased from the gullies towards the ridges, especially on the northern aspects (Tab. 4.3). Precipitation that could not infiltrate or be stored in shallow upslope soils would flow downslope where soils were deeper and posed higher storage capacities. Thus, some fraction of precipitation that was received in upslope areas could not be utilized by the upslope vegetation, which ultimately permitted allocation of more leaf area further downslope. Surface soil water storage could explain LAI_U variations between sites (Fig. 4.9a), however, sub-soil water content dynamics (>0.15m depth) accounted for the majority of total storage dynamics (ΔS) at all sites. Therefore, LAI_O was stronger correlated to ΔS compared to total LAI, as deep stores had little impact on LAI_U.

It is commonly assumed that, vegetation with access to non-local water stores adapts to increased water-availability compared to vegetation affected by local hydro-climatic conditions only (Eagleson 1982). Benyon et al. (2006) illustrated that strongly negative water balances were common features of eucalypt stands on shallow groundwater tables, where trees had access to substantially more water than delivered by annual precipitation. O'Grady et al. (2011) showed that leaf area index (LAI) and the evaporative fraction (ϵ, ET/P) of sites with and without groundwater access converged after accounting for groundwater discharge in the Budyko framework (Budyko 1974). Similar to groundwater access, water redistribution along drainage gradients has the potential to alter plant-water availability (Thompson et al. 2011) as observed in this study. Strong correlation between LAI and soil water storage, as well as LAI and total ET flux indicate that this ecosystem organized in response to water-availability patterns as predicted by eco-hydrological equilibrium theory (Eagleson 1982). Hence, forest ecosystems around the transition from energy to water limitation (aridity index of 1) are expected to be most susceptible to topographic mediated energy and moisture patterns, especially under expected future

changes of precipitation patterns. Eucalypt trees have been shown to deplete soil waters stores throughout drought periods (Mitchell et al. 2012b). Thus, low infiltration capacity and soil water storage capacity at (north-facing) upslope stands on poor and shallow soils might not be able to sustain the actual vegetation under less frequent but potentially higher intensity rainfall patterns in the future. On the other hand, stands in drainage lines and gullies, where soils are deep and can store substantial amounts of water, might experience increased water availability due to increased run-off from upslope areas, which in turn might further enhance spatial heterogeneity.

4.4.3 Measurement uncertainty

Streamflow

Stage heights during high flow periods could not be converted to stream flow with the calibration method used as large outflow volumes could not be captured with containers. However, the general shape of the rating curve should be appropriate until the widest section of the culvert was reached (stage height less than half of the culvert diameter), until which the cross-section increased exponentially. At 50 *cm* diameter, the highest recorded stage height (246.7 mm) was still within the bounds (Fig. 4.2a), but there still remained some uncertainty in the high flow accuracy, due to the lack stream flow volumes collected at high flows. Although stage heights above the highest calibration point only occurred ∼4% of time, those few high flow events contributed largely to the streamflow total (Fig. 4.8b). Nevertheless, the streamflow total was very low compared to the other components of the water balance (Fig. 4.4), and thus not likely a major source of uncertainty for the water balance closure during the monitoring period.

Soil water storage

Soil water storage deficit was difficult to estimate, because soils were either very deep (>3 m) and instrumentation of the entire profile was not feasible or on shallow soils plant available water stored in the (fractured) bedrock could not be quantified. Additionally, soil depth was only determined up to 3 m depth and may have been potentially considerably deeper at the gully plots. Further, deep drainage was not quantified and thus contributed to the uncertainty in storage dynamic estimates. However, mean profile SWC at all plots was lower at the end of the monitoring period compared to the beginning, while SWC deficit was larger on the northern aspect than on the south-facing slope. On the north-facing slope SWC deficit increased from 0.042 $m^3\ m^{-3}$ at N1 to 0.101 $m^3\ m^{-3}$ at N2 and 0.115 $m^3\ m^{-3}$ at N3. In contrast, no clear pattern in relation to drainage position was observed on the south-facing slope, where largest deficit occurred at the mid-slope plot (S2) with 0.052 $m^3\ m^{-3}$ followed the gully plot (0.035 $m^3\ m^{-3}$) and the ridge (0.020 $m^3\ m^{-3}$). Estimated soil water storage deficits (ΔS) ranged from 9 to 107 mm, but he assumption that SWC at 1 m was representative for the remainder of the profile likely overestimated ΔS in soils thicker than 1 m. However ΔS was potentially very small at depth, as SWC dynamics tend to be more buffered with increasing soil depth.

4.5 Conclusion

Large variability of vegetation structure, soil depth and water balance totals were observed over very small spatial extents. Stand LAI ranged from 1.9 to 4.8 $m^2\ m^{-2}$, while soil depth varied between 0.5 and >3 m within several hundred meter distance. Consequently, water balance components were highly variable as well. Measured combined outflows (ET + Q) ranged from 666 to 1179 mm (mean: 858±191 mm) between plots, while inputs (P + ΔS)

spanned from 909 to 1001 mm (mean: 965±33 mm).

Residuals, attributed to deep drainage (D) and measurement uncertainties (e), ranged from -208 to 321 mm (mean 107±199 mm) between plots and were positive on the northern aspects and negative on the lower southern hillslope. While, ET was strongly correlated to A_S and LAI, no significant relationship between landscape position and water balance partitioning was observed with the exception of f_{ET_U}, which was controlled by local slope orientation.

Total stand LAI and total stand ET organized in response soil-water storage capacity. Soil water storage in turn was controlled by soil depth and drainage position, which were strongly correlated due to the catena effect. Therefore, spatial vegetation patterns offer the potential to infer water balance and ecosystem status in complex terrain.

Changes in precipitation patterns are expected to have large implications for eucalypt forests, where trees can deplete soil waters stores throughout drought periods. Stands on exposed (north-facing) upper hillslopes might not be able to sustain the actual vegetation under a changing climate with less frequent but potentially higher intensity rainfall patterns. On the other hand, stands in drainage lines and gullies might profit from increased run-off from upslope areas. Thus, exposed upslope stands are expected be most vulnerable to climate change, as it is more likely that they experience more severe drought stress, leading to potential increases in tree mortality in the future. Particularly, if long-term changes in climatic forcing exceed response time of the vegetation, which might push ecosystems over a threshold into a (less productive) alternative stable state.

Bibliography

Asbjornsen, H. et al. (2011). "Ecohydrological advances and applications in plant-water relations research: a review". In: *Journal of Plant Ecology* 4.1, pp. 3–22.

Ashton, D. H. and O. D. Bassett (1997). "The effects of foraging by the superb lyrebird (Menura novae-hollandiae) in Eucalyptus regnans forests at Beenak, Victoria". In: *Austral Ecology* 22.4, pp. 383–394.

Aston, A. R. (1979). "Rainfall interception by eight small trees". In: *Journal of hydrology* 42.3, pp. 383–396.

Benyon, R. G. and T. M. Doody (2015). "Comparison of interception, forest floor evaporation and transpiration in Pinus radiata and Eucalyptus globulus plantations". In: *Hydrological Processes* 29.6, pp. 1173–1187.

Benyon, R. G. et al. (2006). "Impacts of tree plantations on groundwater in south-eastern Australia". In: *Australian Journal of Botany* 54.2, p. 181.

Beven, K. J. and M. J. Kirkby (1979). "A physically based, variable contributing area model of basin hydrology". In: *Hydrological Sciences Bulletin* 24.1, pp. 43–69.

Brown, A. E. et al. (2005). "A review of paired catchment studies for determining changes in water yield resulting from alterations in vegetation". In: *Journal of Hydrology* 310.1, pp. 28–61.

Budyko, M. I. (1974). *Climate and Life*. Orlando, Fl: Academic.

Crockford, R. H. and D. P. Richardson (2000). "Partitioning of rainfall into throughfall, stemflow and interception: effect of forest type, ground cover and climate". In: *Hydrological processes* 14.16, pp. 2903–2920.

Donohue, R. J. et al. (2007). "On the importance of including vegetation dynamics in Budykos hydrological model". In: *Hydrology and Earth System Sciences* 11, pp. 983–995.

Eagleson, P. (1982). "Ecological optimality in water-limited natural soil-vegetation systems: 1. Theory and hypothesis". In: *Water Resources Research* 18.2, pp. 325–340.

Flerchinger, G. N. et al. (2010). "Surface fluxes and water balance of spatially varying vegetation within a small mountainous headwater catchment". In: *Hydrology and Earth System Sciences* 14.6, pp. 965–978.

Gash, J. H. C. (1979). "An analytical model of rainfall interception by forests". In: *Q.J.R. Meteorol. Soc.* 105.443, pp. 43–55.

Hacke, U. G. et al. (2006). "Scaling of angiosperm xylem structure with safety and efficiency". In: *Tree physiology* 26.6, pp. 689–701.

Hawthorne, S. N. et al. (2013). "The long term effects of thinning treatments on vegetation structure and water yield". In: *Forest Ecology and Management* 310, pp. 983–993.

He, Z.-B. et al. (2014). "Spatial variability of canopy interception in a spruce forest of the semiarid mountain regions of China". In: *Agricultural and Forest Meteorology* 188, pp. 58–63.

Jefferson, A. et al. (2010). "Coevolution of hydrology and topography on a basalt landscape in the Oregon Cascade Range, USA". In: *Earth Surface Processes and Landforms*, pp. 803–816.

Macfarlane, C. et al. (2010). "A new model for predicting understorey leaf area from biomass in eucalypt forest to test the ecohydrological equilibrium theory: Measurement

of understorey LAI in eucalypt forest". In: *Methods in Ecology and Evolution* 1.4, pp. 371–379.

Mitchell, P. J. et al. (2012b). "Responses of evapotranspiration at different topographic positions and catchment water balance following a pronounced drought in a mixed species eucalypt forest, Australia". In: *Journal of Hydrology* 440-441, pp. 62–74.

Neary, D. G. et al. (2009). "Linkages between forest soils and water quality and quantity". In: *Forest Ecology and Management* 258.10, pp. 2269–2281.

Nobre, A. et al. (2011). "Height Above the Nearest Drainage: a hydrologically relevant new terrain model". In: *Journal of Hydrology* 404.1, pp. 13–29.

Nolan, R. H. et al. (2014). "Changes in evapotranspiration following wildfire in resprouting eucalypt forests". In: *Ecohydrology*, pp. 1363–1377.

Nyman, P. et al. (2014). "Downscaling regional climate data to calculate the radiative index of dryness in complex terrain". In: *Australian Metrological and Oceanographic Journal* 64.2, pp. 109–122.

O'Grady, A. P. et al. (2011). "Can we predict groundwater discharge from terrestrial ecosystems using existing eco-hydrological concepts?" In: *Hydrology and Earth System Sciences* 15.12, pp. 3731–3739.

Pfautsch, S. et al. (2016). "Climate determines vascular traits in the ecologically diverse genus *Eucalyptus*". In: *Ecology Letters* 19.3, pp. 240–248.

Poorter, L. et al. (2010). "The importance of wood traits and hydraulic conductance for the performance and life history strategies of 42 rainforest tree species". In: *New Phytologist* 185.2, pp. 481–492.

Rasmussen, C. et al. (2015). "Quantifying Topographic and Vegetation Effects on the Transfer of Energy and Mass to the Critical Zone". In: *Vadose Zone Journal* 14.11.

Savenije, H. H. G. (2010). "Topography driven conceptual modelling (FLEX-Topo)". In: *Hydrology and Earth System Sciences* 14.12, pp. 2681–2692.

Silberstein, R. et al. (2001). "Energy balance of a natural jarrah (Eucalyptus marginata) forest in Western Australia: measurements during the spring and summer". In: *Agricultural and Forest Meteorology* 109.2. 00086, pp. 79–104.

Specht, R. L. (1972). "Water use by perennial evergreen plant communities in Australia and Papua New Guinea". In: *Australian Journal of Botany* 20.3, pp. 273–299.

Specht, R. L. (1983). "Foliage projective covers of overstorey and understorey strata of mature vegetation in Australia". In: *Austral Ecology* 8.4, pp. 433–439.

Specht, R. et al. (2006). "Vegetation structure and biodiversity along the eucalypt forest to rainforest continuum on the serpentinite soil catena in a subhumid area of Central Queensland, Australia". In: *Austral Ecology* 31.3, pp. 394–407.

Thompson, S. E. and G. G. Katul (2011). "Inferring ecosystem parameters from observation of vegetation patterns". In: *Geophysical Research Letters* 38.20.

Thompson, S. E. et al. (2011). "Spatial scale dependence of ecohydrologically mediated water balance partitioning: A synthesis framework for catchment ecohydrology". In: *Water Resources Research* 47.10.

Troch, P. A. et al. (2009). "Climate and vegetation water use efficiency at catchment scales". In: *Hydrological Processes* 23.16, pp. 2409–2414.

Watanabe, M. D. B. and E. Ortega (2011). "Ecosystem services and biogeochemical cycles on a global scale: valuation of water, carbon and nitrogen processes". In: *Environmental Science & Policy* 14.6, pp. 594–604.

Williams, C. A. et al. (2012). "Climate and vegetation controls on the surface water balance: Synthesis of evapotranspiration measured across a global network of flux towers". In: *Water Resources Research* 48.6.

Chapter 5

ET patterns in complex upland forests reveal contrasting topographic thresholds of non-linearity

5.1 Introduction

Forests provide many crucial ecosystem services, e.g. carbon sequestration, water filtration and storage or recreational value (Field et al. 2015; Pan et al. 2011; Viglizzo et al. 2016). These are closely linked to the forest water balance, where evapotranspiration (ET) is usually the largest component (Jasechko et al. 2013; Schlesinger and Jasechko 2014; Good et al. 2015). Therefore, improving predictions of ET will improve estimates of water yield, forest productivity and carbon storage.

ET partitioning still remains a key challenge in eco-hydrology (Asbjornsen et al. 2011) and large areas of forest are often treated as being homogeneous just because they fall in a single climate category. However, ecosystems structures vary spatially in complex terrain, regardless of being water or energy-limited, because topography alters the surface energy and water balance (Alexander et al. 2016; Kitagawa et al. 2014; Zapata-Rios et al. 2016; Gutirrez-Jurado et al. 2013; Flores Cervantes et al. 2014; Pelletier et al. 2013).

Furthermore, spatial heterogeneity within catchments originates from interactions and feedbacks on three temporal scales (assuming same parent material):

1. Catena timescales (thousands of years): Topography driven micro-climatic variations and vegetation patterns will create erosion patterns that will in turn influence soil production, accumulation, quality and therefore plant available water storage capacity (PAWC).

2. Plant community ecology timescales (10s-100s of years): The combination of soil properties and topographically mediated energy and moisture patterns will determine plant water-availability and thus the "optimal" vegetation cover for a given location.

3. Modern timescales (years, sub-yearly): Spatial ET patterns will reflect the first order controls of energy and water inputs as well at the second order controls of the system properties created in response to time scales 1 and 2.

Most importantly, these processes and timescales are not independent, creating interactions and feedbacks that are resulting in co-evolved stable states that yield the current spatially variable ET fluxes (Troch et al. 2015; Pelletier et al. 2013).

Small scale heterogeneity might be crucial for understanding and predicting the hydrologic response of an entire catchment (Nippgen et al. 2015; Emanuel et al. 2014; Jencso and McGlynn 2011; McDonnell 2013) and one way of accounting for spatial patterns is utilizing fully distributed process-based modeling. However, interactions and feedbacks on multiple temporal scales, as well as potentially large differences in dominant processes between ecosystems will complicate model accurate model predictions and might impede model use over large domains (Savenije 2010). Further, the underlying physical process-representation often requires fitting large numbers of model parameters, thus complicating transferability to ecosystems the model was not explicitly calibrated for (McDonnell et al. 2007).

Optical remote sensing products are also being used to represent spatial patterns in lumped models by calibrating the response variable (e.g. LAI) against observed spectral reflectance in a certain wavelength or a combination thereof (Tesemma et al. 2015). However, the spatial resolution of remote sensing products might not be sufficient to capture the spatial vegetation heterogeneity in complex upland terrain (e.g. MODIS).

Light Detection and Ranging (LiDAR) remote sensing provides higher spatial resolution and also more penetration depth into the vegetation layer and thus, in contrast to optical remote sensing, can also provide 3-dimensional vegetation patterns. However, high resolution LiDAR data is gathered in campaigns and consequently the temporal resolution is usually poor. Often, the relationship between parameters of interest (e.g. LAI) and forest structure is used to exploit LiDAR derived metrics such as canopy cover, return densities and return height distribution metrics (Asner et al. 2012; Pope and Treitz 2013; Morsdorf et al. 2006; Jensen et al. 2008; Peduzzi et al. 2012) While LiDAR has been widely used to estimate biomass (Meyer et al. 2013), carbon stocks (Asner et al. 2012; Kristensen et al. 2015), forest growth (Zhao et al. 2018; Yu et al. 2004), LAI (Pope and Treitz 2013; Morsdorf et al. 2006; Jensen et al. 2008; Peduzzi et al. 2012) and basal area (Gobakken and Nsset 2005; Jaskierniak et al. 2015; Jaskierniak et al. 2016), studies using LiDAR to estimate stand sapwood area are rare (Jaskierniak et al. 2015; Jaskierniak et al. 2016; Saito et al. 2015).

In south-east Australia, forest hydrology research has so far mainly focused on catchment-scale response to disturbance (e.g. bushfires, logging) in tall mountain ash (*E. regnans*) forests (Kuczera 1987; Vertessy et al. 1993; Haydon et al. 1997; Watson et al. 1999; Bren et al. 2010; Benyon et al. 2015) and drier mixed species eucalypt forests (Webb et al. 2012; Webb and Jarrett 2013; Bren et al. 2013; Bren and Hopmans 2007; Lane and Mackay 2001; Lane et al. 2010; Nolan et al. 2015). Hence, streamflow response at catchment-scale is

well documented for a range of native eucalypt forests, but relatively little is known about sub-catchment ET patterns and drivers.

In non water-limited Eucalypt forests, where mean annual sap velocities (v_{sap}) are spatially uniform, stand sapwood area (A_S) has been successfully used to predict ET (Benyon et al. 2017) as well as streamflow (Benyon et al. 2015). However, more pronounced vegetation patterns are observed in drier mixed species eucalypt forests (MSEF) (Givnish et al. 2014; Nyman et al. 2014) and seasonal water-limitation presumably cause spatial heterogeneous v_{sap} patterns which complicates ET predictions.

So far, the few studies investigating spatial patterns of water use in MSEF have produced contrasting findings. Mitchell et al. (2012a) found similar v_{sap} at different landscape positions and related sub-catchment ET variability to A_S patterns. In contrast, Gharun et al. (2015) reported strong v_{sap} variations in response to slope aspect and angle but did not consider spatial vegetation patterns. Hence, there remains considerable uncertainty on ET patterns in MSEF.

The above illustrated interactions and feedbacks between vegetation, soils and topography lead to increasing time lags from energy and soil moisture patterns (sub-yearly), to vegetation patterns (10s -100s of years) to soil properties and topography (>1000s of years) in response to climatic forcing. Vegetation and terrain patterns integrate over temporal variability of climatic drivers and water-availability. Consequently, vegetation patterns presumably adapted to long-term climate and thus can potentially be used to infer spatial ET patterns, even when v_{sap} is heterogeneous as well. The aims of this study are therefore to:

1. Quantify the overstory and understory vegetation patterns in response to topography (slope orientation, drainage position), while controlling for other factors (geology, precipitation, temperature).

2. Quantify spatio-temporal overstory and understory ET.

3. Evaluate the relative contribution of factors associated with long (catena), medium (ecology) and short (modern) timescales on overstory and understory ET fluxes.

4. Infer potential patterns of ET partitioning in response to landscape position.

5.2 Methods

5.2.1 LiDAR vegetation models

LiDAR data (ALTM3100EA, 71 KHz scan rate, 0.26 m footprint size, mean point density of 0.9 points m^{-2}, 4 maximum returns) was collected between 19 November 2007 and 10 January 2008. Measured plot scale vegetation properties were scaled to the whole catchment using regression models of LiDAR return indices. Briefly, stand sapwood area (A_S) was measured using sapwood sample cores, overstory LAI (LAI_O) was estimated by digital cover photography (DCP) (Macfarlane et al. 2014) and understory LAI (LAI_U) measured using the line-intercept method (Groeneveld 1997) and tree fern allometrics (see Chapter 2 for details on overstory and Chapter 3 for understory measurements). A_S could be well predicted using the percentage of LiDAR returns that originated from >1.5 m above the ground surface (Fig. 5.1a). The 99th percentile return height was used to scale LAI_O (Fig. 5.1b) and the canopy relief ratio of the understory strata (mean - min return height / (max - min return height)), did explain LAI_U variations best (Fig. 5.1c).

5.2.2 Overstory transpiration

Overstory transpiration (T_O) was scaled from plots to catchment scale by combining mapped A_S and spatially modeled sap velocity (v_{sap}). A_S maps were derived from LiDAR by applying the above mentioned regression model to mapped percentage of returns above

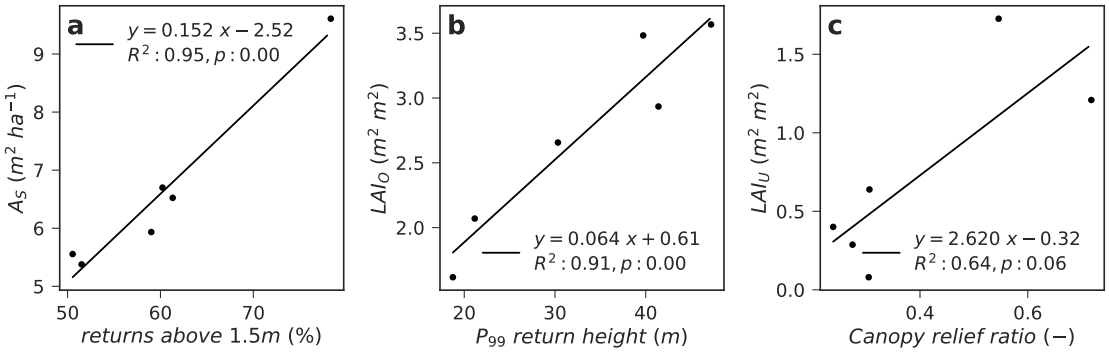

Figure 5.1: Regression models between measured plot-scale vegetation properties and LiDAR metrics: a) Sapwood area (A_S) and percentage of LiDAR returns >1.5 m height above ground, total plot leaf area index (LAI, b) and overstory LAI (LAI_O, c) against the 99th percentile LiDAR return height, d) understory LAI (LAI_U) and canopy relief ratio of the understory strata (mean - min return height / (max - min return height)).

1.5 m height on a 20×20 m spatial resolution. Sap velocity patterns for each 20×20 m pixel were modeled on monthly temporal resolution as a function of monthly mean short-wave radiation load (SWR), northness (Rasmussen et al. 2015) and HAND (Nobre et al. 2011), both metrics describing the landscape position. Northness ($\sin(slope) \times \cos(aspect)$) ranges from -1 (south-facing) to +1 (north-facing) and describes the slope orientation in north-south direction, whereas HAND (height above nearest drainage) captures the drainage position and catena effects. Mean monthly SWR was measured at a weather station in close proximity of the field sites (<4 km). The Random Forest model trained with SWR, northness and HAND was used to predict v_{sap}. SWR was the most important feature (∼0.7) of the model followed by northness (∼0.2) and HAND (∼0.1). Finally, mean monthly spatial T_O patterns were calculated from the product of A_S and v_{sap}.

5.2.3 Sub-canopy short-wave radiation

Spatial sub-canopy radiation maps were generated using the path length model (Nyman et al. 2017) on a 20 x 20 m pixel resolution for every 30 minute interval. Attenuation of below canopy direct radiation depends on path length through the vegetation layer, which in turn is a function of vegetation height and zenith angle of the sun. Vegetation heights for each pixel were derived from LiDAR and the position of the sun relative to each pixel was calculated using pysolar. The diffuse fraction (P_{dif}) was calculated from observed total above canopy radiation using coefficients derived for Melbourne airport (Spencer 1982). Then, the direct above canopy radiation was adjusted according to the path length traveled through vegetation and corrected for slope orientation. Finally, the 30 minute sub-canopy radiation rasters were aggregate to month means. For more details see Chapter 3.

5.2.4 Understory ET

Understory and forest floor evapotranspiration (ET_U) was measured using an evaporation dome (described in detail in chapter 3). The following regression model was fitted to spatially averaged plot-scale ET_U measurements:

$$ET_U = 0.00015\ SWR_U + 0.01459\ LAI_U, \text{ for SWR } >1 \text{ W} \tag{5.1}$$

where SWR_U is the incoming sub-canopy short-wave radiation and LAI_U the understory leaf area index. Based on the lack of night-time ET_U measurements and the evidence of nocturnal ET in the range of 5-20% in other ecosystems (Zeppel et al. 2010; Moore et al. 2008; Ogle et al. 2012; Dios et al. 2015; Dawson et al. 2007) nocturnal ET_U was set to 10% of mean day-time ET_U. The complete ET_U range was most likely not covered during campaigns given the limited number of observations feasible during measurement campaigns and the lack of night-time measurements. Thus, the Random Forests model

could not be used because of the inability to predict outside the bounds of the training data set.

5.2.5 Interception loss

Interception loss was not correlated to LAI or landscape position (see Chapter 4). Therefore, the mean interception loss (237 mm) observed at the six monitoring plots was applied over the entire catchment.

5.2.6 Aridity index down-scaling

Aridity index rasters were generated following Nyman et al. (2014). Large scale, long-term (>20 years) spatial data sets of solar global horizontal irradiance (GHI, 5×5 km), solar direct normal irradiance (DNI, 5×5 km), air temperature (2.5×2.5 km), precipitation (2.5×2.5 km) and cloud fraction (10×10 km) available from the Bureau of Meteorology (BoM) were used to calculate the aridity index (AI) by

$$AI = R_n/\lambda P \tag{5.2}$$

where R_n is the net radiation, P the precipitation and λ the latent heat of vaporisation, which was calculated as a function of air temperature. Net radiation was calculated by

$$R_n = R_s + R_{ld} - R_{lu} \tag{5.3}$$

where R_s is the net shortwave radiation, R_{ld} the incoming longwave radiation and R_{lu} the outgoing longwave radiation. The net shortwave radiation was calculated from

$$R_s = (1 - \alpha_s)\ R_g\ S_{TD} \tag{5.4}$$

Where α_s is the surface albedo, $R - g$ is the global incoming shortwave radiation (GHI) and S_{TD} the topographic downscaling factor. Surface albedo was calculated as a function

of LAI, which in turn was assigned spatially by using four board vegetation categories based on the ecological vegetation classification (EVC). DHI was calculated as a function of DNI and solar elevation and the diffuse radiation defined as the difference between GHI and DHI. The topographic downscaling factor (S_{TD}) accounts for effects of topographic shading, slope and aspect and was calculated using Solar Analyst (ArcGIS, ESRI) for each 20×20 m grid cell by

$$S_{TD} = (DIR_m + DIFF_m)/R_{tile} \tag{5.5}$$

Where DIR_m and $DIFF_m$ are the Solar Analyst outputs for each 20×20m cell and R_{tile} is the average incoming shortwave radiation for the entire 5×5 km tile. The incoming longwave radiation (R_{ld}) was calculated as a function of topographically adjusted temperature using the SRAD model (Moore et al. 1993). Outgoing longwave radiation was calculated as a function of atmospheric emissivity, using the cloud fraction, temperature (Crawford and Duchon 1999) and sky view factor (ArcGIS).

During the measurement period P (∼900 mm) differed largely from the spatial mean P (1275 mm) used to generate the long-term AI raster. However, mean annual solar exposure during the measurement period (14.97 $MJ\ m^{-2}$) agreed well with long-term averages (14.6 $MJ\ m^{-2}$, 1990-2017) at a weather station close-by (Reefton, BoM station 82671). Thus, AI during the measurement period was adjusted by substituting mean precipitation with measured precipitation in the procedure outlined above

$$AI_{adj} = R_{n_{mean}}/\lambda\ P_{measured} \tag{5.6}$$

5.3 Results

5.3.1 Catchment topography

Elevation of the study area spanned from 290 to 616 m.a.s.l. with a mean elevation of 420±78 m (Fig. 5.2a). The catchment drained in west-east direction and thus almost straight north and south-facing flanks made up most of the catchment area (Fig. 5.2b). Slope angles ranged from 0 to 33.6° (Fig. 5.2c) and mean slope angle was 22.5±6.1°. Northness ranged from -0.48 to 0.48 and showed two pronounced peaks representing the north and south-facing flanks (Fig. 5.2d). While HAND ranged from 0 to ∼100 m on the northern and southern aspects, values up to 178 m were reached on western aspects in the head area. Throughout the whole catchment mean HAND was 44.5±39 m. The topographic wetness index (TWI) (Beven and Kirkby 1979) ranged from 3.6 on the ridges to 16.8 in the main channel with a mean of 5.8±1.5 m (Fig. 5.2).

5.3.2 Vegetation patterns

Sapwood area (A_S), overstory leaf area index (LAI_O) as well as understory leaf area index (LAI_U) were significantly larger on southern aspect compared to north-facing hillslopes (Wilcoxon rank-sum test, $p<0.001$). A_S ranged from 3.2 to 10.9 $m^2\ ha^{-1}$ (mean: 6.4 ±1.2 $m^2\ ha^{-1}$) with highest A_S in proximity of the main drainage line and decreasing in upslope direction on both aspects (Fig. 5.2g). Mean LAI_O was 2.6±0.65 $m^2\ m^{-2}$ and spatial patterns due to aspect were more pronounced compared to A_S patterns. Larger LAI_O could be sustained on upper southern hillslopes and LAI_O was less concentrated towards the drainage line as illustrated by a less bell-shaped distribution compared to A_S (Fig. 5.2h). In contrast to LAI_O , LAI_U (mean: 0.46±0.26 $m^2\ m^{-2}$) patterns were more patchy and not as distinct (Fig. 5.2i).

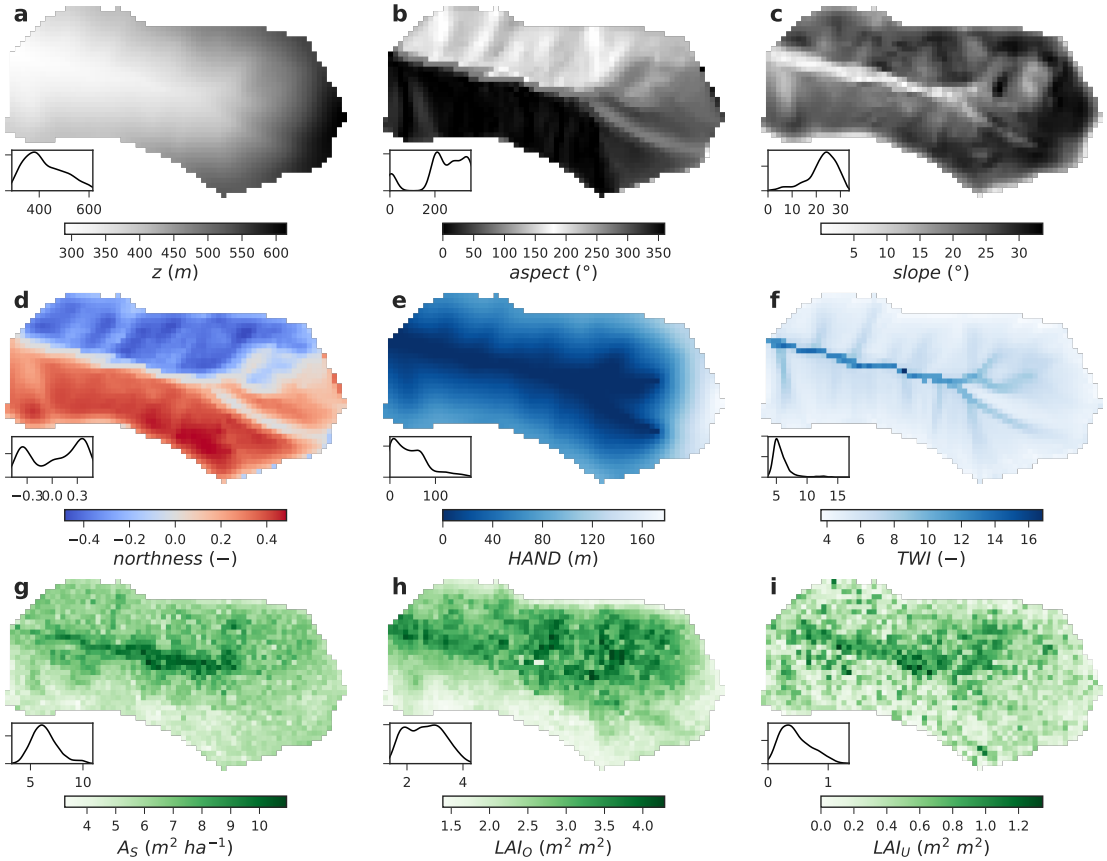

Figure 5.2: Terrain and vegetation characterization of the study area. Maps and inserted kernel densities of a) elevation (z), b) aspect, c) slope, d) northness ((sin(*slope*) × cos(*aspect*))), e) height above nearest drainage (HAND), f) the topographic wetness index (TWI), g) sapwood area (A_S), h) overstory leaf area index (LAI_O)m and i) understory leaf area index (LAI_U).

Spatial A_S and LAI_O patterns were significantly linked to slope orientation and drainage position (Fig. 5.3). Both A_S and LAI_O were significantly higher on southern aspects compared to north-facing locations. The largest differences between aspects were observed at unfavorable drainage positions (high HAND or low TWI). With increasing TWI or decreasing HAND, A_S and LAI_O gains were larger on northern aspects resulting in smallest differences close to drainage lines or in converging landscape positions. Thus, the effect of drainage position on A_S and LAI_O was larger on the north-facing hillslopes, also indicated

by steeper regression line slopes with increasing HAND (Fig. 5.2g) and TWI (Fig. 5.3d,e). Moreover, 29% of A_S variations on the north-facing flank could be explained by HAND, compared to 15% on the southern aspects.

While, LAI_O patterns between aspects were similar to A_S patterns, larger fractions of LAI_O variations could be explained by drainage position. HAND explained 64% of LAI_O variability on northern aspects (Fig. 5.3b), whereas TWI was a slightly better predictor than HAND on the south-facing flank, it only explained 28% of LAI_O variations (Fig. 5.3e).

LAI_U changed less with drainage position compared to LAI_O and A_S and larger LAI_U changes due to drainage position were observed on the southern aspects (Fig. 5.3c,f). At low TWI or high HAND, LAI_U was similar between aspects. However, LAI_U increased in more favorable drainage positions on the southern aspects, while only marginal gains were observed on northern aspects.

5.3.3 Sub-canopy short-wave radiation

Mean sub-canopy short-wave radiation (SWR_U) significantly differed between northern and southern aspects (Wilcoxon rank-sum test, $p<0.001$). The interaction of topography and vegetation patterns caused strong SWR_U contrasts, where higher mean SWR_U was observed on the northern aspects ($6.45\pm2.09\ MJ\ m^{-2}\ d^{-1}$) compared to south-facing slopes ($4.55\pm1.44\ MJ\ m^{-2}\ d^{-1}$). Monthly mean SWR_U ranged from $2.62\pm0.99\ MJ\ m^{-2}\ d^{-1}$ in July to $8.40\pm3.20\ MJ\ m^{-2}\ d^{-1}$ in November with higher SWR_U on the upper hillslopes compared to the gullies (Fig. 5.4). However, SWR_U variations in response to drainage position were larger in magnitude and more pronounced on the northern aspects, where local 'SWR_U lows' extended to upper hillslope areas in drainage lines, a result of increased vegetation density. Peak SWR was recorded in November because steep slope angles (Fig.5.2c) exceeded solar elevation on the upper north-facing hillslope in summer, effectively

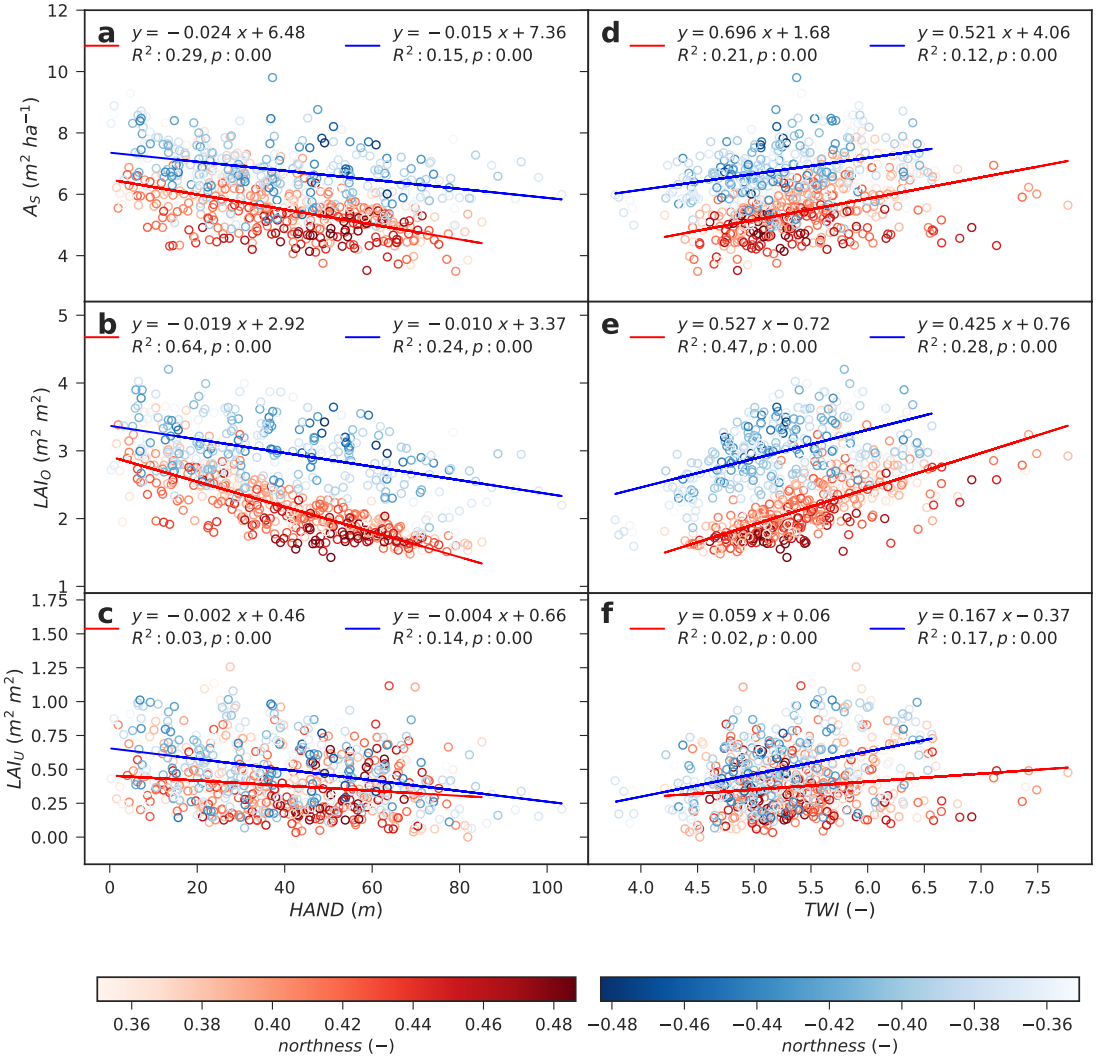

Figure 5.3: Vegetation patterns in relation to landscape position. Sapwood area (A_S, top row), overstory leaf area index (LAI_O, middle row) and understory leaf area index (LAI_U, bottom row) split into north-facing (northness>0.3, red colors) and south-facing (northness<0.3, blue colors). Drainage position is represented by height above nearest drainage (HAND, left column) and the topographic wetness index (TWI, right column).

deceasing mid-day incident angles.

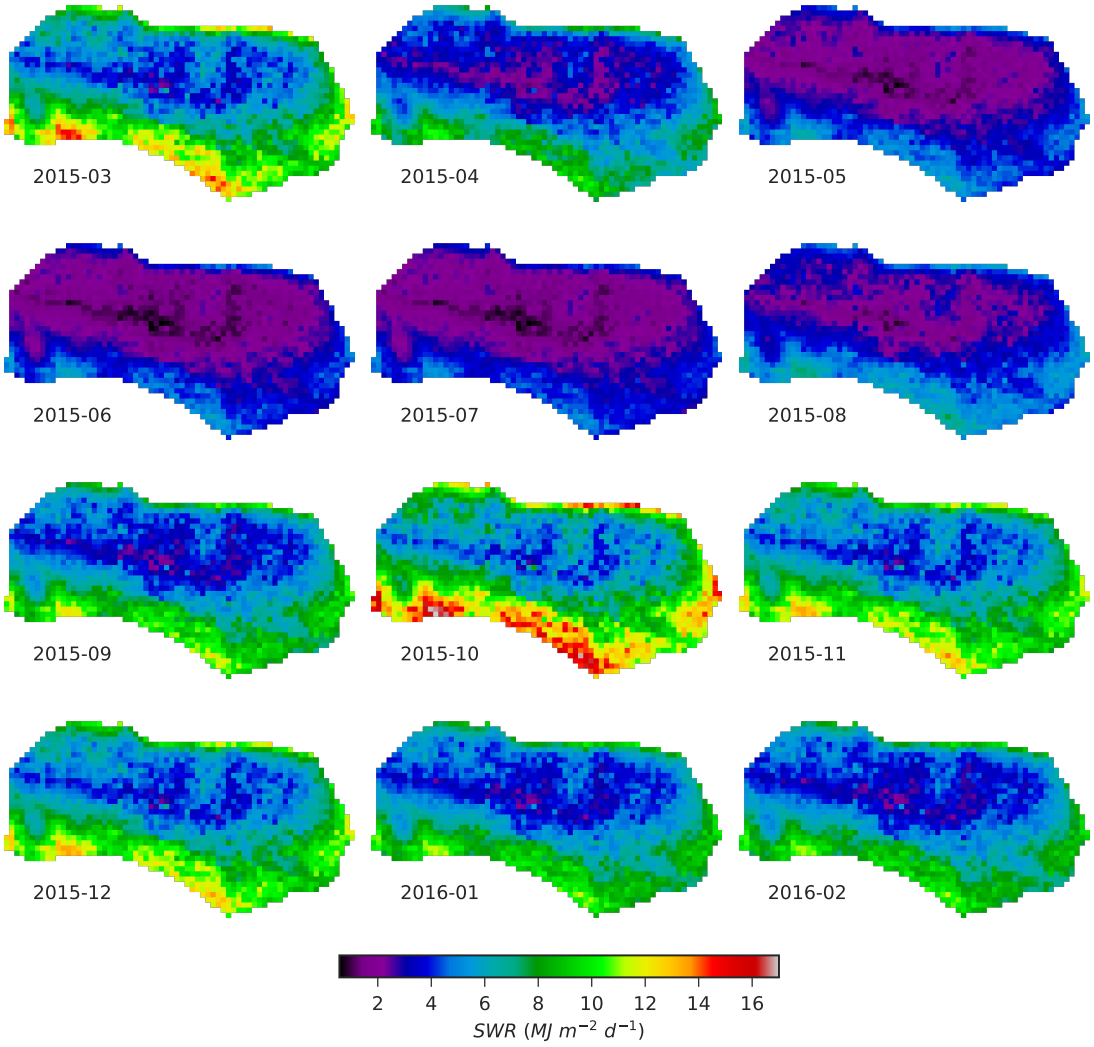

Figure 5.4: Monthly mean sub-canopy radiation load (SWR)

5.3.4 ET patterns

Overstory transpiration

Overstory transpiration (T_O) rates were significantly (Wilcoxon rank-sum test, p<0.001) higher on the southern aspects (mean: 1.37±0.30 $mm\ d^{-1}$) compared to north-facing slopes (mean: 1.03±0.31 $mm\ d^{-1}$) (Fig. 5.5). While T_O was higher in proximity to the main drainage line on both aspects, higher T_O rates were sustained towards the ridges on the southern aspects, particularly in summer (Fig. 5.5). However, mean T_O throughout the

catchment declined from 1.33±0.4 $mm\ d^{-1}$ in March to its minimum of 0.70±0.15 $mm\ d^{-1}$ in July before increasing to peak T_O of 1.63±0.58 $mm\ d^{-1}$ in December (Fig. 5.7a). Along

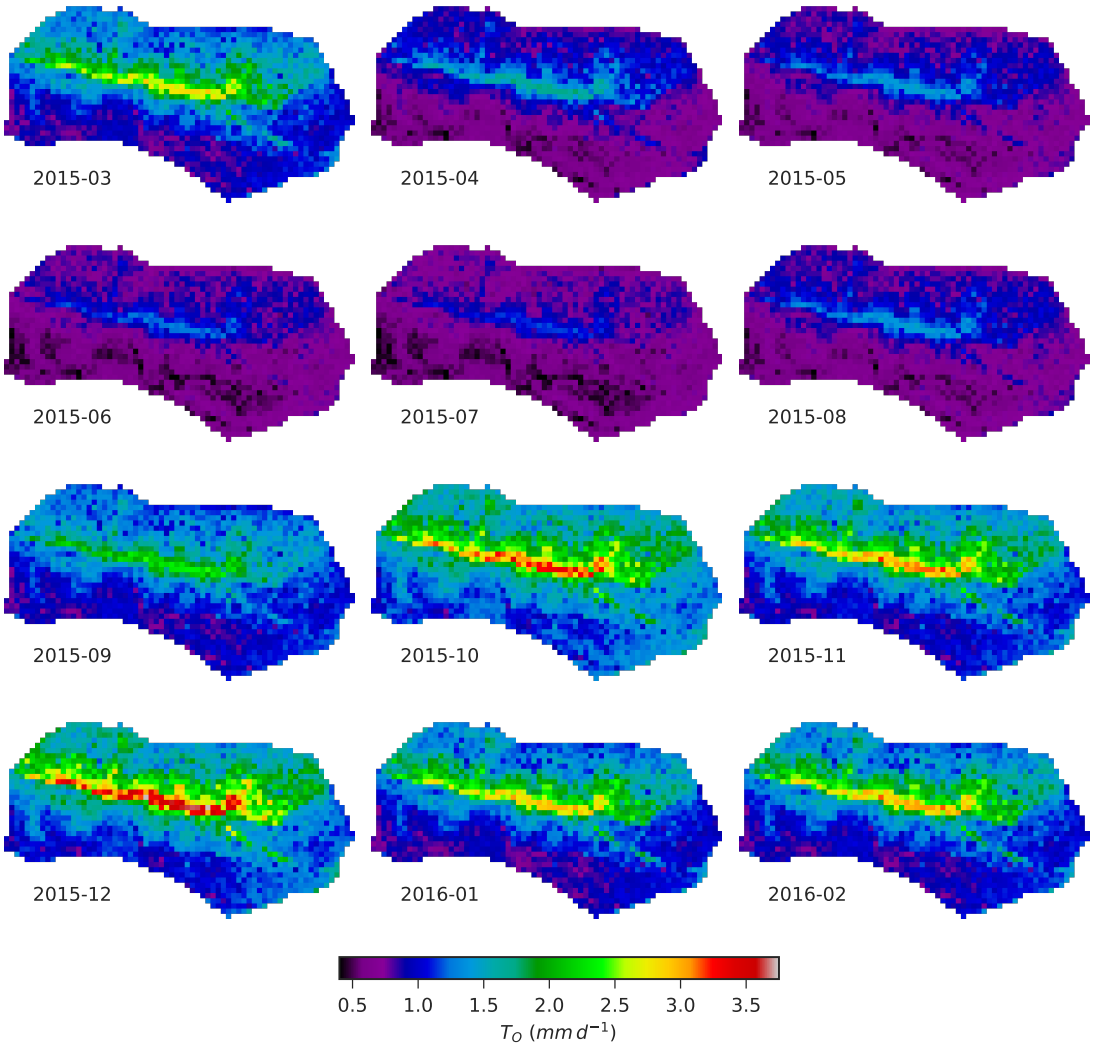

Figure 5.5: Monthly mean overstory transpiration (T_O) rates.

with lowest mean T_O, spatial variability was also lowest in winter (Fig. 5.5 & Fig. 5.7a), while increasing mean T_O, as well as increasing spatial variability were observed from July to October. T_O rates picked up again on southern aspects and in proximity to the channel in December, whereas T_O on the upper north-facing hillslopes declined, resulting in peak mean T_O but also peak spatial variance (Fig. 5.5).

Understory and forest floor evapotranspiration

Understory and forest floor evapotranspiration (ET_U) was generally patchy due to noisy LAI_U patterns (Fig. 5.6). However, general spatio-temporal trends emerged, where ET_U

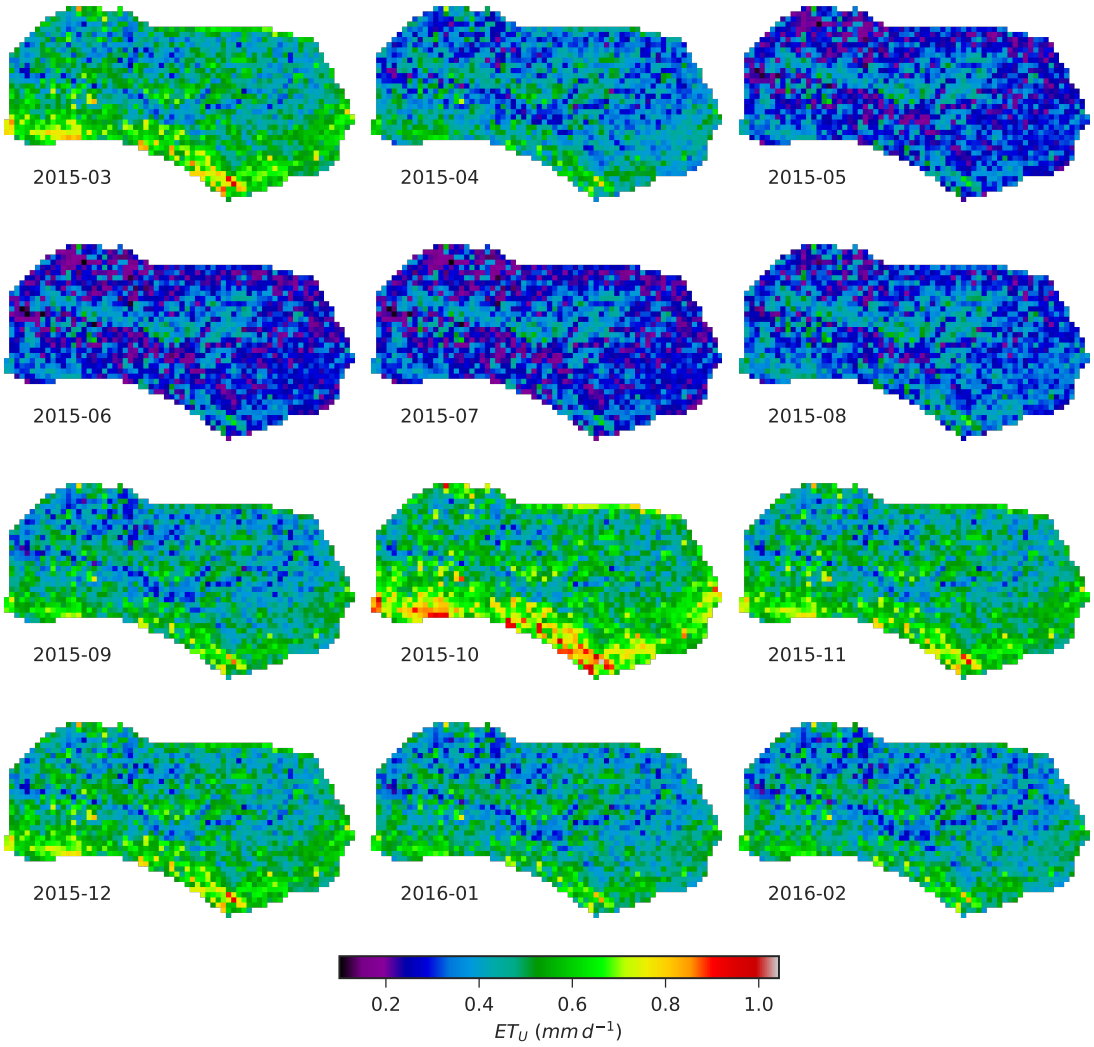

Figure 5.6: Monthly mean understory and forest floor evapotranspiration (ET_U).

was significantly (Wilcoxon rank-sum test, p<0.001) higher on the northern aspect (mean: 0.41±0.09 $mm\ d^{-1}$) compared to south-facing hillslopes (mean: 0.37±0.08 $mm\ d^{-1}$). ET_U was lower during the winter months and highest in early summer. Similar to T_O patterns, monthly means and spatial variability of ET_U were lowest in July (mean: 0.34±0.08

$mm\ d^{-1}$) whereas peak ET_U and peak variability were observed in November (mean: 0.56±0.13 $mm\ d^{-1}$), earlier compared to T_O (Fig.5.7). During winter, ET_U differences between aspects were relatively small, whereas in summer ET_U rates were ∼2-fold higher on the north-facing slope compared to southern aspects. Further, ET_U patterns in response to drainage position varied with aspect. On south-facing slopes, higher ET_U rates were generally observed on the lower hillslope, while the pattern reversed on northern aspects and upper hillslopes posed higher ET_U.

5.3.5 ET drivers

In general, T_O rates were much higher and seasonally more variable than ET_U fluxes (Fig. 5.7a,b).

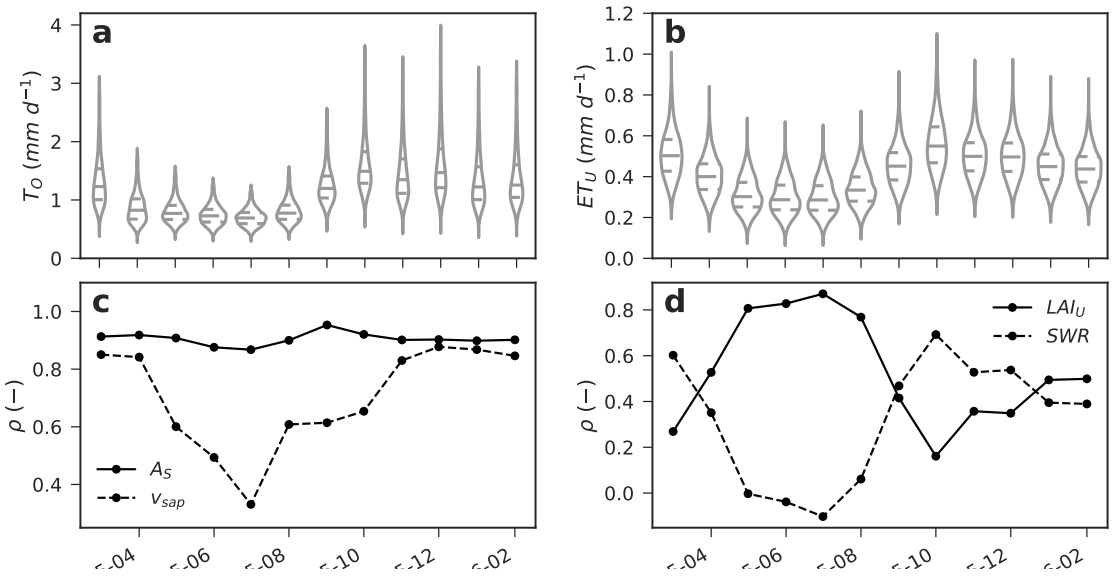

Figure 5.7: Top panels: Violin plots of monthly mean a) overstory transpiration (T_O) and b) understory and forest floor evapotranspiration (ET_U) across the catchment. Bottom panels: Spearman rank correlation coefficients (ρ) between c) monthly T_O and sap velocity (v_{sap}) or sapwood areas (A_S), respectively. ET_U was correlated against understory leaf area index (LAI_U) and sub-canopy short-wave radiation (SWR).

A strong correlation between spatial A_S patterns and monthly T_O rates was observed

throughout the monitoring period (Fig. 5.7c). In contrast, sap velocity (v_{sap}) influence on T_O patterns showed a clear seasonal pattern, where v_{sap} patterns correlated well with T_O patterns from November to April (Spearman $\rho > 0.8$) but then declined until July before slowly recovering (Fig. 5.7c). Thus, spatial T_O patterns during the summer months were shaped by both spatial A_S as well as v_{sap} patterns, whereas in winter A_S patterns caused most of the spatial heterogeneity of T_O.

A similar pattern was observed when correlating ET_U with SWR_U and LAI_U (Fig. 5.7c). During winter, when mean ET_U and variability was lowest, correlation with SWR_U was lowest as well, whereas in summer LAI_U and SWR_U were similarly important.

5.3.6 ET partitioning

Annual T_O ranged from 195 to 891 mm (mean: 425±127 mm, Fig. 5.8a), while ET_U contributed 68 to 279 mm (mean: 146±32 mm, Fig. 5.8b). T_O rates were significantly higher on the southern aspects and increased towards favorable drainage positions. However, T_O fluxes decreased more abruptly in upslope direction on northern aspects compared to south-facing hillslopes (Fig. 5.8a).

While, ET_U was significantly higher on the northern aspects, differences were not as large compared to annual T_O patterns (Fig. 5.8a). Drainage position had contrasting effect on north and south-facing slopes. On the southern aspect, ET_U was highest in drainage lines, whereas ET_U fluxes near the ridges dominated on the northern aspect.

Annual ET ranged from 596 to 1309 mm (mean: 808 ±126 mm) and spatial patterns were mainly shaped by T_O patterns (Fig. 5.8c,d). The T_O fraction ($f_{T_O} = T_O / (T_O + ET_U)$) spanned a large range from 0.48 to 0.91 (mean: 0.78±0.05) and was significantly (Wilcoxon rank-sum test, $p<0.001$) larger on the southern compared to the northern aspects (Fig. 5.8c). T_O contribution were particularly large on the lower (south-facing) hillslopes, whereas

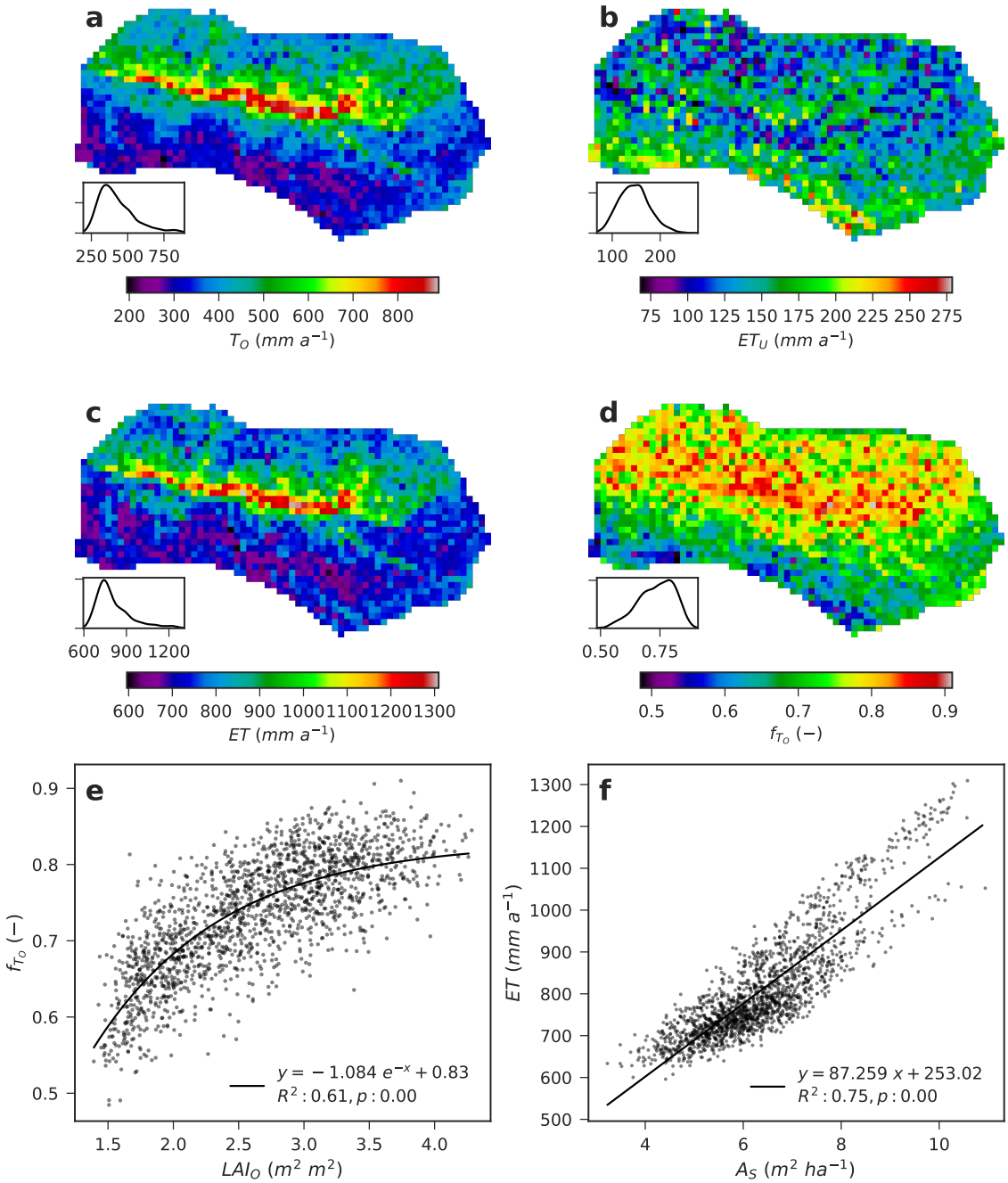

Figure 5.8: Spatial patterns of mean annual a) overstory transpiration (T_O), b) understory and forest floor evapotranspiration (ET_U), c) annual total ET, d) the T_O fraction ($f_{T_O} = T_O\ /\ (T_O\ + ET_U)$), e) the T_O fraction in relation to overstory leaf area index (LAI_O) and annual ET in relation to sapwood area index (A_S).

f_{T_O} was lowest on the upper north-facing slopes . While the overstory LAI could explain 61% of observed f_{T_O} (Fig. 5.8e), annual ET patterns were well correlated to A_S patterns (Fig. 5.8f)

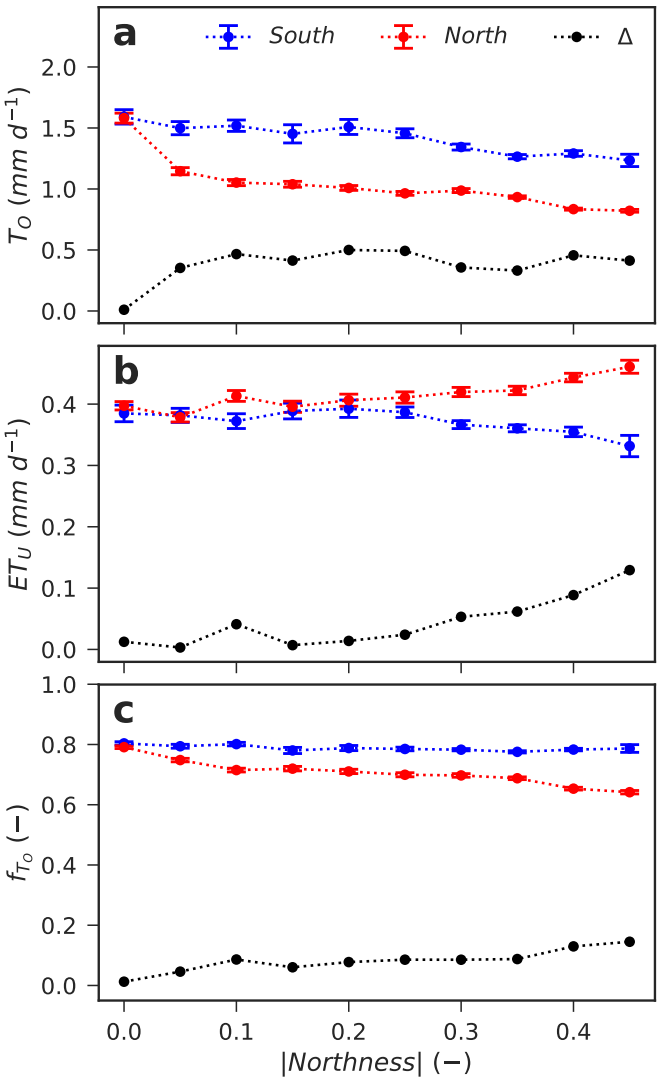

Figure 5.9: Effect of slope orientation on ET patterns. ET patterns were split into northern and southern aspect, aggregated in 0.05 northness ($\sin(slope) \times \cos(aspect)$) bins. Class means, standard error of the mean and the difference between southern and northern aspects in each bin are shown. T_O: overstory transpiration, ET_U: understory and forest floor evapotranspiration, F_{T_O}: T_O / (T_O + ET_U).

Northness ($\sin(slope) \times \cos(aspect)$), a proxy for the strength of slope inclination in

north or south direction, revealed characteristic T_O, ET_U and f_{T_O} patterns (Fig. 5.9a). In relatively flat areas (absolute northness 0-0.05) mean T_O between aspects was similar but variability was larger on northern aspects (North: 1.58±0.45 $mm\ d^{-1}$, South: 1.58±0.31 $mm\ d^{-1}$) (Fig. 5.9a). A relatively small increase in absolute northness (0.05-0.10) caused a steep decrease to 1.15±0.22 $mm\ d^{-1}$ on the northern aspects, while T_O on the southern aspects only slightly declined to 1.50±0.31 $mm\ d^{-1}$. After this initial drop in T_O on the northern aspects, T_O declined gradually with increasing absolute northness on both aspects and differences between north and south slopes ranged from 0.45 to 0.5 $mm\ d^{-1}$. However, with declining T_O, the spatial variability also deceased on the northern aspect resulting in larger spatial variability on moderate and steep south-facing slopes. $\Delta\ T_O$ decrease between an absolute northness of 0.3 and 0.35 was caused by steep slopes in predominantly western aspects in the head area of the catchment, where relative small divergence towards southern or northern aspects resulted in relative large absolute northness values (Fig. 5.2b-d).

In contrast small and moderate absolute northness seemed to have little impact on ET_U (Fig. 5.9b), with an exception at an absolute northness around 0.1, caused by the converging area in the transition from the south-facing flank to the west-facing head area (Fig. 5.2b-d). However, ET_U on the northern aspects exponentially increased above an absolute northness of 0.25, while an exponential decrease was observed on the south-facing slopes. Consequently, a 2-fold increase in absolute northness (0.2 to 0.45) resulted in a 10-fold $\Delta\ T_O$ increase from 0.013 to 0.13 $mm\ d^{-1}$.

f_{T_O} remained constant on the south-facing slopes around 0.8 regardless of absolute northness (Fig. 5.9c). Neglecting the ET_U increase around 0.1 absolute northness, f_{T_O} gradually decreased on the northern aspects from 0.79±0.05 to 0.64±0.04. Thus, $\Delta\ f_{T_O}$ increased almost linear from 0.01 to 0.15 with increasing absolute northness.

Topographic controls on energy and water fluxes manifested in a large spread around the

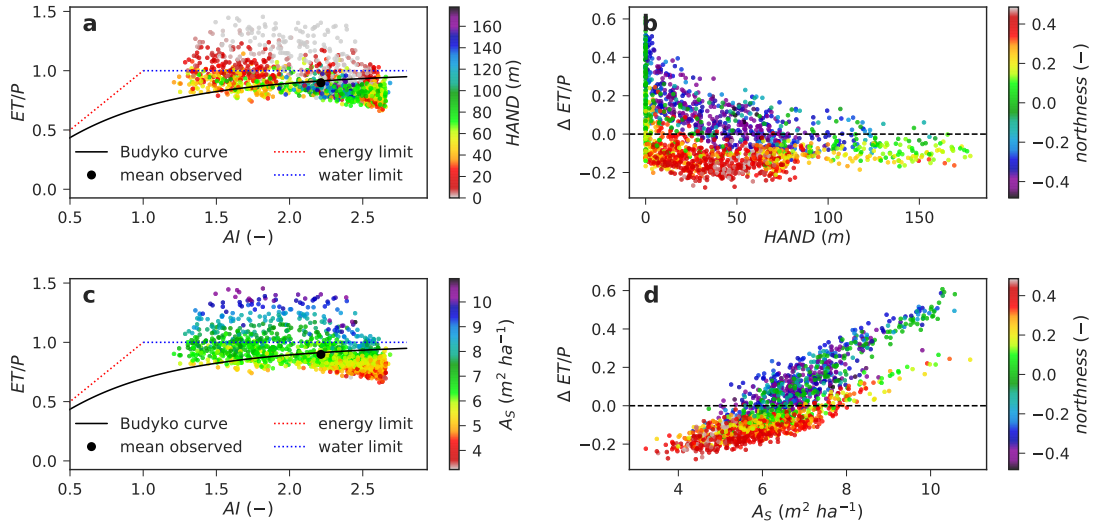

Figure 5.10: Sub-catchment (20×20 m) ET values plotted in the Budyko frame work (a,b) and model residuals in relation to (b) height above nearest drainage (HAND) and (d) sapwood area index (A_S).

mean aridity (2.21±0.39) ranging from 1.21 to 2.69 (Fig. 5.10a,c). While, the mean observed ET agreed well with the estimate using the Budyko framework, considerable deviations around the curve were observed on finer spatial scales (20×20 m pixels) basis (Fig. 5.10a,c). ET at favorable drainage position (low HAND) and on southern aspects (negative northness) was strongly underestimated using the Budyko framework (Fig. 5.10a,b). In contrast, ET on northern aspects (positive northness) and closer to ridges (high HAND) was overestimated in the Budyko framework. Deviations around the Budyko curve were significantly ($p<0.001$) correlated to aridity (r=-0.69), northness (r=-0.62), HAND (r=-0.39) and TWI (r=0.44). However, sapwood area was stronger related to residuals (r=0.85) than any topographic index (Fig. 5.10d).

5.4 Discussion

Regression models using LiDAR data reveled distinct vegetation patterns in response to landscape position, which in turn manifested in characteristic spatio-temporal ET patterns. While sapwood area (A_S) and overstory leaf area index (LAI_O) were significantly larger on southern aspects, drainage position exerted stronger control on A_S and LAI_O patterns on northern aspects than on south-facing slopes. Understory leaf area index (LAI_U) was significantly larger on southern aspects as well, but in contrast to A_S and LAI_O, LAI_U patterns were more responsive to changes in drainage position on southern aspects. A combination of quasi static A_S patterns and dynamic sap velocity (v_{sap}) patterns in response to shorter-term hydro-climatic conditions resulted in significantly higher transpiration (T_O) rates on southern aspects. T_O was lower and spatially more uniform in winter, whereas mean T_O as well as spatial variability peaked in summer. Further, A_S exerted control on spatial T_O patterns throughout the year, whereas v_{sap} mainly enhanced spatial heterogeneity during summer. In contrast, understory and forest floor evapotranspiration (ET_U) was significantly higher on northern aspects and while structural parameters (LAI_U) also controlled winter fluxes, short-term climatic conditions became more important in summer. Moreover, distinct patterns of ET partitioning emerged in response to landscape position, where the annual T_O fraction (f_{T_O}) was significantly higher on southern slopes. Contrasting, non-linear T_O and ET_U patterns were unveiled in relation to northness (Fig. 5.9), a proxy for the strength of slope inclination facing north or south. The northness threshold triggering diverging non-linear patterns between aspects was lower for T_O than for ET_U. While strong T_O deviation at low absolute northness was observed between aspects, higher absolute northness had similar effects at both aspects. In contrast, ET_U between aspects remained at similar levels until moderate slope inclination,

after which ET_U fluxes exponentially increased on northern aspects, while simultaneously decreasing on southern aspects. Interestingly, f_{T_O} remained stable on the southern slopes regardless of slope inclination, whereas f_{T_O} gradually decreased with increasing northness on the north-facing slopes. Further, LAI_O could explain 61% of f_{T_O} variations entire catchment.

5.4.1 Vegetation patterns

A_S and LAI_U concentration along the main drainage lines could be partially attributed to species patterns. *Pomaderris aspera*, which had exceptionally high A_S (see Chapter 2), was almost exclusively abundant at lower southern hillslopes. Similarly, broad leaved understory species (tree ferns, sedges, water ferns, etc.), which contributed the largest fraction to ET_U were mainly abundant on the lower slopes and converging areas on southern aspects and thus LAI_U tended to be higher in those locations.

Larger absolute A_S and LAI_O gains along the drainage gradient on northern aspects compared to south-facing slopes were most likely caused by shallower, poorer developed soils and higher short-wave radiation (SWR) loads. Higher SWR due to slope orientation, less canopy cover and thus higher soil evaporation rates manifested in greater competition for plants on northern aspects and generally lower soil moisture. Lower moisture content in turn impeded pedogenesis, leading to lower soil water storage capacity and potentially lower infiltration rates on north-facing slopes. Consequently, smaller precipitation fractions were stored "locally" and more water was redistributed in downslope areas on norther aspects resulting in larger contrasts between upslope and downslope areas compared to southern aspects (Niu et al. 2014).

Less sensitivity of LAI_U to drainage position might have been caused by shallower rooting depth of understory species and thus the inability to access deep soil moisture. Larger LAI_U

dynamics on southern aspects could be explained by non-linear response of sub-canopy radiation loads to slope orientation and vegetation patterns (Zou et al. 2007; Nyman et al. 2017). Relatively low solar elevation caused radiation to penetrate considerably more biomass on southern aspects compared to north-facing slopes, particularly at lower hillslope positions. Thus, surface evaporation is higher on northern aspects and consequently litter and surface soil moisture lower (Nyman et al. 2015), ultimately restricting the topsoil development (Geroy et al. 2011) and offering less favorable growing conditions for understory vegetation.

The general patchiness of LAI_U could be related to several factors. Firstly, uncertainties associated with vertical LiDAR precision ($\pm$20 cm) likely introduced noise when analyzing returns closed to the ground surface. Secondly, the likelihood of understory returns and thus sample size, decreased with overstory cover using a discrete four return LiDAR scanner. Further, shallow rooting depth of understory vegetation might have caused vegetation adaptation on small spatial scales in response to surface moisture patterns due to local micro-topography or throughfall patterns.

5.4.2 ET patterns

Annual T_O of pixels in the catchment ranged from 196 to 892 mm, spanning the range observed in Heathy Dry forests (Yunusa et al. 2010) to wet *E. regnans* forests (Benyon et al. 2017), with <1 km spatial extent. Generally higher T_O rates in favorable drainage position and on southern aspects can be explained by higher moisture content (Martinez et al. 2008) and deeper (Tesfa et al. 2009), more developed soils (Rasmussen and Tabor 2007; Geroy et al. 2011) on polar-facing slopes and in lower drainage positions, resulting in more plant available water. Further, water redistribution in downward direction can contribute to high T_O in favorable drainage positions (Niu et al. 2014; Thompson et al.

2011). Thus, T_O peaked in December on the south-facing slopes, whereas maximum T_O on the northern aspects was observed in October (Fig. 5.5) and thereafter probably became water-limited. Very few other studies have investigated spatio-temporal water use patterns or evapotranspiration patterns in mixed species eucalypt forests. Gharun et al. (2015) also found varying v_{sap} rates in relation to landscape position, where v_{sap} and spatial variability where also highest in summer and lowest during winter. Further, highest mean annual sap velocity were reported on steep southern aspects and in flat areas. However, they did not report vegetation patterns, e.g. LAI or A_S. In contrast, Mitchell et al. (2012a) found similar sap velocity rates across species and tree sizes at different landscape positions and related majority of the ET signal to structural vegetation changes due to elevation gradients. However, majority of their research catchment was south-east and south-westerly facing and thus lacked potentially strong contrasts due to northerly aspects. In non-water limited Eucalypt forests, where sap velocity, stand structure and species composition were spatially more homogeneous, A_S patterns explained annual ET (Benyon et al. 2017; Benyon et al. 2015) and stream flow (Benyon et al. 2017). Close links between vegetation patterns and topography, soils and climate have be illustrated in a broad range of ecosystems outside of Australia (Flores Cervantes et al. 2014; Rasmussen et al. 2015; Hwang et al. 2011; Zapata-Rios et al. 2016; Gutirrez-Jurado et al. 2013; Pelletier et al. 2013). The fact that A_S patterns could explain T_O in all seasons despite v_{sap} heterogeneity points towards optimization of vegetation to hydro-climatic conditions at a given landscape position in the studied ecosystem. A_S, LAI_O decline from gullies to ridges was stronger and more abrupt on northern aspects (Fig. 5.2g,h) and soils were deeper in mid-slope positions on southern aspects (see Chapter 2). Hence, higher T_O rates could be sustained on steeper upslope areas at southern aspects compared to north-facing slopes (Fig.5.5, Fig. 5.8a, Fig. 5.9a).

Annual ET_U ranged from 68 to 279 mm, thus exceeding the range from limited experimental data on ET_U in SE Australian MSEF (144 mm (Mitchell et al. 2012b), 285-323 mm (Nolan et al. 2014)) over very short spatial extents. In contrast to T_O, ET_U was significantly higher on northern aspects compared to southern aspects and contrasting ET_U patterns in relation to drainage position were observed between aspects. While SWR decreased from the ridges to gullies on the south-facing slopes (Fig. 5.4), LAI_U did also increase in response to drainage position (Fig. 5.2i & Fig. 5.3c,f), resulting in higher ET_U in downslope areas (Fig. 5.6). Thus, T_O and ET_U decreased in similar fashion with increasing absolute northness (Fig. 5.9a,b). In contrast, LAI_U patterns due to drainage position were less pronounced on northern aspects (Fig. 5.2i & Fig. 5.3c,f), while SWR_U increases up to 3-fold (Fig. 5.4). The generally more patchy ET_U patterns were caused by heterogeneous LAI_U patterns, discussed earlier. However, the ET_U model was able to capture general trends that emerged from ET_U plot observations, where ET_U decreased in down-slope direction on the northern aspects, while increasing on the south-facing transect (see Chapter 3).

fT_O observed in the study area (0.48 to 0.91) spanned a large range of previously reported plot studies carried out in contrasting eucalypt ecosystems ranging from ∼50% in open woodlands in Western Australia (Mitchell et al. 2009) to 0.58-0.76 in dry and damp MSEF in central and northern Victoria (Nolan et al. 2014; Mitchell et al. 2012b) and to 0.81 - 0.89 in E. regnans forests (Benyon et al. 2017), illustrating the strong topographic control in the studied ecosystem. Stable fT_O on southern aspects, while fT_O decreased on north-facing slopes can be attributed to feedbacks between slope orientation and vegetation patterns. Less plant available water due to shallower soils lead to sparser canopy cover and thus less plant water use. On southern aspects, reduced canopy cover had comparatively little impact on SWR_U, because radiation had to penetrate upslope vegetation due to

low incident angles (Nyman et al. 2017). In contrast, radiation path length through the vegetation layer was short and mostly affected by "local" vegetation on northern aspects. Therefore, a potentially strong feedback evolves, where decreasing canopy cover resulted in higher SWR_U which in turn causes higher soil evaporation and thus lower soil moisture and LAI_U. While T_O was regulated in response to water-availability, ET_U was not. Despite lowering LAI_U and thus understory transpiration, ET_U will shift more and more to soil and litter evaporation. Hence, decreasing LAI_O had opposing effects between aspects and mainly caused declines in f_{T_O} on upper north-facing slopes. Consequently, LAI_O could explain f_{T_O} because it captured T_O patterns via links to A_S as well as ET_U via modifying sub canopy SWR patterns. Further, a saturating relationship between LAI_O and f_{T_O} (Fig. 5.8d) indicated that LAI_O variations in the lower range have large consequences for ET partitioning, while increasing LAI_O had comparatively little impact on fT_O at high LAI_O. No significant relation between interception loss and LAI (R^2 : 0.01, p=0.89, see chapter 4) or landscape position was found, and thus ET partitioning in the study was restricted on T_O and ET_U.

The limitation of lumped models to predict sub-catchment processes and patterns in heterogeneous forested headwater catchments was illustrated by the large scatter around the Budyko curve using topographically adjusted aridity index and scaled ET measurements on 20 m spatial resolution (Fig. 5.10). The significance of "non-local" water subsidies in this ecosystem became evident by the fact that 17.8% of the catchment area plots above the theoretical water limit (Fig. 5.10a,b) confirming recent studies illustrating effects of contribution groundwater and lateral water movement in the Budyko framework (Condon and Maxwell 2017; Rouholahnejad Freund and Kirchner 2017). However, both the scatter around the Budyko curve and and spatial sub-catchment ET patterns were explained well by sapwood area patterns (Fig. 5.8f & Fig. 5.10d). Hence, vegetation and terrain patterns

could potentially be used to predict small scale sub-catchment ET patterns using the Budyko framework.

Spatio-temporal patterns presented in this Chapter are largely unvalidated model outputs, scaled from on intensive plot measurements. However, time and monetary restrains (sap flow sensor costs) prohibited a more thorough, replicated study design that would have enabled more thorough validation of spatio-temporal patterns. Thus, future research following up work on this work could seek to test whether observed water balance patterns hold in other forest ecosystems in SE Australia and ultimately explore the potential use of terrain and vegetation patterns to infer ecosystem state and functioning at sub-catchment scale.

5.5 Conclusion

This study revealed large spatio-temporal ET patterns despite a relatively uniform nature of the site, same geology, precipitation input and climate. However, topography controls - via slope orientation and drainage position - manifested in highly variable ET rates over spatial extent of 100s of meters, which correspond to ranges observed in arid open woodlands in Western Australia and heathy dry forests of northern Victoria to wet mountain ash forests in the Victorian highlands. Sapwood area, overstory and understory leaf area index were significantly higher on southern aspects. While, more vegetation on south-facing slopes translated to higher overstory transpiration rates compared to northern aspects, understory and forest floor ET was higher on north-facing slopes, particularly close to ridge tops. Thus, ET partitioning was stable on southern aspects, whereas the contribution of overstory transpiration gradually decreased in upslope direction on north-facing slopes. Moreover, topographic thresholds triggering diverging ET patterns between aspects were lower for the overstory than for the understory. The degree to which structural

properties or climatic forcing control ET patterns did underlie strong seasonality, where climatic impact was strongest during summer and lowest in winter. Thus, much of the observed differences originated from topographic effects at timescales of soil development which determined plant available water capacity and on intermediate time scales the establishment of vegetation communities. Vegetation patterns then interacted with present hydro-climate and topography leading to distinct transpiration and sub-canopy micro-climatic patterns which drive understory ET. Strong observed links between vegetation patterns, topography, water and energy fluxes illustrated dominant topographic control in this ecosystems characteristic for large parts of SE Australian forests. Moreover, remotely sensed vegetation and terrain patterns unveiled their potential to be used to downscale large-scale lumped models (e.g. Budyko framework) in complex upland forests.

Bibliography

Alexander, C. et al. (2016). "Micro-topography driven vegetation patterns in open mosaic landscapes". In: *Ecological Indicators* 60, pp. 906–920.

Asbjornsen, H. et al. (2011). "Ecohydrological advances and applications in plant-water relations research: a review". In: *Journal of Plant Ecology* 4.1, pp. 3–22.

Asner, G. P. et al. (2012). "A universal airborne LiDAR approach for tropical forest carbon mapping". In: *Oecologia* 168.4, pp. 1147–1160.

Benyon, R. G. et al. (2015). "Use of a forest sapwood area index to explain long-term variability in mean annual evapotranspiration and streamflow in moist eucalypt forests: streamflow predicted from sapwood area". In: *Water Resources Research* 51.7, pp. 5318–5331.

Benyon, R. G. et al. (2017). "Stand-level variation in evapotranspiration in non-water-limited eucalypt forests". In: *Journal of Hydrology* 551, pp. 233–244.

Beven, K. J. and M. J. Kirkby (1979). "A physically based, variable contributing area model of basin hydrology". In: *Hydrological Sciences Bulletin* 24.1, pp. 43–69.

Bren, L. and P. Hopmans (2007). "Paired catchments observations on the water yield of mature eucalypt and immature radiata pine plantations in Victoria, Australia". In: *Journal of Hydrology* 336.3, pp. 416–429.

Bren, L. et al. (2010). "Longer-term water use of native eucalyptus forest after logging and regeneration: The Coranderrk experiment". In: *Journal of Hydrology* 384.1, pp. 52–64.

Bren, L. et al. (2013). “Impacts of native forest harvesting on flows into the MurrayDarling Basin system”. In: *Australian Forestry* 76.2, pp. 91–100.

Condon, L. E. and R. M. Maxwell (2017). “Systematic shifts in Budyko relationships caused by groundwater storage changes”. In: *Hydrology and Earth System Sciences* 21.2, pp. 1117–1135.

Crawford, T. M. and C. E. Duchon (1999). “An Improved Parameterization for Estimating Effective Atmospheric Emissivity for Use in Calculating Daytime Downwelling Longwave Radiation”. In: *J. Appl. Meteor.* 38.4, pp. 474–480.

Dawson, T. E. et al. (2007). “Nighttime transpiration in woody plants from contrasting ecosystems”. In: *Tree Physiology* 27.4, pp. 561–575.

Dios, V. R. Resco de et al. (2015). “Processes driving nocturnal transpiration and implications for estimating land evapotranspiration”. In: *Scientific Reports* 5, p. 10975.

Emanuel, R. E. et al. (2014). “Vegetation and topographic influences on the connectivity of shallow groundwater between hillslopes and streams”. In: *Ecohydrology* 7.2, pp. 887–895.

Field, J. P. et al. (2015). “Critical Zone Services: Expanding Context, Constraints, and Currency beyond Ecosystem Services”. In: *Vadose Zone Journal* 14.1.

Flores Cervantes, J. H. et al. (2014). “A geomorphic perspective on terrain-modulated organization of vegetation productivity: analysis in two semiarid grassland ecosystems in Southwestern United States”. In: *Ecohydrology* 7.2, pp. 242–257.

Geroy, I. et al. (2011). “Aspect influences on soil water retention and storage”. In: *Hydrological Processes* 25.25, pp. 3836–3842.

Gharun, M. et al. (2015). “Mapping spatial and temporal variation in tree water use with an elevation model and gridded temperature data”. In: *Agricultural and Forest Meteorology* 200, pp. 249–257.

Givnish, T. J. et al. (2014). “Determinants of maximum tree height in Eucalyptus species along a rainfall gradient in Victoria, Australia”. In: *Ecology* 95.11, pp. 2991–3007.

Gobakken, T. and E. Nsset (2005). “Weibull and percentile models for lidar-based estimation of basal area distribution”. In: *Scandinavian Journal of Forest Research* 20.6, pp. 490–502.

Good, S. P. et al. (2015). “Hydrologic connectivity constrains partitioning of global terrestrial water fluxes”. In: *Science* 349.6244, pp. 175–177.

Groeneveld, D. P. (1997). “Vertical point quadrat sampling and an extinction factor to calculate leaf area index”. In: *Journal of Arid Environments* 36, pp. 475–485.

Gutirrez-Jurado, H. A. et al. (2013). “On the observed ecohydrologic dynamics of a semiarid basin with aspect-delimited ecosystems: ecohydrologic dynamics of a semiarid basin”. In: *Water Resources Research* 49.12, pp. 8263–8284.

Haydon, S. R. et al. (1997). “Variation in sapwood area and throughfall with forest age in mountain ash (Eucalyptus regnans F. Muell.)” In: *Journal of Hydrology* 187.3, pp. 351–366.

Hwang, T. et al. (2011). “Topography-mediated controls on local vegetation phenology estimated from MODIS vegetation index”. In: *Landscape Ecology* 26.4, pp. 541–556.

Jasechko, S. et al. (2013). “Terrestrial water fluxes dominated by transpiration”. In: *Nature* 496.7445, pp. 347–350.

Jaskierniak, D. et al. (2016). “Predicting long-term streamflow variability in moist eucalypt forests using forest growth models and a sapwood area index: PREDICTING STREAMFLOW WITH FOREST GROWTH MODELS”. In: *Water Resources Research* 52.4, pp. 3052–3067.

Jaskierniak, D. et al. (2015). "Using Tree Detection Algorithms to Predict Stand Sapwood Area, Basal Area and Stocking Density in Eucalyptus regnans Forest". In: *Remote Sensing* 7.6, pp. 7298–7323.

Jencso, K. G. and B. L. McGlynn (2011). "Hierarchical controls on runoff generation: Topographically driven hydrologic connectivity, geology, and vegetation". In: *Water Resources Research* 47.11.

Jensen, J. L. R. et al. (2008). "Discrete return lidar-based prediction of leaf area index in two conifer forests". In: *Remote Sensing of Environment* 112.10, pp. 3947–3957.

Kitagawa, R. et al. (2014). "Spatial pattern of forest structure mediated by topography in a steep mountain basin in West Tanzawa, Japan". In: *Journal of Forest Research* 19.1, pp. 205–214.

Kristensen, T. et al. (2015). "Mapping Above- and Below-Ground Carbon Pools in Boreal Forests: The Case for Airborne Lidar". In: *PLOS ONE* 10.10. Ed. by K. P. Vadrevu, e0138450.

Kuczera, G. (1987). "Prediction of water yield reductions following a bushfire in ash-mixed species eucalypt forest". In: *Journal of Hydrology* 94.3, pp. 215–236.

Lane, P. N. and S. M. Mackay (2001). "Streamflow response of mixed-species eucalypt forests to patch cutting and thinning treatments". In: *Forest Ecology and Management* 143.1, pp. 131–142.

Lane, P. et al. (2010). "Modelling the long term water yield impact of wildfire and other forest disturbance in Eucalypt forests". In: *Environmental Modelling & Software* 25.4, pp. 467–478.

Macfarlane, C. et al. (2014). "Digital canopy photography: Exposed and in the raw". In: *Agricultural and Forest Meteorology* 197, pp. 244–253.

Martinez, C. et al. (2008). "Spatiotemporal distribution of nearsurface and root zone soil moisture at the catchment scale". In: *Hydrological Processes* 22.14, pp. 2699–2714.

McDonnell, J. J. et al. (2007). "Moving beyond heterogeneity and process complexity: A new vision for watershed hydrology". In: *Water Resources Research* 43.7, n/a–n/a.

McDonnell, J. J. (2013). "Are all runoff processes the same?" In: *Hydrological Processes* 27.26, pp. 4103–4111.

Meyer, V. et al. (2013). "Detecting tropical forest biomass dynamics from repeated airborne lidar measurements". In: *Biogeosciences* 10.8, pp. 5421–5438.

Mitchell, P. J. et al. (2009). "Partitioning of evapotranspiration in a semi-arid eucalypt woodland in south-western Australia". In: *Agricultural and Forest Meteorology* 149.1, pp. 25–37.

Mitchell, P. J. et al. (2012a). "Capturing within catchment variation in evapotranspiration from montane forests using LiDAR canopy profiles with measured and modelled fluxes of water: capturing variation in evapotranspiration using lidar". In: *Ecohydrology* 5.6, pp. 708–720.

Mitchell, P. J. et al. (2012b). "Responses of evapotranspiration at different topographic positions and catchment water balance following a pronounced drought in a mixed species eucalypt forest, Australia". In: *Journal of Hydrology* 440-441, pp. 62–74.

Moore, G. W. et al. (2008). "Nocturnal transpiration in riparian Tamarix thickets authenticated by sap flux, eddy covariance and leaf gas exchange measurements". In: *Tree Physiology* 28.4, p. 521.

Moore, I. D. et al. (1993). "Modelling environmental heterogeneity in forested landscapes". In: *Journal of Hydrology* 150.2, pp. 717–747.

Morsdorf, F. et al. (2006). "Estimation of LAI and fractional cover from small footprint airborne laser scanning data based on gap fraction". In: *Remote Sensing of Environment* 104.1, pp. 50–61.

Nippgen, F. et al. (2015). "The spatial and temporal evolution of contributing areas". In: *Water Resources Research* 51.6, pp. 4550–4573.

Niu, G.-Y. et al. (2014). "An integrated modelling framework of catchment-scale ecohydrological processes: 2. The role of water subsidy by overland flow on vegetation dynamics in a semi-arid catchment". In: *Ecohydrology* 7.2, pp. 815–827.

Nobre, A. et al. (2011). "Height Above the Nearest Drainage: a hydrologically relevant new terrain model". In: *Journal of Hydrology* 404.1, pp. 13–29.

Nolan, R. H. et al. (2014). "Changes in evapotranspiration following wildfire in resprouting eucalypt forests". In: *Ecohydrology*, pp. 1363–1377.

Nolan, R. H. et al. (2015). "Trends in evapotranspiration and streamflow following wildfire in resprouting eucalypt forests". In: *Journal of Hydrology* 524, pp. 614–624.

Nyman, P. et al. (2014). "Downscaling regional climate data to calculate the radiative index of dryness in complex terrain". In: *Australian Metrological and Oceanographic Journal* 64.2, pp. 109–122.

Nyman, P. et al. (2015). "Quantifying the effects of topographic aspect on water content and temperature in fine surface fuel". In: *International Journal of Wildland Fire* 24.8, pp. 1129–1142.

Nyman, P. et al. (2017). "Evaluating models of shortwave radiation below Eucalyptus canopies in SE Australia". In: *Agricultural and Forest Meteorology* 246, pp. 51–63.

Ogle, K. et al. (2012). "Differential daytime and night-time stomatal behavior in plants from North American deserts". In: *New Phytologist* 194.2, pp. 464–476.

Pan, Y. et al. (2011). “A Large and Persistent Carbon Sink in the Worlds Forests”. In: *Science* 333.6045, pp. 988–993.

Peduzzi, A. et al. (2012). “Estimating leaf area index in intensively managed pine plantations using airborne laser scanner data”. In: *Forest Ecology and Management* 270, pp. 54–65.

Pelletier, J. D. et al. (2013). “Coevolution of nonlinear trends in vegetation, soils, and topography with elevation and slope aspect: A case study in the sky islands of southern Arizona”. In: *Journal of Geophysical Research: Earth Surface* 118.2, pp. 741–758.

Pope, G. and P. Treitz (2013). “Leaf Area Index (LAI) Estimation in Boreal Mixedwood Forest of Ontario, Canada Using Light Detection and Ranging (LiDAR) and WorldView-2 Imagery”. In: *Remote Sensing* 5.10, pp. 5040–5063.

Rasmussen, C. and N. J. Tabor (2007). “Applying a Quantitative Pedogenic Energy Model across a Range of Environmental Gradients”. In: *Soil Science Society of America Journal* 71.6, p. 1719.

Rasmussen, C. et al. (2015). “Quantifying Topographic and Vegetation Effects on the Transfer of Energy and Mass to the Critical Zone”. In: *Vadose Zone Journal* 14.11.

Rouholahnejad Freund, E. and J. W. Kirchner (2017). “A Budyko framework for estimating how spatial heterogeneity and lateral moisture redistribution affect average evapotranspiration rates as seen from the atmosphere”. In: *Hydrology and Earth System Sciences* 21.1, pp. 217–233.

Saito, T. et al. (2015). “Using airborne LiDAR to determine total sapwood area for estimating stand transpiration in plantations”. In: *Hydrological Processes* 29.24, pp. 5071–5087.

Savenije, H. H. G. (2010). “Topography driven conceptual modelling (FLEX-Topo)”. In: *Hydrology and Earth System Sciences* 14.12, pp. 2681–2692.

Schlesinger, W. H. and S. Jasechko (2014). “Transpiration in the global water cycle”. In: *Agricultural and Forest Meteorology* 189, pp. 115–117.

Spencer, J. W. (1982). “A comparison of methods for estimating hourly diffuse solar radiation from global solar radiation”. In: *Solar Energy* 29.1, pp. 19–32.

Tesemma, Z. K. et al. (2015). “Including the dynamic relationship between climatic variables and leaf area index in a hydrological model to improve streamflow prediction under a changing climate”. In: *Hydrology and Earth System Sciences* 19.6, pp. 2821–2836.

Tesfa, T. K. et al. (2009). “Modeling soil depth from topographic and land cover attributes”. In: *Water Resources Research* 45.10.

Thompson, S. E. et al. (2011). “Spatial scale dependence of ecohydrologically mediated water balance partitioning: A synthesis framework for catchment ecohydrology”. In: *Water Resources Research* 47.10.

Troch, P. A. et al. (2015). “Catchment coevolution: A useful framework for improving predictions of hydrological change?” In: *Water Resources Research* 51.7, pp. 4903–4922.

Vertessy, R. A. et al. (1993). “Predicting water yield from a mountain ash forest catchment using a terrain analysis based catchment model”. In: *Journal of Hydrology* 150.2, pp. 665–700.

Viglizzo, E. et al. (2016). “Partition of some key regulating services in terrestrial ecosystems: Meta-analysis and review”. In: *Science of The Total Environment* 562, pp. 47–60.

Watson, F. G. R. et al. (1999). “Large-scale modelling of forest hydrological processes and their long-term effect on water yield”. In: *Hydrol. Process.* 13.5, pp. 689–700.

Webb, A. A. and B. W. Jarrett (2013). “Hydrological response to wildfire, integrated logging and dry mixed species eucalypt forest regeneration: The Yambulla experiment”. In: *Forest Ecology and Management* 306, pp. 107–117.

Webb, A. A. et al. (2012). “Longer-term changes in streamflow following logging and mixed species eucalypt forest regeneration: The Karuah experiment”. In: *Journal of Hydrology* 464, pp. 412–422.

Yu, X. et al. (2004). “Automatic detection of harvested trees and determination of forest growth using airborne laser scanning”. In: *Remote Sensing of Environment* 90.4, pp. 451–462.

Yunusa, I. A. et al. (2010). “Topographical and seasonal trends in transpiration by two co-occurring Eucalyptus species during two contrasting years in a low rainfall environment”. In: *Agricultural and Forest Meteorology* 150.9, pp. 1234–1244.

Zapata-Rios, X. et al. (2016). “Influence of terrain aspect on water partitioning, vegetation structure and vegetation greening in high-elevation catchments in northern New Mexico: Terrain Aspect, Water Partitioning, Vegetation Greening in High-elevation Catchments”. In: *Ecohydrology* 9.5, pp. 782–795.

Zeppel, M. et al. (2010). “Rates of nocturnal transpiration in two evergreen temperate woodland species with differing water-use strategies”. In: *Tree Physiology* 30.8, pp. 988–1000.

Zhao, K. et al. (2018). “Utility of multitemporal lidar for forest and carbon monitoring: Tree growth, biomass dynamics, and carbon flux”. In: *Remote Sensing of Environment* 204, pp. 883–897.

Zou, C. B. et al. (2007). “Effects of topography and woody plant canopy cover on near-ground solar radiation: Relevant energy inputs for ecohydrology and hydropedology”. In: *Geophysical Research Letters* 34.24.

Chapter 6

Synthesis

This thesis is the first quantitative study to comprehensively investigate how topographic controls on the Critical Zone structure determine spatial ET patterns in mixed species eucalypt forests (MSEF) at sub-catchment scale (as illustrated in Figure 6.1). Systematically distributed, intensive monitoring plots enabled robust scaling of evapotranspiration (ET) using LiDAR derived vegetation patterns, and thus allowed assessing the effect of aspect, slope angle, drainage position and the combination thereof on vegetation patterns, soil depth and understory and overstory ET.

Chapter two demonstrated that overstory vegetation patterns and structure adjust to water-availability patterns, determined by topographic control on soil depth, water redistribution and radiation loads (Fig. 6.1). Safety versus productivity trade-offs (Hacke et al. 2006; Poorter et al. 2010) at dry sites on shallow soils were confirmed by slower growth rates, smaller trees and less stand sapwood area. The observed vegetation patterns in relation to topographic control on water-availability confirm opportunistic establishment (Brooks et al. 2015) and growth (Griebel et al. 2017) of overstory vegetation in relation to energy and moisture patterns. Spatial water-limitation patterns that shaped the vegetation structure were also evident in contrasting seasonal sap velocity patterns. Trees at well buffered sites on deep soils (gullies and south-facing mid-slope) had highest transpiration

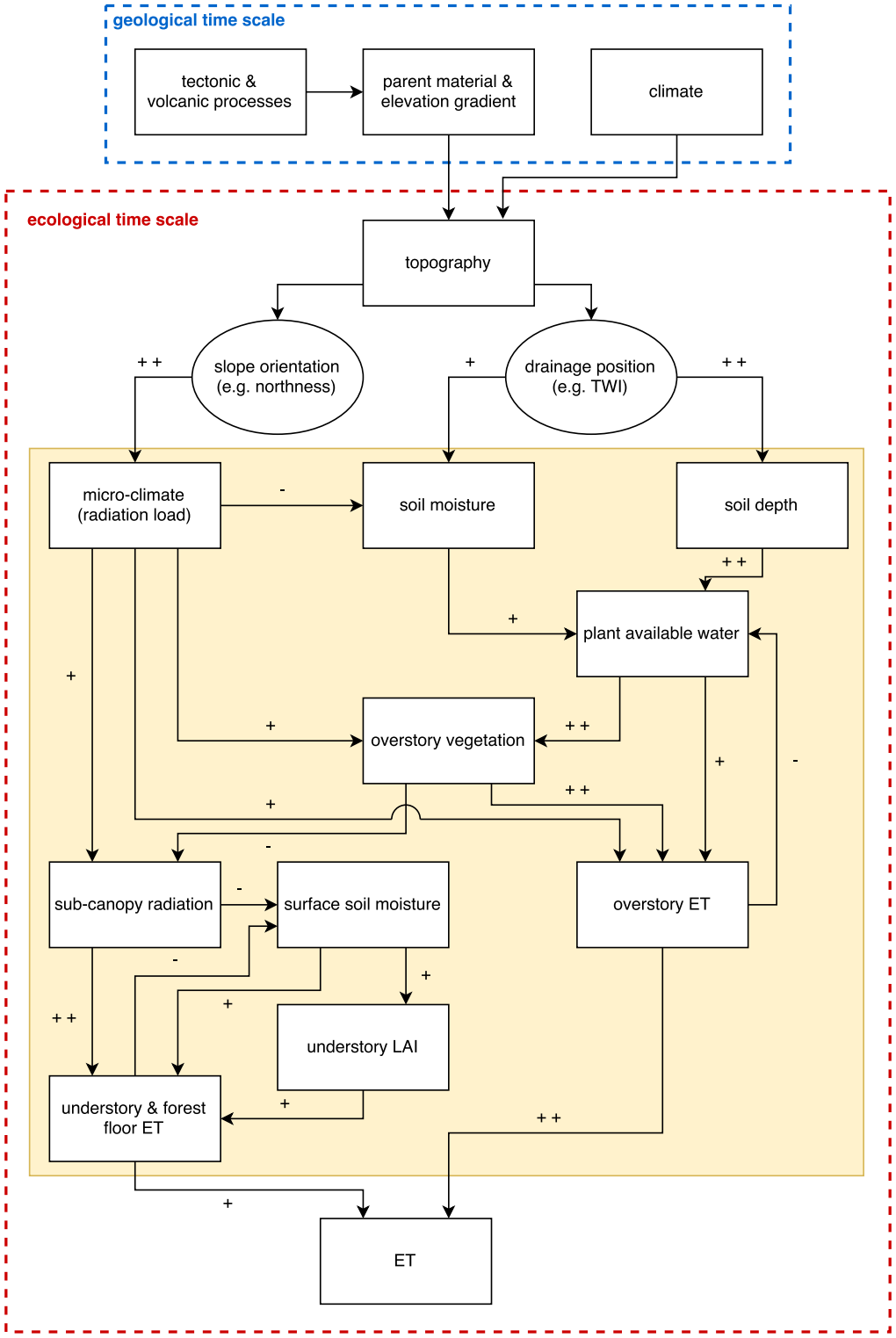

Figure 6.1: Conceptual model describing topographic controls on Critical Zone structure and processes unveiled in this thesis, which determined evapotranspiration patterns. Plus and minus signs indicate direction and strength of relationships.

rates during summer, whereas transpiration rates at sites with shallow soils showed almost no seasonality due to water-limitation in summer. Consequently, mean annual sap velocity was higher on the south-facing plots, but increased on both transects in downslope direction incline with similar sap velocity patterns of another recent study in MSEF (Gharun et al. 2015). Sapwood area patterns further amplified sap velocity contrasts between sites, leading to even larger differences in plot-specific transpiration rates. With decreasing temporal resolution (from hours and days to annual) overstory transpiration controls shifted from atmospheric demand (VPD and SWR) to vegetation structural properties (tree height, DBH, A_S). Thus, annual overstory transpiration (T_O) was mainly controlled by sapwood area index and water-availability patterns in relation to soil depth and topographic redistribution. Further, sapwood area index (A_S) alone explained 89% of the variability in annual stand transpiration despite heterogeneous sap velocity patterns, extending the applicability of A_S from non water-limited (Benyon et al. 2017) to (periodically) water-limited eucalypt forests.

Chapter three illustrated that the understory organized to surface soil moisture patterns. Understory LAI decreased with decreasing soil moisture, and species composition shifted from broad-leaved species (tree ferns, ferns, sedges etc.) to prickly, small-leaved xeric species. Sub-canopy short-wave radiation load (SWR_U) was the main driver of understory and forest floor ET (ET_U), with surface soil moisture playing only a secondary role. In contrast to T_O, soil depth variations did not affect ET_U directly due to shallow rooting depth of understory vegetation. However, the catena effect on soil depth controlled overstory vegetation patterns, as shown in chapter two. Interactions of overstory vegetation and topography in turn resulted in contrasting sub-canopy radiation patterns, surface SWC and understory LAI patterns in response to landscape position. ET_U was generally higher on northern aspects compared to the south-facing slope but drainage position had adverse

effects on ET_U between aspects. In contrast to T_O, ET_U was higher on the upper north-facing hillslope, while higher ET_U was observed on the lower southern aspects. However, the interaction of energy, moisture and vegetation patterns, mediated ET_U differences between landscape positions, since high sub-canopy SWR resulted in lower mean SWC and a lower plot-scale LAI.

Chapter four illustrated the combined effects of aspect and drainage position (quantified by northness, TWI and HAND) on water balance partitioning, which markedly diverged along the south and north-facing transects. All plots on northern aspects had a positive annual water balance (P>ET). In contrast, only the ridge plot on the south-facing slope had a positive water balance, with plots on the lower slopes having higher ET than rainfall. Vegetation patterns organized in relation to water-availability, as predicted by the eco-hydrological equilibrium theory (Eagleson 1982). However, in contrast to expectations, interception loss patterns did not vary with landscape position, despite a large LAI gradient (Aston 1979; Gash 1979). Higher atmospheric demand in open canopies on ridges compared to denser canopy cover in gullies might have offset LAI patterns, as speculated in other studies that did not find significant LAI - interception loss relationships in eucalypt forests either (Nolan et al. 2014; Benyon and Doody 2015). Further, topographic controls on ET varied strongly between overstory and understory. Overstory contribution to total ET increased with more favorable drainage position and soil depths. In contrast, slope orientation controlled understory contributions to total ET. However, vegetation patterns (A_S and LAI) explained ∼90% of the variation in ET between plots.

Chapter five illustrated that the study design, which used distributed plots at systematically varied landscape positions, enabled up-scaling ET in a robust way. This allowed untangling the topographic controls on vegetation and ET patterns.

LAI and A_S were larger on southern aspects, but LAI and A_S gains in relation to

drainage position were higher on northern aspects. Strong spatial terrain and vegetation patterns translated to spatially heterogeneous ET patterns, where overstory transpiration (4.5-fold), understory and forest floor ET (3.5-fold) and total ET rates (2-fold) varied strongly. The observed ranges over as little as 200 m distance typically occur in ecosystems several hundred of kilometers apart. However, spatial variability of total ET was mitigated by uniform interception loss patterns and contrasting overstory and understory patterns with drainage position on northern aspects. T_O dominated ET_U throughout most of the catchment, which appears to be a typical feature of south-east Australian forest stands (Nolan et al. 2014; Mitchell et al. 2012b; Benyon et al. 2017). However, on upper north-facing hillslopes, similar ET_U and T_O was observed, comparable to open arid eucalypt woodlands in Western Australia (Mitchell et al. 2009).

Moreover, this study unveiled contrasting, non-linear overstory and understory patterns with slope inclination between aspects. Small slope inclination already caused strong divergence of T_O patterns between northern and southern aspects. In contrast, ET_U was similar between aspects until moderate slope inclination, after which ET_U increased exponentially on norther-facing slopes while decreasing on southern aspects. As a result, the ratio of T_O to ET_U (f_{T_O}) was stable on southern aspects and decreasing with increasing slope inclination on northern aspects.

The individual effects of slope orientation and drainage position on spatial ET patterns were weak ($R^2 : 0.2 - 0.3$), whereas A_S index alone explained 75% of spatial variation in annual ET despite such heterogeneous forest structures, highlighting organization of vegetation in response to water-availability as a result of complex non-linear interactions between slope orientation and drainage position.

ET predictions using the Budyko framework matched mean observed ET surprisingly well given the spatial heterogeneities of the CZ demonstrated in earlier chapters. However,

substantial biases were unraveled when using topographically down-scaled aridity index at 20 m spatial resolution. ET on southern aspects and favorable drainage positions was strongly underestimated, while ET on north-facing slopes and close to ridges was overestimated in the Budyko framework. Model residuals were linked to topography and sapwood area index, which alone explained ∼72% of the deviation from the Budyko curve. Moreover, the importance of topographic water redistribution in this ecosystem is illustrated by the fact that ET in ∼18% of the catchment area exceeded precipitation inputs and thus plot above the water limit in the Budyko framework (Fig. 5.10).

6.1 Implications

This study has demonstrated that sapwood area index (A_S) can predict annual overstory transpiration rates across a broad range of conditions, where tree size, species composition, soil depth and seasonal water-limitation were highly spatially variable. While previous studies illustrated that A_S could predict stand-level ET in non water-limited forests (Benyon et al. 2015; Benyon et al. 2017), the findings presented here extend the applicability of using sapwood area index to predict transpiration patterns of (periodically) water-limited eucalypt forests in complex terrain. Vegetation patterns can be conceptualized as the "signature" of the Critical Zone at a given landscape position, because vegetation integrates over short-term climatic fluctuations while adapting to topographically controlled patterns of energy and water-availability. LiDAR derived sapwood area, understory LAI and terrain attributes can be used in combination with observations of incoming short-wave radiation to scale plot-scale overstory and understory transpiration measurements. Further, A_S explained large parts of residuals around the Budyko curve, illustrating the potential of using A_S patterns to down-scale ET estimates of lumped models. Thus, increasing availability of high resolution data (UAVs or high resolution satellites) of vegetation and

terrain patterns offers the potential to i) infer spatial organization of Critical Zone patterns and ii) down-scale lumped models for operational purposes.

ET estimates from six systematically distributed plots varied strongly and while mean ET from the six plots agreed relatively well with mean scaled ET, biased plot selection (e.g. convenient access in proximity of roads) could result in strongly biased ET estimates in other studies. Thus, experimental design in general and plot selection in particular are of utmost importance in heterogeneous ecosystems.

A growing number of studies indicated an increase in water stress on ecosystems, and increasing tree mortality rates are frequently linked to hydraulic failure during extreme events (e.g. prolonged heat waves or droughts) (Mantgem et al. 2009; Williams et al. 2013). Even ecosystems in wet climates, e.g. tropical rain forests, previously thought to be least susceptible to drought stress, were identified as being vulnerable to decreasing water-availability (Phillips et al. 2009).

Further, Choat et al. (2012) demonstrated similar safety margins to hydraulic failure in wet and dry forest ecosystems, indicating that not only dry ecosystems are vulnerable to climate change but also previously assumed resilient ecosystems. However, these studies neglected effects of topographic controls on water-availability, potentially to underestimating ecosystem vulnerability towards climate change. However, the findings presented in this study suggest that strong topographic control on soil depth and radiation loads in steep terrain could lead to large differential responses under climate change. Furthermore, the increasing importance of atmospheric drought on carbon and water fluxes has recently been acknowledged (Novick et al. 2016) and an increase in atmospheric demand will be further amplified on northern slopes, but potentially mediated on southern aspects. Moreover, potential shifts to less frequent but higher intensity precipitation events would result in higher run-off ratios on sites with shallow soils, where storage capacity is exceeded more

quickly. Thus, even at similar precipitation totals, water-availability on shallow soils might be reduced considerably. Consequently, vegetation on shallow soils is expected to experience more drought stress due to decreased water-availability and increasing atmospheric demand. This will be especially notable on northern aspects, where a reduction in overstory LAI will substantially increase sub-canopy radiation load and soil evaporation, which diminishes potential water conservation attempts of the overstory vegetation. However, higher runoff ratios at upslope areas will result in more water subsidies to downslope areas, mediating or potentially even reducing drought stress, particularly on lower hillslope positions. Therefore, resilience of forest ecosystems to climate change in complex terrain is expected to vary substantially with landscape position. Moreover, topographic amplification of projected change in long-term climatic forcing increases the likelihood of exceeding the response time of the present vegetation, which might push ecosystems over a threshold into a less productive alternative stable state.

This clearly calls for explicit incorporation of topographic controls on climatic forcing and water-availability into broad-scale modeling frameworks and needs to be considered for management strategies of water and forest resources under a changing climate.

6.2 Future research

While differences in spatio-temporal patterns of ET were partly due to water-limitation, the origin and contribution of different water pools (soil vs. rock vs. groundwater) remain unclear. Future research could link spatio-temporal water use patterns with moisture characterization below the soil profile using geophysical methods (electrical resistivity tomography, ground penetrating radar) or measurements of isotopic composition of xylem water to gain further insights into spatial water-availability patterns and topographic control on shifts from energy to water-limitation. In addition, the assumption that uniform

interception loss patterns in complex terrain, despite strong LAI patterns, were driven by differential atmospheric demand could be evaluated with stratified measurements of atmospheric demand in the canopy alongside throughfall measurements.

Slower growth rates and higher ET_U contributions on norther aspects indicated high temporal persistence of contrasts in this ecosystem. However, stem growth was only measured of a limited number of trees in this study. Thus a more detailed assessment of forest growth patterns in complex terrain would enable to link hydrological, ecological and biogeochemical cycles. In particular, spatial patterns of water-use efficiency and biological productivity will provide insights into how topographic controls shape Critical Zone evolution in complex terrain.

Ultimately, this thesis illustrated the potential of using remotely sensed vegetation and terrain patterns to up-scale ET measurements in heterogeneous forests. Further, strong correlation of A_S with the residuals around the Budyko curve encourages using vegetation and terrain patterns to down-scale ET estimates of lumped models. Universal applicability of the concept will require further assessment in different ecosystems.

Bibliography

Aston, A. R. (1979). "Rainfall interception by eight small trees". In: *Journal of hydrology* 42.3, pp. 383–396.

Benyon, R. G. and T. M. Doody (2015). "Comparison of interception, forest floor evaporation and transpiration in Pinus radiata and Eucalyptus globulus plantations". In: *Hydrological Processes* 29.6, pp. 1173–1187.

Benyon, R. G. et al. (2015). "Use of a forest sapwood area index to explain long-term variability in mean annual evapotranspiration and streamflow in moist eucalypt forests: streamflow predicted from sapwood area". In: *Water Resources Research* 51.7, pp. 5318–5331.

Benyon, R. G. et al. (2017). "Stand-level variation in evapotranspiration in non-water-limited eucalypt forests". In: *Journal of Hydrology* 551, pp. 233–244.

Brooks, P. D. et al. (2015). "Hydrological partitioning in the critical zone: Recent advances and opportunities for developing transferable understanding of water cycle dynamics". In: *Water Resources Research* 51.9, pp. 6973–6987.

Choat, B. et al. (2012). "Global convergence in the vulnerability of forests to drought". In: *Nature* 491.7426, pp. 752–755.

Eagleson, P. (1982). "Ecological optimality in water-limited natural soil-vegetation systems: 1. Theory and hypothesis". In: *Water Resources Research* 18.2, pp. 325–340.

Gash, J. H. C. (1979). “An analytical model of rainfall interception by forests”. In: *Q.J.R. Meteorol. Soc.* 105.443, pp. 43–55.

Gharun, M. et al. (2015). “Mapping spatial and temporal variation in tree water use with an elevation model and gridded temperature data”. In: *Agricultural and Forest Meteorology* 200, pp. 249–257.

Griebel, A. et al. (2017). “Evergreen and ever growing Stem and canopy growth dynamics of a temperate eucalypt forest”. In: *Forest Ecology and Management* 389, pp. 417–426.

Hacke, U. G. et al. (2006). “Scaling of angiosperm xylem structure with safety and efficiency”. In: *Tree physiology* 26.6, pp. 689–701.

Mantgem, P. J. v. et al. (2009). “Widespread Increase of Tree Mortality Rates in the Western United States”. In: *Science* 323.5913, pp. 521–524.

Mitchell, P. J. et al. (2009). “Partitioning of evapotranspiration in a semi-arid eucalypt woodland in south-western Australia”. In: *Agricultural and Forest Meteorology* 149.1, pp. 25–37.

Mitchell, P. J. et al. (2012b). “Responses of evapotranspiration at different topographic positions and catchment water balance following a pronounced drought in a mixed species eucalypt forest, Australia”. In: *Journal of Hydrology* 440-441, pp. 62–74.

Nolan, R. H. et al. (2014). “Changes in evapotranspiration following wildfire in resprouting eucalypt forests”. In: *Ecohydrology*, pp. 1363–1377.

Novick, K. A. et al. (2016). “The increasing importance of atmospheric demand for ecosystem water and carbon fluxes”. In: *Nature Clim. Change* 6.11, pp. 1023–1027.

Phillips, O. L. et al. (2009). “Drought Sensitivity of the Amazon Rainforest”. In: *Science* 323.5919, pp. 1344–1347.

Poorter, L. et al. (2010). “The importance of wood traits and hydraulic conductance for the performance and life history strategies of 42 rainforest tree species”. In: *New Phytologist* 185.2, pp. 481–492.

Williams, A. P. et al. (2013). “Temperature as a potent driver of regional forest drought stress and tree mortality”. In: *Nature Clim. Change* 3.3, pp. 292–297.